UNIVERSITAT POLITÈCNICA DE CATALUNYA

Doctoral Programme:

AUTOMÀTICA, ROBÒTICA I VISIÓ

Thesis:

Modelling and Vibration Control for a Submerged Piezoelectric Cantilever Beam

Bin Wang

Advisors:

Dr. Ramon Costa Castelló

Prof. Jing Na

June 2022

Universitat Politècnica de Catalunya

Automatic Control Department

Title:
Modelling and Vibration Control for a Submerged Piezoelectric Cantilever Beam

This PhD thesis was completed at:

Institut de Robòtica i Informàtica Industrial, CSIC-UPC
C/ Llorens i Artigas 4-6. 08028 Barcelona, Spain

Advisors:
Dr. Ramon Costa Castelló
Prof. Jing Na

To my family

Acknowledgments

I would like to take this chance to express my deep and sincere gratitude to my research supervisors, Professor Ramon Costa Castelló and Professor Jing Na for giving me the opportunity to do doctoral research and providing invaluable guidance during all these years. I am really appreciated for both your patience, encouragement and insightful comments.

My sincere thanks also goes to Professor Xavier Escaler, Oscar de la Torre and Xavier Sanchez Botello, for their help on conducting the experiments.

Again, I would like to give my sincere thanks to Professor Jing Na, for his continuous support since my Master's studies. I was fortunate to have him as both my Master's thesis advisor and doctoral thesis advisor. Thanks to him for his recommendation for me to pursue doctoral degree abroad.

A debt of gratitude also owes to Professor Weijun Su, Professor Tingli Su, Professor Xuebo Jin and Professor Yu Guo , for their help and support in my career growth.

I would also like to give my special thanks to all the colleagues and friends in Barcelona, for their encouragement and support in both academic and daily life.

Last but not least, I would like to express my sincere thanks to my family, for supporting all the things in my life.

Finantial Support: This work was supported in part by the Chinese Scholarship Council under Grant 201908530215; in part by the Horizon 2020 research and innovation program under Grant 814958 (AFC4HYDRO); in part by the National Natural Science Foundation of China under Grants 61922037 and 61873115; in part by the Yunnan Fundamental Research Project under Grant 202001AV070001; in part by the project Grant RTI2018-096001-B-C32 (DOVELAR).

Contents

List of Figures

List of Tables

Part I

Preamble

Chapter 1

Introduction

1.1 Motivation

The climate change and the health problems caused by the utilization of the fossil fuels have attracted great attentions with the rapid growth of global population. Exploring green energies to replace traditional fossil fuels is regarded the most effective and promising way to solve these problems [3]. The main contributors to the green energies include solar energy, wind energy, hydro energy and hydrogen energy. Hydro energy is one of the most attractive clean energy among different kinds of sustainable energies [4, 5]. To obtain hydro energy, hydraulic turbine is an essential element that can transform water's kinetic energy to mechanical energy. In the power system including various power resources, variations in either power generation from other kinds of resources or special demands of hydro power directly affect the hydraulic turbines [6]. The turbines have to change the power output constantly in order to fulfill these demands. As a result, hydraulic turbines work at different design points with varying load conditions. In other words, hydraulic turbines experience unsteady flows under different load conditions [1]. These unstable flows intensely degrade the hydraulic turbines.

To improve the efficiency and performance of the hydraulic turbines, it is essential to develop an active flow control system to ensure the turbine work safely in various operating conditions. This is the main purpose of the EU-funded AFC4Hydro project [7]. By designing the active flow control strategies, the hydraulic turbines can work at their best efficiency points. Recently, some results show the dynamics of fluid-structure interaction can be modelled by using COMSOL [8] or ANSYS [9]. However, these models are mainly focus on the modal analysis and are difficult to be utilized for controller design. Due to the fact that unstable flow conditions severely affect the turbine systems, the estimation of the system parameters is not trivial. Although the natural frequency can be estimated by using the finite element analysis [10], the procedure is time consuming. The control may not be realized in real time. Under the framework of the AFC4Hydro project, this thesis mainly addresses the modelling, parameter estimation and vibration control of the structure-fluid interaction problem for the hydraulic turbine system.

One of the main challenge is reducing vibration caused by the cavitation. Cavitation occurs in many mechanical systems with fluid dynamics and can cause significant deformation of mechanical structures. This phenomenon is devastating in high-speed rotating scenarios where rapid pressure changes of the swirling fluid generate intense shock waves. In particular, a rapid expansion from a thin vortex to a much broader vortex with severe vibration (also known as vortex breakdown phenomenon) can significantly deteriorate or even damage the mechanical structure of the engineering applications [11]. In [12], the

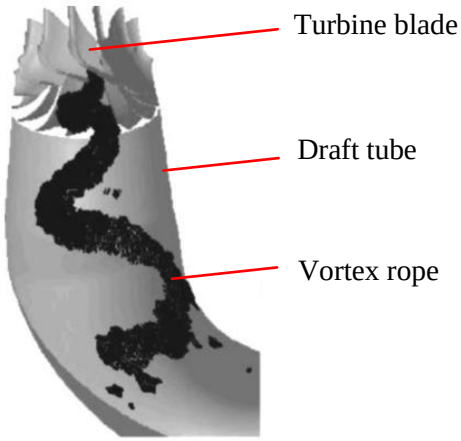

Figure 1.1: Vortex in the Francis turbine [1]

physical phenomena is reviewed and the main effects of cavitation are discussed. In [13], the cavitation instabilities are summarized. Numerical methods describing the cavitation turbulent flows are presented. How to cope with vortex breakdown phenomenon and prevent the vibration of the mechanical structure become a meaningful topic [14]. Figure. 1.1 shows the profile of the vortex in the typical Francis turbine. The vibrations induced by the vortex breaking are different with various load conditions [1]. These vibrations lead to damage to the runner blades and the shaft, which in return deteriorate the performance on the power output.

The main goal of this thesis is to cope with the vibrations caused by vortex breakdown in the water turbine system. To achieve this, the first step is to develop the mathematical model of the plant. For the purpose of focusing on the vibration of the rotating wheel (runner) of the water turbine system, we assume that the blade of the wheel can be partly described by a flexible cantilever beam. Then the problem is transformed to the beam-fluid interaction problem and the main goal becomes vibration suppression of the beam in fluid. The sketch of the beam-fluid interaction system is shown in Figure 1.2.

For the beam-fluid interaction problem, modelling of beam and fluid as well as beam-fluid interaction are significant to describe the system dynamics. During the past decades, many researchers have been interested in modelling of beam to explore modal dynamics [15] [16] [17] due to its application in many engineering practice. The well known Euler–Bernoulli beam [15], Timoshenko beam [18] and Rayleigh beam [19] were investigated, leading to the developments of a broad class of beam models [20, 21]. In [22], a piezoelectric laminate beam model was developed using piezoelectric actuator and sensor. In [23], the Rayleigh damping was included into the Euler–Bernoulli beam to represent a flexible-link robot. However, most of these beam models are described by using partial differential equations (PDE). Although the modelling of the beam and the simplification of several PDE models have been studied in the above-mentioned literatures, a model that is suitable for online estimating the parameters of the submerged beam by using the piezoelectric actuator and strain gauge was not developed yet.

In this thesis, we will firstly focus on the modelling of beam and fluid respectively. Because there are many literature regarding beam dynamics and also fluid dynamics, the problems mainly remain in beam-fluid interaction dynamics. For the beam, the main problem is how to cope with the distributed parameter system described by partial differential equation. For distributed parameter systems, unlike lumped parameter systems, it is more difficult to analyze and conduct control strategies in a direct manner.

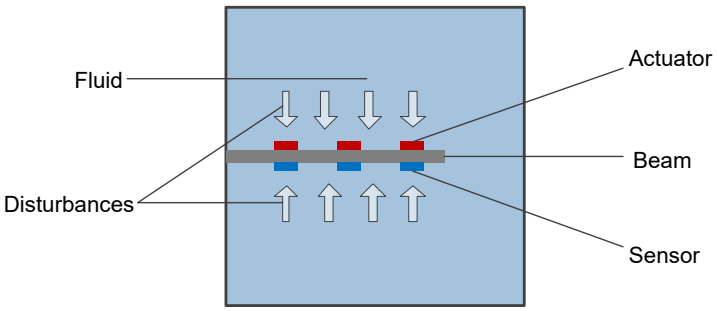

Figure 1.2: Sketch of beam-fluid interaction system

For the fluid, due to the complexity and difficulty to implement the ideal flow equation (Navier-Stokes equation) in practical applications, proper assumptions and approximations are necessary. For the fluid-structure interaction, it is critical to create mathematic models that can describe the dynamics of beam-fluid interaction, and at the same time, easy to implement.

Automatic control plays an important role in both protecting the devices and improving the efficiency of the applications. For the beam-fluid interaction problems, appropriate control strategies can effectively suppress the vibration of the beam. In particular, smart materials (e.g. piezoelectric materials) are generating a lot of interests for the design of vibration control [24]. Such materials can apply control forces on the structures, thus the vibration can be suppressed with appropriate controllers. Although there are many literature regarding the control of mechanical structures like beams and plates [25–27], very few control strategies have been developed for beam-fluid interactions. To guarantee the safety of the hydro turbines (i.e. the fluid-structure interaction) under various scenarios, it is very significant to introduce new control methods regarding these specific problems. At the same time, due to the fact that unknown dynamics can seriously degrade the control performance, it is useful to investigate parameter estimation methods and unknown dynamics estimation techniques.

Another challenging issue is that the accurate beam-fluid interaction model is described by partial differential equation (PDE). Compared with the ordinary differential equation (ODE), PDE is difficult to find the analytical solution. This makes the modelling and control of such system difficult and time-consuming. Some well known approximations (e.g. finite element method, finite difference method) have been used to cope with PDE. As a result, convergence of approximations and stabilization of the transformed system become interesting research areas. In a word, it is worth investigating the approximation methods and appropriate simplifications to model and control of the beam-fluid interaction system as well as many other systems described by PDE.

For the above reasons, in this thesis we will explore the fundamental principles of beam-fluid interaction problems and develop suitable models to describe the problems. After this, we will focus on the parameter estimation and control strategies of the beam and the beam submerged in fluid under various flow scenarios.

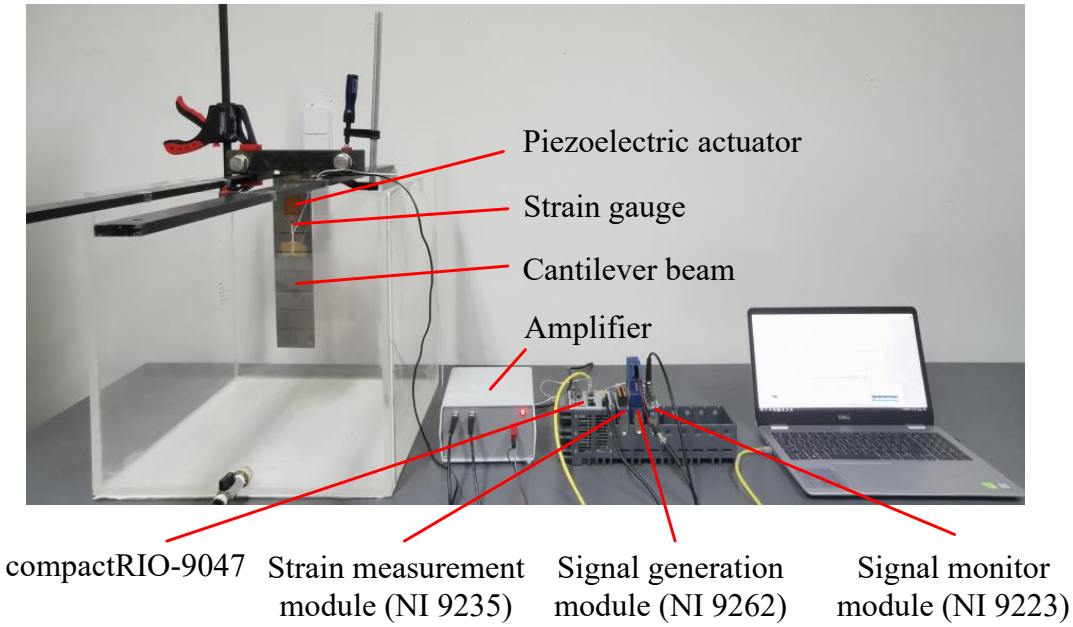

Figure 1.3: Test bench of the beam system

1.2 Experimental apparatus of the beam system

This work is conducted mainly based on the test bench as shown in Figure 1.3. We can see that a steel cantilever beam is vertically placed in a cubic tank. We use a piezoelectric actuator (type number: P-876.A12) from PI Ceramic GmbH to excite the beam. The voltage applied on the actuator is an amplified signal (ranges: $\pm$100V) from the voltage amplifier and the original voltage signal (ranges: $\pm$10V) is generated from NI 9262 module which is a simultaneously updating analog output module from National Instruments. The NI 9223 module is used to monitor the amplified signal. To configure the sensor subsystem, we use a strain gauge (type number: WFLA-6-11-3LDBTB) from Tokyo Measuring Instruments Laboratory to measure the strain of the beam. The NI 9235 quarter-bridge strain measurement module is used to collect the signal of the strain gauge. A bridge offset nulling calibration is introduced to eliminate the offset of the strain gauge. For the real-time control purpose, we use compactRIO-9047 from National Instruments. The geometric and material properties of the steel beam and the piezoelectric actuator are described in Table 1.1 [28] and Table 1.2 [29] , respectively. The specific characteristics of the hardware configuration are summarized in the following subsections.

Table 1.1: Material properties of the beam

Variables	Values
Density of the beam (ρ)	$7723.13\ kg/m^3$
Cross sectional area (A)	$0.00008\ m^2$
Young's modulus of elasticity (E)	$1.93 \times 10^{11} N/m^2$
Bending moment of inertia (I)	$6.67 \times 10^{-12} m^4$
Damping factor (C)	$9.8 \times 10^7 N/(m/s)$
Length of the beam (L)	$0.36\ m$

Table 1.2: Material data of the piezoelectric ceramics

Variables	Values
Young's modulus of elasticity (E_p)	$7.06 \cdot 10^{10} N/m^2$
Piezoelectric coefficient (d_{31})	$-1.8 \cdot 10^{-10} C/N$
Effective moment arm (r_a)	$0.001\ m$

1.2.1 Strain gauge

The strain gauge we use in the experiments is a waterproof strain gauge (type number: WFLA-6-11-3LDBTB) from Tokyo Measuring Instruments Laboratory. The strain gauge is shown in Figure 1.4 and the main characteristics are summarized as follows

- Applicable specimen: Metal, Glass, Ceramics
- Operational temperature(°C) : 0 to +80°C
- Temperature compensation range(°C) : +10 to +80°C
- Applicable adhesive: CN, P-2
- Backing: Epoxy
- Element: Cu-Ni
- Strain limit: 3% (30000 × 10^6 strain)
- Dimensions of the gauge: 6 mm × 2.2 mm
- Dimensions of the backing: 25 mm × 11 mm × 1.5 mm

1.2.2 Piezoelectric actuator

In the experiments, we use a piezoelectric actuator (type number: P-876.SP1) from PI Ceramic GmbH to excite the beam. The piezoelectric actuator is shown in Figure 1.5 and the main characteristics are given as

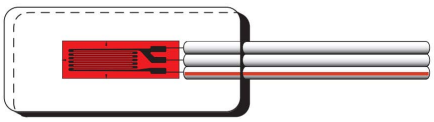

Figure 1.4: Photo of the strain gauge (type number: WFLA-6-11-3LDBTB)

Figure 1.5: Photo of the piezoelectric actuator (type number: P-876.A12)

- Operating voltage range: -100 V to 400 V
- Piezo ceramic: PIC255
- Piezoceramic height: 200 µm
- Dimensions: 61 mm × 35 mm × 0.5 mm

1.2.3 Strain measurement module (NI 9235)

The strain measurement module (NI 9235) is chosen to collect the strain data of the beam in the experiments. The module is shown in Figure 1.6 and the main characteristics are summarized as follows

- Spring terminal connectivity
- Simultaneous dynamic strain analog input
- Built-in voltage excitation for quarter-bridge sensors
- 120 Ω strain gauge measurements
- -40 °C to 70 °C operating range, 5 g vibration, 50 g shock

1.2.4 Signal generation module (NI 9262)

In the experiments, the excitation signal and the control signal are all generated through the signal generation module (NI 9262). The NI 9262 module is a simultaneously updating analog output module. The module is shown in Figure 1.7 and the main characteristics are summarized as follows

- Output range: ±10 V
- 6-Channel C Series Voltage Output Module
- 16-bit resolution

1.2.5 Signal monitor module (NI 9223)

The signal monitor module (NI 9223) is a 4-Channel 16-Bit simultaneous analog input module. In the experiments, it is used to monitor the amplified voltage applied on the piezoelectric actuator. The module is shown in Figure 1.8.

Figure 1.6: Photo of the strain measurement module (NI 9235)

Figure 1.7: Photo of the signal generation module (NI 9262)

Figure 1.8: Photo of the signal monitor module (NI 9223)

1.2.6 compactRIO-9047

To control the beam system in real time, compactRIO-9047 is selected which includes a Kintex-7 70T FPGA with LabVIEW FPGA Module. The compactRIO-9047 is shown in Figure 1.9 and the main characteristics are summarized as follows

Figure 1.9: Photo of compactRIO-9047

- CPU: Intel Atom E3940
- Number of cores: 4
- CPU frequency: 1.6 GHz (base), 1.8 GHz (burst)
- On-die L2 cache: 2 MB
- Supported C Series module programming modes: Real-Time (NI-DAQmx), Real-Time Scan (I/O Variables), LabVIEW FPGA
- Maximum input or output frequency: 1 MHz
- I/O standard compatibility: 5 V TTL
- I/O voltage protection ±30 V

1.3 Thesis objectives

The overall objective of the research is to develop a modern modelling and control framework for the beam submerged in fluid in order to fulfil the demanding requirements for vibration suppression and control performance. Comparing with the beam in air, there are many challenges on the modelling and control for beam in fluid due to nonlinear and strong-coupled characteristics. The global objectives can be listed as follows:

1. Develop control-oriented models. For the beam, different models will be introduced and the feasibility for control will be verified. For the fluid dynamics, we will introduce Navier-Stokes equation to describe the flow in a box. In order to construct the beam-fluid interaction system, we will introduce the distributed force from the fluid to the beam. To simplify the fluid dynamics, a combined simplified force will be derived. To handle the model, it will be necessary to discretize the model with appropriate discretization methods due to the fact that the analytical solution of the PDE system is difficult to obtain. We will use finite difference method to get the approximation solution of the system. We will then implement the system in MATLAB to see the behavior of the beam system.

2. Investigate the parameter estimation methods to online estimate the unknown parameters of the beam system. For the system considering the first vibration mode, the states can be measured or estimated, the parameter estimation methods can be designed based on the states. For the higher-order system considering multiple vibration modes, we design the parameter estimation algorithms based on the input and output, which can be directly measured from the system. New adaptive laws will be studied based on the proposed estimation framework.

3. Design control algorithms together with unknown dynamics estimation methods to suppress the vibration, so as to alleviate the degradation of the system. Specifically, for the control of the beam immersed in fluid, we will investigate unknown dynamics estimation methods to estimate the unknown force imposed on the beam. In no doubt the distributed control will be complicated and the implementation will be time-consuming. To solve this problem, proper simplification of both the model and the control strategy will be investigated. Unknown system dynamics estimator (USDE) based controller will be designed. In addition, adaptive control will be investigated for the beam system.

4. Study the applicability of the designed control framework with simulations and experiments. Simulations of different parameter estimation methods and control strategies will be conducted in MATLAB. Since the complicated model together will high performance but time-consuming controls are difficult to implement in practice due to the limitation of the computer processor, appropriate simplifications (e.g. model reduction) will be proposed for practical experiments.

1.4 Outline of the thesis

This thesis mainly focuses on the modelling, parameter estimation and vibration control of a submerged piezoelectric cantilever beam. In this chapter, the motivation, experimental apparatus of the beam system and thesis objectives have been described.

The rest of the thesis is organized as follows:

- **Chapter 2**, "Modelling of the submerged piezoelectric cantilever beam", provides the system models described by both the PDE and ODE. By using the Hamilton's principle, a PDE model is presented considering the piezoelectric actuator, the Kelvin-Voigt damping and the fluid force. The ODE model is then derived with the help of Galerkin's method.

- **Chapter 3**, "Adaptive parameter estimation for first mode system", gives a new adaptive parameter estimation framework to online estimate unknown system parameters considering the first vibration mode. To obtain the system states, the Levant exact differentiator via sliding mode technique is constructed. Instead of using the observer/predictor error as in the classical parameter estimation methods, a novel adaptive law which is driven by the parameter estimation error is proposed.

- **Chapter 4**, "Adaptive parameter estimation for the beam system with multi-modes", deals with parameter estimation of the beam system with multi-modes. A novel adaptive parameter estimation strategy is introduced to estimate the unknown system parameters in real time. Specifically, a time-varying gain is designed to handle the effects of regressor to enhance convergence performance and simplify the tuning of learning gains.

- **Chapter 5**, "Unknown dynamics estimator based vibration control for the beam", provides an estimator based vibration control strategy to both suppress the vibration and estimate the unknown system dynamics. Different to the function approximation based methods, the proposed control has a simple structure which is more realistic to implement in practice. In the proposed estimator, only one parameter need to be tuned depends on the bandwidth of the filter. The estimated unknown dynamics is compensated into the controller and thus makes the system more robust to unknown external disturbances. The stability and convergence properties of the proposed control is proved by using Lyapunov theory.

- **Chapter 6**, "Adaptive vibration control for the beam", presents an adaptive control scheme for the beam system with uncertainties. By using the parameter estimation error based adaptive law, the system parameters can be online updated. To suppress the vibration of the beam, the adaptive controller is designed and the stability is proved.

- **Chapter 7**, "Conclusions and future work", gives the conclusions of this thesis and a proposal for future research.

The diagram and logic of the thesis structure is provided in Figure. 1.10.

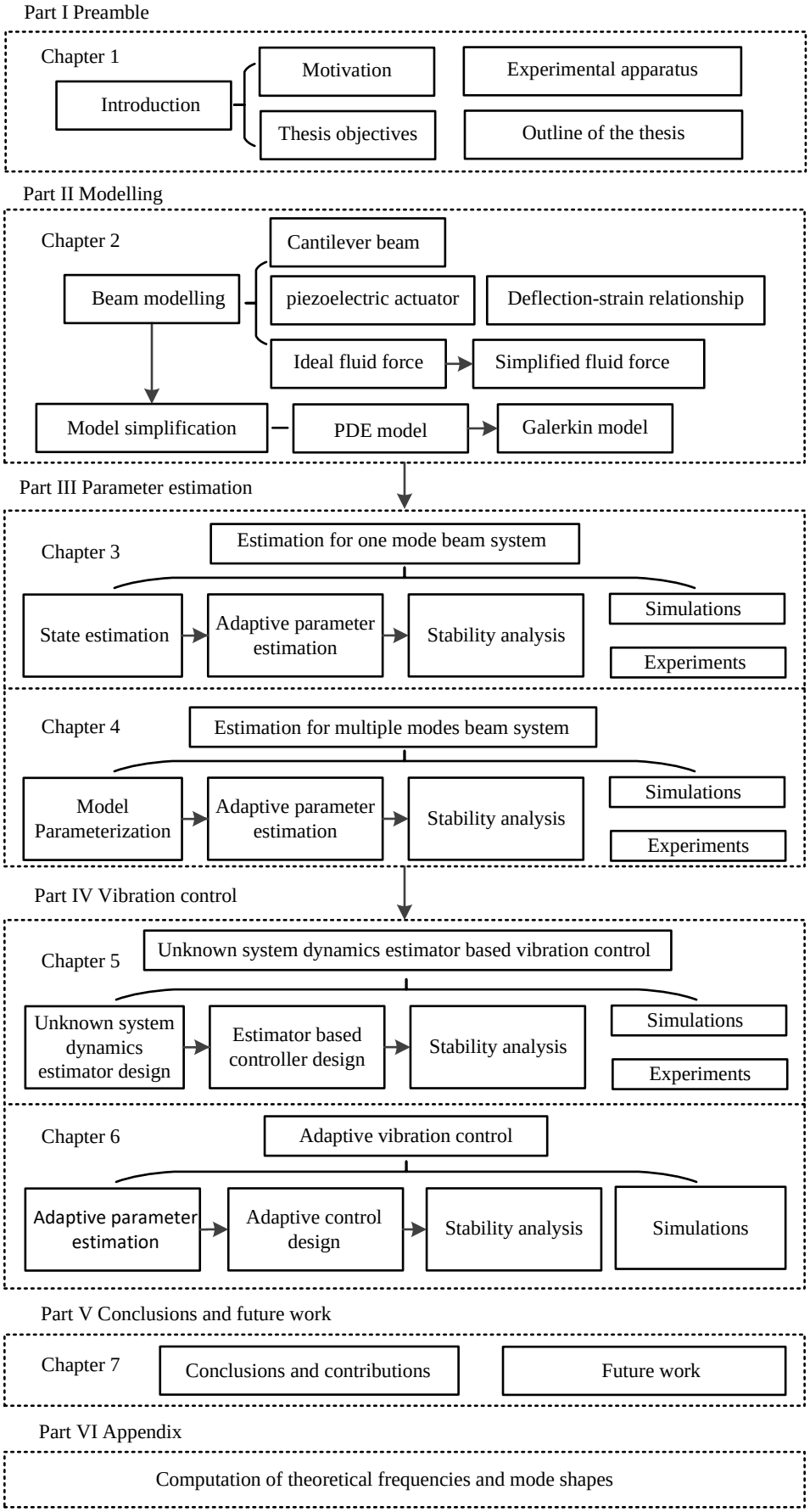

Figure 1.10: Diagram and logic of the thesis structure

Part II

Modelling of the Beam System

Chapter 2

Modelling of the submerged beam

2.1 Introduction

In this chapter, modelling of the beam together with the fluid dynamics is done. A brief overview of the beam theories is presented. To describe the dynamics of a submerged piezoelectric beam, Euler-Bernoulli equation and Navier–Stokes equation are taken into considered. Piezoelectric effects are included in the system model and the strain-deflection relationship is derived for the experiment purpose. A tradeoff is made between the accuracy and the practicability to fulfill the demand of the real plant.

2.2 State of art

There are many beam theories in the literature considering different behaviour for the vibrating beam. The Euler-Bernoulli model was firstly presented by Jacob Bernoulli and then accepted by Leonhard Euler in the 18th century. Jacob Bernoulli first discovered the curvature of the elastic beam is proportional to the bending moment and his nephew Daniel Bernoulli first formulated the motion equation of a vibrating beam. Leonhard Euler accepted Jacob Bernoulli's theory in the studies of the shape of elastic beams under various loading conditions [30]. The sketch of a flexible cantilever beam is shown in Figure. 2.1.

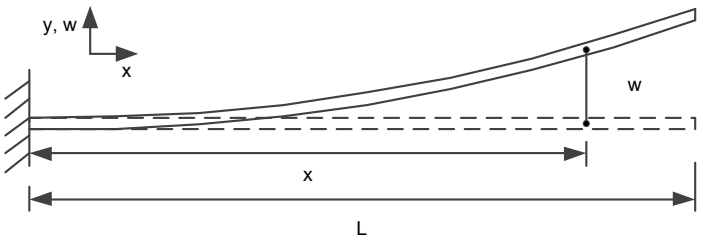

Figure 2.1: Sketch of a flexible cantilever beam

The partial differential equation for the Euler-Bernoulli beam model can be written as

$$\rho A \frac{\partial^2 w(x,t)}{\partial t^2} + EI \frac{\partial^4 w(x,t)}{\partial x^4} = f(x,t) \tag{2.1}$$

where $w(x,t)$ is the transverse displacement at position x and time t, ρ is the density assumed to be a constant, A is the cross-sectional area, E is the Young's modulus of elasticity, I is the bending moment

of inertia, and $f(x,t)$ is the forcing function of both space and time. Four possible boundary conditions shown in Figure. 2.2 can be listed as

- $\frac{\partial^2 w}{\partial x^2} = 0, \quad w = 0$ for hinged end (Figure 2.2 (a));
- $\frac{\partial w}{\partial x} = 0, \quad w = 0$ for clamped end (Figure 2.2 (b));
- $\frac{\partial^2 w}{\partial x^2} = 0, \quad \frac{\partial^3 w}{\partial x^3} = 0$ for free end (Figure 2.2 (c));
- $\frac{\partial w}{\partial x} = 0, \quad \frac{\partial^3 w}{\partial x^3} = 0$ for sliding end (Figure 2.2 (d)).

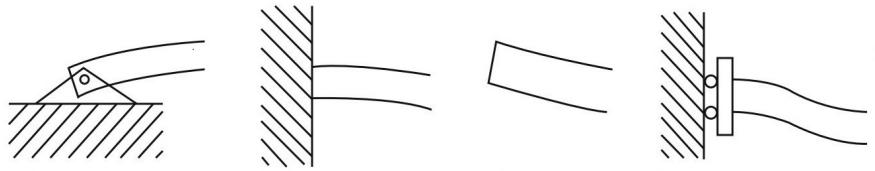

Figure 2.2: Four types of boundary conditions: (a) hinged; (b) clamped; (c) free; (d) sliding. [2]

The Euler-Bernoulli beam theory, also known as classical beam theory, is the most commonly used in many engineering problems mainly because it is simple and reasonable for approximations in many scenarios. For example, in the analysis of nonlinear dynamics, Euler-Bernoulli beam model is widely used. As one of the most well-known nonlinear systems, rotating beams have even become a benchmark plant for validating nonlinear effects. In [31], Chung and Yoo analysed dynamic characteristics of a rotating beam by using finite element method. Stability analysis of the rotating beam is further investigated in [32]. Vibration analysis of a multi-layer composite beam is then carried out in [33]. In [34], a rotating thin-walled cantilever beam is modelled and the nonlinear dynamics are analysed. For variable speed rotating beams, a nonlinear model is presented in [20, 35].

The Euler-Bernoulli model normally tend to slightly overestimate the natural frequency of the vibrating beam. In order to improve the model, Rayleigh included the effect of rotational inertia of the cross-sectional area in 1877 [30]. The governing equation of Rayleigh beam model can be given as

$$\rho A \frac{\partial^2 w(x,t)}{\partial t^2} + EI \frac{\partial^4 w(x,t)}{\partial x^4} - \rho I \frac{\partial^4 w(x,t)}{\partial x^2 \partial t^2} = f(x,t) \tag{2.2}$$

with four possible boundary conditions

- $\frac{\partial^2 w}{\partial x^2} = 0, w = 0$ for hinged end (Figure 2.2 (a));
- $\frac{\partial w}{\partial x} = 0, w = 0$ for clamped end (Figure 2.2 (b));
- $\frac{\partial^2 w}{\partial x^2} = 0, \quad \frac{\partial^3 w}{\partial x^3} - \rho I \frac{\partial^3 w}{\partial x \partial t^2} = 0$ for free end (Figure 2.2 (c));
- $\frac{\partial w}{\partial x} = 0, \quad \frac{\partial^3 w}{\partial x^3} - \rho I \frac{\partial^3 w}{\partial x \partial t^2} = 0$ for sliding end (Figure 2.2 (d)).

Many investigations have been conducted based on the Rayleigh beam theory. The dynamics of a rotating Rayleigh beam with an added force is studied in [36]. In [21, 37], the vibration and stability of axially moving Rayleigh beams are investigated. The Rayleigh beam model partially corrects the overestimation of natural frequencies in the Euler-Bernoulli model. However, the natural frequencies are still overestimated.

The shear beam model added the shear distortion to the Euler-Bernoulli model [30]. This considerably improves the estimation of the natural frequencies. The governing equation of the shear beam model can be stated as follows

$$\begin{aligned} \rho A \frac{\partial^2 w(x,t)}{\partial t^2} - GA_s \left(\frac{\partial^2 w(x,t)}{\partial x^2} - \frac{\partial \alpha(x,t)}{\partial x} \right) &= f(x,t) \\ EI \frac{\partial^2 \alpha(x,t)}{\partial x^2} + GA_s \left(\frac{\partial w(x,t)}{\partial x} - \alpha(x,t) \right) &= 0, \end{aligned} \tag{2.3}$$

where G is the shear modulus, $\alpha(x,t)$ denotes the rotation angle due to bending, $A_s = A/k$, with A being the cross-sectional area and k the shear correction coefficient, depends on the shape of the cross section. Four possible boundary conditions can be listed as

- $\frac{\partial \alpha}{\partial x} = 0, w = 0$ for hinged end (Figure 2.2 (a));
- $\alpha = 0, w = 0$ for clamped end (Figure 2.2 (b));
- $\frac{\partial \alpha}{\partial x} = 0, GA_s \left(\frac{\partial w}{\partial x} - \alpha \right) = 0$ for free end (Figure 2.2 (c));
- $\alpha = 0, \left(\frac{\partial w}{\partial x} - \alpha \right) = 0$ for sliding end (Figure 2.2 (d)).

The Shear beam model is often used for the analysis of building behavior [38–40]. In [39], a multistory building considering coupling actions is described by the shear beam model. Modelling by the shear beam approach is proved effective in the analysis of torsionally coupled buildings. In [40], a shear beam model is used to analyse the nonlinear properties of the reinforced concrete and the nature of strong motion for a seven-story building with earthquake excitation.

Timoshenko formulated the beam model by adding both the effect of shear and effect of rotation into the Euler-Bernoulli model [41]. The governing equation of the Timoshenko beam model is [38]

$$\begin{aligned} \rho A \frac{\partial^2 w(x,t)}{\partial t^2} - GA_s \left(\frac{\partial^2 w(x,t)}{\partial x^2} - \frac{\partial \alpha(x,t)}{\partial x} \right) &= f(x,t) \\ \rho I \frac{\partial^2 \alpha(x,t)}{\partial t^2} - EI \frac{\partial^2 \alpha(x,t)}{\partial x^2} - GA_s \left(\frac{\partial w(x,t)}{\partial x} - \alpha(x,t) \right) &= 0, \end{aligned} \tag{2.4}$$

and the boundary conditions are identical to those of shear beam model.

For scenarios that can not neglect shear and rotary effects, the Timoshenko beam theory is regarded as a major improvement for non-slender beams with high frequencies. Properties of the natural frequencies and modes of Timoshenko beam model can be found in [42]. In [43], the advantages of Timoshenko beam model are shown in the vibration analysis of multi-walled carbon nanotubes, where the effects of shear deformation and rotary inertia are significant and considering high vibration modes. Different beam models are summarized in Table 2.1.

Euler-Bernoulli beam	Rayleigh beam	Shear beam	Timoshenko beam
[30] [31] [32] [33] [34]	[30] [36]	[30] [39]	[30] [41]
[20] [35] [44] [45]	[21] [37]	[40]	[42] [43]

Table 2.1: Summary of different beam models in the literature

Over the past years, the submerged beam has attracted a lot of research interests. The fluid flow can be generally classified into three different types as shown in Figure 2.3. The regular flow represents the behavior of general evolvement of the fluid. The rebound flow is the flow back to the beam from the wall. The external flow is the flow input from outside. In [46], a cantilevered Euler–Bernoulli beam submerged

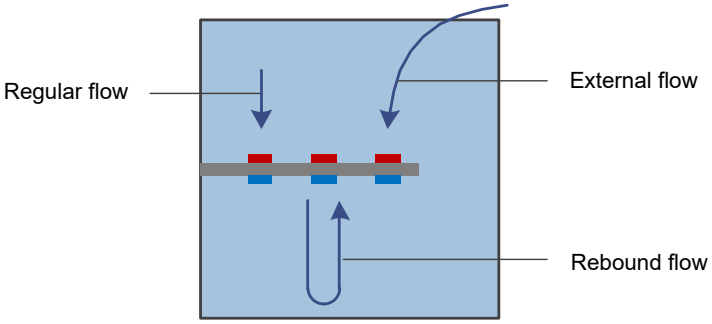

Figure 2.3: Different fluid flow interacting with the beam

in Newtonian fluid is modeled. A simplified analytical fluid–structure interaction model is derived. In trying to calculate the coupled frequencies of vibration of a partially submerged beam, [47] provides an theoretical model that describes the vibrational behavior of the submerged beam. In [48], the vortex is modeled by a nonlinear oscillator satisfying the van der Pol equation. As a result, the structure-fluid interaction can be described by the wake oscillator and a one degree-of-freedom structural oscillator.

In addition to model the complex structure-fluid interaction dynamics, there are many literature working on the simplified fluid forces. In this way, the fluid forces can be directly integrated to the beam models. In [49], the fluid dynamics are simplified as a combination of inviscid forces and viscous forces. In [50], a flexible slender cantilevered beam is modeled interacting with an incompressible fluid. The fluid is modeled by using an added mass and a summation of forces including the shear force, the viscous force and the axial tension. We can see that the key point of the simplified beam-fluid interaction problems can be summarized as: construct the virtual flow considering different behaviors of fluid; select or create appropriate methods to simplify the solving procedure. Some of these considerations can also be found in the literature. In [51], Eftekhari and Jafari propose a mixed modal-differential quadrature method to study the dynamic behavior of beams in contact with fluid. This methodology uses the modal technique for the structure while it applies the differential quadrature method for the fluid. Thus, the governing partial differential equations of the beam and fluid are reduced to a set of ordinary differential equations in time. Later, some similar results are obtained in [52]. In [53], free vibration and stability of a cantilever beam attached to an axially moving base in fluid is studied by using Galerkin approach. For Euler-Bernoulli beam, a semi-analytical technique called differential transformation method is employed for solving a fluid-structure interaction in [54].

Most of the above-mentioned models are developed by using PDEs. Although the PDE based models can describe the detailed dynamics of the beam system, it is hard to implement them in real applications due to the limitation of the hardware (e.g., bandwidth and local memory capacity). In this thesis, we will focus on both the PDE and ODE models for the system modelling and analysis. In order to obtain system parameters and suppress the vibration in reality, we will mainly deal with the simplified ODE model.

2.3 Beam Modelling

In this section, we will derive the beam model based on Euler-Bernoulli beam theory. The piezoelectric actuator model will be included in the beam model. In order to collect the output information with strain gauge in the experiments, we will derive the relationship between deflection and strain. The derived beam model will be then simplified with different simplification methods.

2.3.1 Cantilever beam model

The sketch of the cantilever beam considering the flapwise deflection is depicted in Figure 2.4.

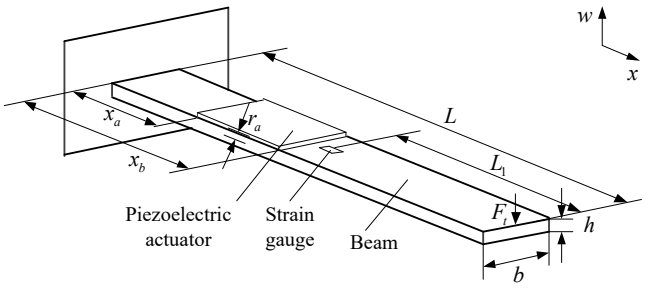

Figure 2.4: Sketch of the piezoelectric cantilever beam

For an inextensible beam (neglecting the strech deformation), the kinetic energy T can be given as [35, 55]

$$T = \int_0^L \frac{1}{2} m V_y^2 dx = \frac{1}{2} \rho A \int_0^L \left(\frac{\partial w}{\partial t} \right)^2 dx \tag{2.5}$$

where m is the mass of the cantilever beam, V_y is the flapwise velocity, ρ is the density, A is the cross-sectional area of the beam ($A = b \cdot h$, b is the beam width and h is the beam thickness), w is the flapwise displacement and L is the length of the beam.

To describe the dynamics associated with damping, the Kelvin-Voigt damping model is considered. Based on the Kelvin-Voigt hypothesis, the conservative moment M_c and the non-conservative moment M_{nc} can be given as [56, 57]

$$M_c = EI \frac{\partial^2 w}{\partial x^2} \tag{2.6}$$

$$M_{nc} = CI \frac{d}{dt} \left(\frac{\partial^2 w}{\partial x^2} \right) \tag{2.7}$$

where E is the Young's modulus, I is the Bending moment of inertia and C is the damping factor of the beam.

Considering the flapwise deformation [58], the potential energy (or strain energy) U of an inextensible beam may be obtained by using the conservative moment (2.6) [57, 59]

$$U = \frac{1}{2} \int_0^L EI \left(\frac{\partial^2 w}{\partial x^2} \right)^2 dx. \tag{2.8}$$

Using the non-conservative moment (2.7), the non-conservative force F_{nc} can be written as [57]

$$F_{nc} = \int_0^L \frac{\partial^2}{\partial x^2} M_{nc} dx = \int_0^L CI \frac{\partial^2}{\partial x^2} \left[\frac{d}{dt} \left(\frac{\partial^2 w}{\partial x^2} \right) \right] dx. \tag{2.9}$$

Therefore, the variation of works done of the non-conservative force F_{nc} and the piezoelectric force F_{ac} are given as [57]

$$\begin{aligned}\delta W &= -(F_{nc} + F_{ac})\delta w dx \\ &= \int_0^L -\left\{ CI\frac{\partial^2}{\partial x^2}\left[\frac{d}{dt}\left(\frac{\partial^2 w}{\partial x^2}\right)\right] + F_{ac}\right\}\delta w dx.\end{aligned} \tag{2.10}$$

By using the variation and integrating (2.5), (2.8) and (2.10) by parts respectively, one could have

$$\begin{aligned}\int_{t_1}^{t_2}\delta T dt &= \rho A\int_{t_1}^{t_2}\int_0^L \frac{\partial w}{\partial t}\delta\frac{\partial w}{\partial t}dxdt \\ &= \rho A\int_0^L\left(\frac{\partial w}{\partial t}\delta w\Big|_{t_1}^{t_2}\right)dx - \rho A\int_0^L\int_{t_1}^{t_2}\frac{\partial^2 w}{\partial t^2}\delta w dt dx \\ &= -\rho A\int_0^L\int_{t_1}^{t_2}\frac{\partial^2 w}{\partial t^2}\delta w dt dx\end{aligned} \tag{2.11}$$

$$\begin{aligned}\int_{t_1}^{t_2}\delta U dt &= EI\int_{t_1}^{t_2}\int_0^L \frac{\partial^2 w}{\partial x^2}\delta\frac{\partial^2 w}{\partial x}dxdt \\ &= EI\int_{t_1}^{t_2}\left(\frac{\partial^2 w}{\partial x^2}\delta w\Big|_0^L - \int_0^L\frac{\partial^3 w}{\partial x^3}\delta\frac{\partial w}{\partial x}dx\right)dt \\ &= EI\int_{t_1}^{t_2}\left(\frac{\partial^2 w}{\partial x^2}\delta\frac{\partial w}{\partial x}\Big|_0^L - \frac{\partial^3 w}{\partial x^3}\delta w\Big|_0^L + \int_0^L\frac{\partial^4 w}{\partial x^4}\delta w dx\right)dt\end{aligned} \tag{2.12}$$

$$\int_{t_1}^{t_2}\delta W = \int_{t_1}^{t_2}\int_0^L -\left\{ CI\frac{\partial^2}{\partial x^2}\left[\frac{d}{dt}\left(\frac{\partial^2 w}{\partial x^2}\right)\right] + F_{ac}\right\}\delta w dx dt. \tag{2.13}$$

For deformable bodies with infinite number of degrees of freedom, the states of the systems can be represented by using continuous functions of time and space. For such bodies, the Hamilton's principle is given by

$$\int_{t_1}^{t_2}\left[\delta T - (\delta U - \delta W)\right]dt = 0 \tag{2.14}$$

where t_1 and t_2 are the initial and final times.

Substituting (2.11), (2.12) and (2.13) into (2.14), we have

$$\begin{aligned}&-\int_{t_1}^{t_2}\int_0^L(\rho A\frac{\partial^2 w}{\partial t^2} + EI\frac{\partial^4 w}{\partial x^4} + CI\frac{\partial^5 w}{\partial t\partial x^4} + F_{ac})\delta w dx dt \\ &- EI\int_{t_1}^{t_2}\left(\frac{\partial^2 w}{\partial x^2}\delta\frac{\partial w}{\partial x}\Big|_0^L - \frac{\partial^3 w}{\partial x^3}\delta w\Big|_0^L\right)dt = 0.\end{aligned} \tag{2.15}$$

As δw is an nonzero arbitrary variation, the terms with double integrals in (2.15) are set equal to zero. Then, the governing equation of motion can be written as

$$\rho A\frac{\partial^2 w}{\partial t^2} + EI\frac{\partial^4 w}{\partial x^4} + CI\frac{\partial^5 w}{\partial t\partial x^4} + F_{ac} = 0. \tag{2.16}$$

The boundary conditions are obtained by setting the single integrals in (2.15) equal to zero as

$$w|_{x=0} = 0;\ \frac{\partial w}{\partial x}\Big|_{x=0} = 0;\ \frac{\partial^2 w}{\partial x^2}\Big|_{x=L} = 0;\ \frac{\partial^3 w}{\partial x^3}\Big|_{x=L} = 0. \tag{2.17}$$

This means at the fixed end both the deflection and the slope are zero. At the free end of the cantilever beam, there are no bending moments or shear forces.

2.3.2 Cantilever beam with piezoelectric actuator

It is common to assume that the piezoelectric actuator's layer is much thinner than the cantilever beam. The effect of the bonding material and the layer are negligible. In addition, the twisting (shear) effect is not considered [60].

The voltage applied to the actuator introduces strain in the actuator. Since there is a distance between the actuator and the neutral surface, the strain introduces counteracting control moment on the mechanical structure. The control moment can be described as [60, 61]

$$M_a = r_a d_{31} E_p U_a(x,t) \tag{2.18}$$

where r_a is the effective moment arm (distance between the surface of the beam and the mid-plane of the piezoelectric actuator), d_{31} is the transverse piezoelectric coefficient [29], E_p is the Young's modulus of the piezoelectric patch and $U_a(x,t)$ is the imposed actuator voltage.

The voltage applied on the piezoelectric actuator can be given as

$$U_a(x,t) = U_a(t)\left[H\left(x - x_a\right) - H\left(x - x_b\right)\right] \tag{2.19}$$

where x_a, x_b represent the two ends of the piezoelectric actuator as shown in Figure 2.4. $H(\cdot)$ is the Heaviside step function which is defined as

$$H\left(x - x_i\right) = \begin{cases} 0 & x < x_i \\ 1 & x \geq x_i \end{cases} \tag{2.20}$$

The piezoelectric force can be written as

$$F_{ac} = \int_0^L \frac{\partial^2}{\partial x^2} M_a dx. \tag{2.21}$$

Substituting (2.21) into (2.13), we have

$$\rho A \frac{\partial^2 w}{\partial t^2} + EI\frac{\partial^4 w}{\partial x^4} + CI\frac{\partial^5 w}{\partial t \partial x^4} + \frac{\partial^2 M_a}{\partial x^2} = 0. \tag{2.22}$$

2.3.3 Deflection calculation from strain

From the stress-strain relationship in the Kelvin-Voigt model, the strain can be written as

$$\varepsilon(t) = \frac{\sigma}{E}\left(1 - e^{-t/\lambda}\right) \tag{2.23}$$

where σ is bending stress, $\varepsilon(t)$ is strain and $\lambda = C/E$ is the retardation time .

When we calculate strain $\varepsilon(t)$ from the known bending stress σ, the strain can be approximately given as

$$\varepsilon(t) = \frac{\sigma}{E}. \tag{2.24}$$

The theoretical force F_t for a cantilever beam can be calculated as [62]

$$F_t = \frac{3EIw}{L^3}. \tag{2.25}$$

Then the bending stress can be given by

$$\sigma = \frac{Mh}{2I} = \frac{F_t L_1 h}{2I} = \frac{3EwL_1 h}{2L^3} \tag{2.26}$$

where L_1 is the distance from the strain gauge to the theoretical force location.

Consider the stress-strain relationship from (2.24), we have the deflection-strain relationship as

$$w = \frac{2L^3\varepsilon}{3L_1 h} \tag{2.27}$$

Note that the deflection-strain relationship will be only used in experiments to transform the strain to displacement and will not be included in the model. This is because displacement and velocity are more straightforward for analysis in practice compared to strain.

Remark 2.1. *Compared to the classical formulation of Euler-Bernoulli beam, we included the effect of Kelvin-Voigt damping (2.7) and the piezoelectric force (2.21) in this work. Besides, the deflection-strain relationship is derived. The derived model (2.22) together with the deflection-strain relationship (2.27) make it possible to represent the practical beam bonding with the piezoelectric actuator and the strain gauge.*

2.3.4 Ideal fluid force

Ideally, the fluid dynamics should be described by the Navier-Stokes equation. The Navier-Stokes equation is a partial differential equation that describes the flow of incompressible fluid. In the 18th century, the equation is introduced by French engineer Claude-Louis Navier, which is an extension of the Euler equation and includes the element of viscosity for the more realistic problems in viscous fluids.

2.3.4.1 Navier–Stokes equation

Euler's original equation can be written as

$$\frac{\partial \mathbf{V}}{\partial t} + (\mathbf{V} \cdot \nabla)\mathbf{V} = -\frac{1}{\rho_d}\nabla P, \tag{2.28}$$

where $\mathbf{V}$ is the fluid velocity vector, P is the fluid pressure, ρ_d is the fluid density, and ∇ indicates the gradient differential operator.

The Navier–Stokes equation is given as

$$\frac{\partial \mathbf{V}}{\partial t} + (\mathbf{V} \cdot \nabla)\mathbf{V} = -\frac{1}{\rho_d}\nabla P + v\nabla^2\mathbf{V}, \tag{2.29}$$

where v is the kinematic viscosity, ∇^2 is the Laplacian operator.

2.3.4.2 Continuity equation

In fluid dynamics, the conservation of mass can be achieved by the mass continuity equation given as

$$\nabla \cdot \mathbf{V} = 0, \tag{2.30}$$

which means that the divergence of the velocity field is zero everywhere.

2.3.4.3 Pressure poisson equation

The continuity equation (2.30) acts as a constraint for computing the pressure. However, there is only velocity but no pressure in the continuity equation, which means there is no explicit form to couple velocity and the pressure considering the continuity equation. Thus, we derive pressure poisson equation as follows.

For two-dimensional incompressible flow, equation (2.29) and (2.30) can be written as

$$\frac{\partial V_y}{\partial t} + V_y \cdot \frac{\partial V_y}{\partial y} + V_z \cdot \frac{\partial V_y}{\partial z} = -\frac{1}{\rho}\frac{\partial p}{\partial y} + v \cdot \left(\frac{\partial^2 V_y}{\partial y^2} + \frac{\partial^2 V_y}{\partial z^2}\right) \tag{2.31}$$

$$\frac{\partial V_z}{\partial t} + V_y \cdot \frac{\partial V_z}{\partial y} + V_z \cdot \frac{\partial V_z}{\partial z} = -\frac{1}{\rho}\frac{\partial p}{\partial z} + v \cdot \left(\frac{\partial^2 V_z}{\partial y^2} + \frac{\partial^2 V_z}{\partial z^2}\right) \tag{2.32}$$

$$\frac{\partial V_y}{\partial y} + \frac{\partial V_z}{\partial z} = 0 \tag{2.33}$$

Differentiating (2.31) with respect to y to provide

$$\frac{\partial}{\partial t}\left(\frac{\partial V_y}{\partial y}\right) + \frac{\partial V_y}{\partial y} \cdot \frac{\partial V_y}{\partial y} + V_y \cdot \frac{\partial^2 V_y}{\partial y^2} + \frac{\partial V_z}{\partial y} \cdot \frac{\partial V_y}{\partial z} + V_z \cdot \frac{\partial^2 V_y}{\partial z \partial y} = -\frac{1}{\rho}\frac{\partial^2 p}{\partial y^2} + v \cdot \frac{\partial}{\partial y}\left(\nabla^2 V_y\right) \tag{2.34}$$

Similarly, differentiating (2.32) with respect to z to provide

$$\frac{\partial}{\partial t}\left(\frac{\partial V_z}{\partial z}\right) + \frac{\partial V_y}{\partial z} \cdot \frac{\partial V_z}{\partial y} + V_y \cdot \frac{\partial^2 V_z}{\partial y \partial z} + \frac{\partial V_z}{\partial z} \cdot \frac{\partial V_z}{\partial z} + V_z \cdot \frac{\partial^2 V_z}{\partial z^2} = -\frac{1}{\rho}\frac{\partial^2 p}{\partial z^2} + v \cdot \frac{\partial}{\partial z}\left(\nabla^2 V_z\right) \tag{2.35}$$

Addition of equations (2.34) and (2.35) yields

$$\begin{aligned} &\frac{\partial}{\partial t}\left(\frac{\partial V_y}{\partial y} + \frac{\partial V_z}{\partial z}\right) + \left(\frac{\partial V_y}{\partial y}\right)^2 + \left(\frac{\partial V_z}{\partial z}\right)^2 + 2 \cdot \frac{\partial V_z}{\partial y} \cdot \frac{\partial V_y}{\partial z} + V_y\left(\frac{\partial^2 V_y}{\partial y^2} + \frac{\partial^2 V_z}{\partial y \partial z}\right) \\ &+ V_z\left(\frac{\partial^2 V_z}{\partial z^2} + \frac{\partial^2 V_y}{\partial z \partial y}\right) = -\frac{1}{\rho}\left(\frac{\partial^2 p}{\partial y^2} + \frac{\partial^2 p}{\partial z^2}\right) + v\left[\frac{\partial}{\partial y}\left(\nabla^2 V_y\right) + \frac{\partial}{\partial z}\left(\nabla^2 V_z\right)\right] \end{aligned} \tag{2.36}$$

Considering the continuity equation (2.33), we have

$$\frac{\partial}{\partial t}\left(\frac{\partial V_y}{\partial y} + \frac{\partial V_z}{\partial z}\right) = 0 \tag{2.37}$$

$$\frac{\partial^2 V_y}{\partial y^2} + \frac{\partial^2 V_z}{\partial y \partial z} = \frac{\partial}{\partial y}\left(\frac{\partial V_y}{\partial y} + \frac{\partial V_z}{\partial z}\right) = 0 \tag{2.38}$$

$$\frac{\partial^2 V_z}{\partial z^2} + \frac{\partial^2 V_y}{\partial z \partial y} = \frac{\partial}{\partial z}\left(\frac{\partial V_y}{\partial y} + \frac{\partial V_z}{\partial z}\right) = 0 \tag{2.39}$$

$$\begin{aligned} \frac{\partial}{\partial y}\left(\nabla^2 V_y\right) + \frac{\partial}{\partial z}\left(\nabla^2 V_z\right) &= \frac{\partial}{\partial y}\left(\frac{\partial^2 V_z}{\partial y^2} + \frac{\partial^2 V_z}{\partial z^2}\right) + \frac{\partial}{\partial z}\left(\frac{\partial^2 V_z}{\partial y^2} + \frac{\partial^2 V_z}{\partial z^2}\right) \\ &= \frac{\partial^2}{\partial y^2}\left(\frac{\partial V_y}{\partial y} + \frac{\partial V_z}{\partial z}\right) + \frac{\partial^2}{\partial z^2}\left(\frac{\partial V_y}{\partial y} + \frac{\partial V_z}{\partial z}\right) = 0 \end{aligned} \tag{2.40}$$

Thus, equation (2.36) reduces to

$$\frac{\partial^2 p}{\partial x^2} + \frac{\partial^2 p}{\partial y^2} = -\rho\left[\left(\frac{\partial V_y}{\partial y}\right)^2 + \left(\frac{\partial V_z}{\partial z}\right)^2 + 2 \cdot \frac{\partial V_z}{\partial y} \cdot \frac{\partial V_y}{\partial z}\right] \tag{2.41}$$

This equation is called pressure poisson equation.

2.3.4.4 Discretization of the Navier-Stokes equations and the pressure poisson equation

Now, we have the system equation including the Navier-Stokes equations and the pressure poisson equation as

$$\frac{\partial V_y}{\partial t} + V_y \cdot \frac{\partial V_y}{\partial y} + V_z \cdot \frac{\partial V_y}{\partial z} = -\frac{1}{\rho}\frac{\partial p}{\partial y} + v \cdot \left(\frac{\partial^2 V_y}{\partial y^2} + \frac{\partial^2 V_y}{\partial z^2}\right) \tag{2.42}$$

$$\frac{\partial V_z}{\partial t} + V_y \cdot \frac{\partial V_z}{\partial y} + V_z \cdot \frac{\partial V_z}{\partial z} = -\frac{1}{\rho}\frac{\partial p}{\partial z} + v \cdot \left(\frac{\partial^2 V_z}{\partial y^2} + \frac{\partial^2 V_z}{\partial z^2}\right) \tag{2.43}$$

$$\frac{\partial^2 p}{\partial y^2} + \frac{\partial^2 p}{\partial z^2} = -\rho \left[\left(\frac{\partial V_y}{\partial y}\right)^2 + \left(\frac{\partial V_z}{\partial z}\right)^2 + 2 \cdot \frac{\partial V_z}{\partial y} \cdot \frac{\partial V_y}{\partial z}\right] \tag{2.44}$$

The discretized equations can be written as

$$\begin{aligned}
&\frac{V^{n+1}_{y(i,j)} - V^n_{y(i,j)}}{\Delta t} + V^n_{y(i,j)} \frac{V^n_{y(i,j)} - V^n_{y(i-1,j)}}{\Delta y} + V^n_{z(i,j)} \frac{V^n_{y(i,j)} - V^n_{y(i,j-1)}}{\Delta z} \\
&= -\frac{1}{\rho}\frac{p^n_{i+1,j} - p^n_{i-1,j}}{2\Delta y} + v\left(\frac{V^n_{y(i+1,j)} - 2V^n_{y(i,j)} + V^n_{y(i-1,j)}}{\Delta y^2} + \frac{V^n_{y(i,j+1)} - 2V^n_{y(i,j)} + V^n_{y(i,j-1)}}{\Delta z^2}\right)
\end{aligned} \tag{2.45}$$

$$\begin{aligned}
&\frac{V^{n+1}_{z(i,j)} - V^n_{z(i,j)}}{\Delta t} + V^n_{y(i,j)} \frac{V^n_{z(i,j)} - V^n_{z(i-1,j)}}{\Delta y} + V^n_{z(i,j)} \frac{V^n_{z(i,j)} - V^n_{z(i,j-1)}}{\Delta z} \\
&= -\frac{1}{\rho}\frac{p^n_{i+1,j} - p^n_{i-1,j}}{2\Delta y} + v\left(\frac{V^n_{z(i+1,j)} - 2V^n_{z(i,j)} + V^n_{z(i-1,j)}}{\Delta y^2} + \frac{V^n_{z(i,j+1)} - 2V^n_{z(i,j)} + V^n_{z(i,j-1)}}{\Delta z^2}\right)
\end{aligned} \tag{2.46}$$

$$\begin{aligned}
&\frac{p^n_{i+1,j} - 2p^n_{i,j} + p^n_{i-1,j}}{\Delta y^2} + \frac{p^n_{i,j+1} - 2p^n_{i,j} + p^n_{i,j-1}}{\Delta z^2} \\
&= \rho\left[\frac{1}{\Delta t}\left(\frac{V_{y(i+1,j)} - V_{y(i-1,j)}}{2\Delta y} + \frac{V_{z(i,j+1)} - V_{z(i,j-1)}}{2\Delta z}\right) - \frac{V_{y(i+1,j)} - V_{y(i-1,j)}}{2\Delta y}\frac{V_{y(i+1,j)} - V_{y(i-1,j)}}{2\Delta y}\right. \\
&\left. - 2\frac{V_{y(i,j+1)} - V_{y(i,j-1)}}{2\Delta z}\frac{V_{z(i+1,j)} - V_{z(i-1,j)}}{2\Delta y} - \frac{V_{z(i,j+1)} - V_{z(i,j-1)}}{2\Delta z}\frac{V_{z(i,j+1)} - V_{z(i,j-1)}}{2\Delta z}\right]
\end{aligned} \tag{2.47}$$

where n denotes the current time point and $n+1$ the next time point, and spacial notations are shown in Figure 2.5.

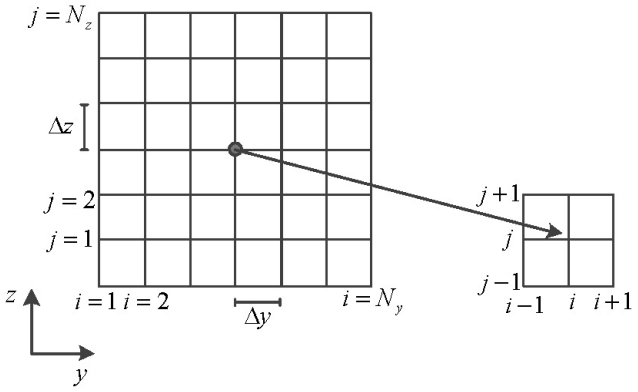

Figure 2.5: Notations for fluid domain

We reorganise equations (2.45), (2.46) and (2.47), the following discretized form can be derived

$$\begin{aligned} V_{y(i,j)}^{n+1} =& V_{y(i,j)}^{n} - V_{y(i,j)}^{n}\frac{\Delta t}{\Delta y}\left(V_{y(i,j)}^{n} - V_{y(i-1,j)}^{n}\right) - V_{z(i,j)}^{n}\frac{\Delta t}{\Delta z}\left(V_{y(i,j)}^{n} - V_{y(i,j-1)}^{n}\right) \\ & - \frac{\Delta t}{\rho 2\Delta y}\left(p_{i+1,j}^{n} - p_{i-1,j}^{n}\right) + v\left(\frac{\Delta t}{\Delta y^2}\left(V_{y(i+1,j)}^{n} - 2V_{y(i,j)}^{n} + V_{y(i-1,j)}^{n}\right)\right. \\ & \left. + \frac{\Delta t}{\Delta z^2}\left(V_{y(i,j+1)}^{n} - 2V_{y(i,j)}^{n} + V_{y(i,j-1)}^{n}\right)\right) \end{aligned} \tag{2.48}$$

$$\begin{aligned} V_{z(i,j)}^{n+1} =& V_{z(i,j)}^{n} - V_{z(i,j)}^{n}\frac{\Delta t}{\Delta y}\left(V_{z(i,j)}^{n} - V_{z(i-1,j)}^{n}\right) - V_{y(i,j)}^{n}\frac{\Delta t}{\Delta z}\left(V_{z(i,j)}^{n} - V_{z(i,j-1)}^{n}\right) \\ & - \frac{\Delta t}{\rho 2\Delta y}\left(p_{i+1,j}^{n} - p_{i-1,j}^{n}\right) + v\left(\frac{\Delta t}{\Delta y^2}\left(V_{z(i,j)}^{n} - 2V_{z(i,j)}^{n} + V_{z(i-1,j)}^{n}\right)\right. \\ & \left. + \frac{\Delta t}{\Delta z^2}\left(V_{z(i,j+1)}^{n} - 2V_{z(i,j)}^{n} + V_{z(i,j-1)}^{n}\right)\right) \end{aligned} \tag{2.49}$$

$$\begin{aligned} p_{i,j}^{n} =& \frac{\left(p_{i+1,j}^{n} + p_{i-1,j}^{n}\right)\Delta z^2 + \left(p_{i,j+1}^{n} + p_{i,j-1}^{n}\right)\Delta y^2}{2\left(\Delta y^2 + \Delta z^2\right)} \\ & - \frac{\rho\Delta y^2\Delta z^2}{2\left(\Delta y^2 + \Delta z^2\right)} \times \left[\frac{1}{\Delta t}\left(\frac{V_{y(i+1,j)} - V_{y(i-1,j)}}{2\Delta y} + \frac{V_{z(i,j+1)} - V_{z(i,j-1)}}{2\Delta z}\right)\right. \\ & - \frac{V_{y(i+1,j)} - V_{y(i-1,j)}}{2\Delta y}\frac{V_{y(i+1,j)} - V_{y(i-1,j)}}{2\Delta y} \\ & \left. - 2\frac{V_{y(i,j+1)} - V_{y(i,j-1)}}{2\Delta z}\frac{V_{z(i+1,j)} - V_{z(i-1,j)}}{2\Delta y} - \frac{V_{z(i,j+1)} - V_{z(i,j-1)}}{2\Delta z}\frac{V_{z(i,j+1)} - V_{z(i,j-1)}}{2\Delta z}\right] \end{aligned} \tag{2.50}$$

2.3.4.5 Boundary conditions

- At the left and right boundary:

$$V_y = 0; \quad V_z = 0 \tag{2.51}$$

- At the bottom boundary:

$$V_z = 0; \quad V_y = 0 \tag{2.52}$$

- At the top boundary:

$$V_z = 0 \tag{2.53}$$

Now, we can obtain the fluid force (2.50) everywhere in the fluid domain by using the Navier-Stokes equations (2.48)-(2.49) and the boundary conditions (2.51)-(2.53). Figure 2.6 and Figure 2.7 show the pressure distribution at the 1st second and the 2nd second respectively. We can see that the pressure and their directions change everywhere in the fluid domain at the two different time points.

It should be noted the fluid force (2.50) has no analytical solution. To obtain the solution, approximated numerical solution can be found by iteration. Therefore, this fluid force can be used for theoretical analysis without considering the computation time. For the real time estimation and control, we will make further simplifications to fulfill the requirements of fast response and practical implementations in the following section.

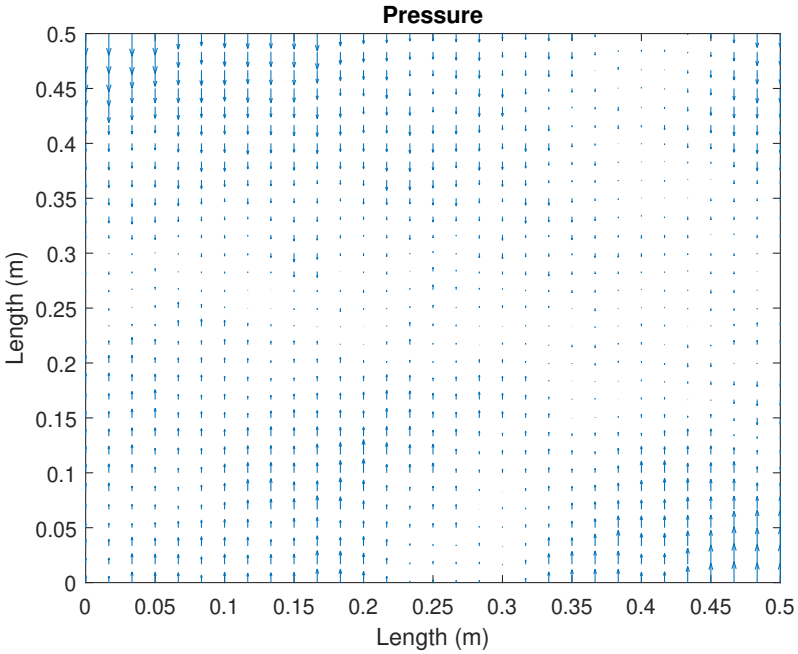

Figure 2.6: Pressure in the fluid domain at the 1st second

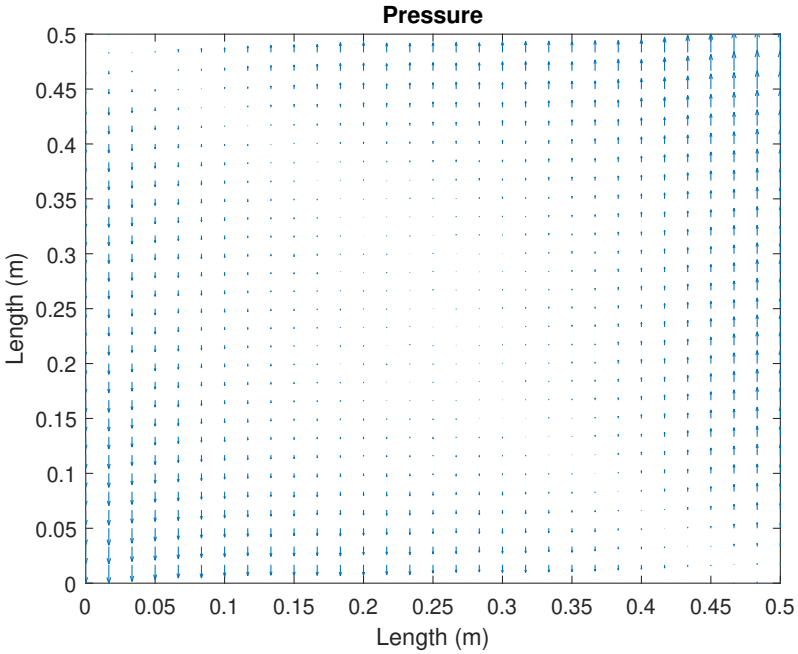

Figure 2.7: Pressure in the fluid domain at the 2nd second

2.3.5 Simplified fluid force

In the beam-structure interaction problem, dealing with the Navier–Stokes equation is hard for online parameter estimation and real-time control due to the limitation of the hardware. Certain assumptions and simplifications are desired to be made. In this thesis, we assume the fluid works under stokes flow [63, 64]. This assumption is suitable for the situation of the submerged beam. The stokes flow is useful for a low Reynolds number flow. The Reynolds number is a ratio measuring the relative importance of inertia forces (or fictitious forces) and viscous forces defined by [65]

$$\mathrm{Re} = \frac{DU_d\rho_d}{v}, \tag{2.54}$$

where D is the diameter of the domain occupied by the fluid, U_d is the flow speed, ρ_d is the fluid density and v is the viscosity.

Then the Navier–Stokes equation can be simplified and the fluid dynamics can be described by the Reynolds equation as [66]

$$12v\frac{\partial(Pw_h)}{\partial t} = \nabla\cdot\left[(1+6K_n)\,h^3P\nabla P\right], \tag{2.55}$$

where v is the viscosity of fluid, P is the pressure, w_h is the distance between the beam and the wall and K_n is the Knudsen number (the ratio describes the relationship of the mean free path of the fluid molecule and the distance of the gap).

Further, we assume the Knudsen number is negligibly small, the Reynolds equation (2.55) reduces to

$$\frac{\partial(Pw_h)}{\partial t} = \frac{h^3}{12v}\left(\frac{1}{2}\nabla^2P^2\right). \tag{2.56}$$

Under the above assumptions and simplifications, we will introduce the main components of the fluid force for the beam-fluid interaction in the following subsections.

2.3.5.1 Added inertia force

Since the vibration of the beam would influence the surrounding fluid, the created force due to the acceleration of the fluid has effect on the beam [67, 68]. The resulted added inertia force can be written as

$$F_a = m_a\frac{\partial^2 w}{\partial t^2}, \tag{2.57}$$

where m_a is the added mass per unit length of the beam. For a rectangular beam, the value of m_a can be given as [68]

$$m_a = C_a\rho_d A, \tag{2.58}$$

where C_a is the correction factor determined by the gap between the beam and the rigid wall. ρ_d is the density of the fluid and A is the cross sectional area.

The added inertia force is of critical importance in fluid-structure interactions [69]. In [70], an empirical added mass formulation is derived for the submerged cantilever plates. The frequencies and mode shapes are determined by using Rayleigh–Ritz method. In [71], the added mass effect has been discussed and simulated on a francis turbine runner, the vibration problems in hydraulic turbine systems are summarized. However, few investigations have addressed the online system parameter estimation and vibration control for the piezoelectric cantilever beam considering the added inertia force. Therefore, in this work, we will take into consideration of the added inertia force on modelling of the fluid-beam

interaction. Moreover, online parameter estimation and vibration control for the submerged beam will be studied.

2.3.5.2 Squeeze flow force

For the beam-fluid interaction problem in the water turbine system, the squeeze flow force is one of the dominated forces. The squeeze force is generated from the movement of the beam towards the wall. The fluid squeeze out when the beam approach to the wall and the pressure increases. When the beam moves away from the wall, a suddenly drag is applied on the beam because the fluid fills back to the gap [72].

To approximate the squeeze flow force, we linearize (2.56) about an assumed operating point. We let w_0 being the average gap distance and P_0 being the static pressure, then we have the gap distance as

$$w_h = w_0 + w \tag{2.59}$$

where w is the the oscillation amplitude of the beam, and the pressure as

$$P = P_0 + \bar{P} \tag{2.60}$$

where $\bar{P}$ is the pressure variation of P_0.

We assume the fluid motion is in the vertical direction to the beam, the linearized Reynolds equation can be derived as

$$\frac{\partial P^*}{\partial t} = \frac{w_0^2 P_0}{12vb^2}\frac{\partial^2 P^*}{\partial \xi^2} - \frac{1}{w_0}\frac{\partial w_h}{\partial t} \tag{2.61}$$

where $P^* = \bar{P}/P_0$ and $\xi = w_h/b$.

One can obtain the solution of (2.61) by using the eigenfunction method as [66]

$$P^* = -\frac{z_0}{w_0}\sum_{n \text{ odd}} \frac{4}{n\pi}[\sin n\pi\xi]e^{-\alpha_n t} \tag{2.62}$$

where z_0 is an imaginary step input and

$$\alpha_n = \frac{w_0^2 P_0 n^2 \pi^2}{12vb^2}. \tag{2.63}$$

The squeeze flow force F_s acting on the beam is

$$F_s(t) = P_0 bL \int_0^1 P^*(t,\xi)d\xi \tag{2.64}$$

and the Laplace transformation is [66]

$$F_s(s) = \left[\frac{96vLb^3}{\pi^4 w_0^3}\sum_{n \text{ odd}} \frac{1}{n^4}\frac{1}{1+\frac{s}{\alpha_n}}\right] sz(s) \tag{2.65}$$

where $z(s)$ is the Laplace transform of the displacement of the beam $w(t)$.

It can be observed from (2.65) the magnitude of the coefficients is dominated by the first term with $n = 1$. The other terms with $n \geq 2$ are negligible compared with the first term. Therefore, we can use the first term to approximate the force as

$$F_s(s) = \frac{96vLb^3}{\pi^4 w_0^3}\frac{1}{1+\frac{s}{\alpha_n}} sz(s). \tag{2.66}$$

Consequently, the squeeze flow force can be simplified as

$$F_s(t) = b_s\frac{\partial w}{\partial t}. \tag{2.67}$$

It can be seen the squeeze flow force is finally reduced to a damping force. The direction of the force is opposite to the vibration of the beam.

2.3.5.3 Total fluid force

The total fluid force F_z can be finally derived by combining the main force components affect on the beam as

$$F_z = F_a + F_s = m_a \frac{\partial^2 w}{\partial t^2} + b_s \frac{\partial w}{\partial t} \tag{2.68}$$

where F_a is the added inertia force due to the added fluid mass on the submerged beam, F_s is the squeeze flow force resulted from the interaction of the beam and fluid.

2.3.6 Model of the submerged beam

Considering the fluid force (2.68) along with the dry beam (2.22), the model of the submerged beam can be written as

$$(\rho A + m_a)\frac{\partial^2 w}{\partial t^2} + EI\frac{\partial^4 w}{\partial x^4} + CI\frac{\partial^5 w}{\partial t \partial x^4} + \frac{\partial^2 M_a}{\partial x^2} + b_s \frac{\partial w}{\partial t} = 0. \tag{2.69}$$

The derived PDE model (2.69) describes the dynamics of the submerged beam by considering the Kelvin-Voigt damping, the piezoelectric effect and the fluid force. The model can better describe the characteristics of a real beam compared to the beam model in [22] due to the effect of the damping in practice. Compared to the proportional (Rayleigh) damping considered in [23], the Kelvin-Voigt damping included in (2.22) has its advantage in representing the behaviour of stress and strain state [73]. In addition, the proposed model included the lumped fluid force which can describe the dynamics of the beam-fluid interaction.

2.4 Beam model discretization

To manipulate the PDE model (2.69), one effective way is to discretize the PDE to obtain the numerical solution because the analytical solution is difficult to be found at the moment [74]. In this section, we will focus on the beam model discretization by using finite difference method. We will mainly discrete space domain to develop a semi-discrete model. After further discrete the time domain, a fully discrete model can also be obtained.

2.4.1 Finite difference method

For partial differential equations, finite difference method (FDM) is an effective way to obtain the numerical solution [75]. This method is versatile and simple to implement on a computer. The basic idea is to determine the variables according to the neighbouring or surrounding points as shown in Figure 2.8.

1. The finite difference equation of first derivative is [74]
$$\left.\frac{\partial w}{\partial x}\right|_k = \frac{w_{k+1} - w_k}{\Delta x} \tag{2.70}$$
where k and $k+1$ represent the current node and the next node as shown in Figure 2.8.

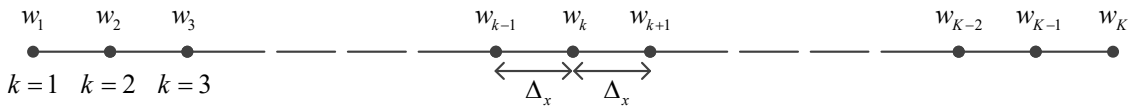

Figure 2.8: Notations for the finite difference scheme

2. The finite difference equation of second derivative is
$$\left.\frac{\partial^2 w}{\partial x^2}\right|_k = \frac{w_{k+1} - 2w_k + w_{k-1}}{(\Delta x)^2}. \tag{2.71}$$

3. The finite difference equation of third derivative is
$$\left.\frac{\partial^3 w}{\partial x^3}\right|_k = \frac{w_{k+2} - 2w_{k+1} + 2w_{k-1} - w_{k-2}}{(\Delta x)^3}. \tag{2.72}$$

4. The finite difference equation of fourth derivative is
$$\left.\frac{\partial^4 w}{\partial x^4}\right|_k = \frac{w_{k+2} - 4w_{k+1} + 6w_k - 4w_{k-1} + w_{k-2}}{(\Delta x)^4}. \tag{2.73}$$

The above-mentioned equations (2.70)-(2.73) are called centered difference approximation. There are also forward difference approximations and backward difference approximations as following

1. Forward difference approximations of the first and second derivatives:
$$\left.\frac{\partial w}{\partial x}\right|_k = \frac{-3w_k + 4w_{k+1} - w_{k+2}}{2\Delta x}. \tag{2.74}$$
$$\left.\frac{\partial^2 w}{\partial x^2}\right|_k = \frac{2w_k - 5w_{k+1} + 4w_{k+2} - w_{k+3}}{(\Delta x)^2}. \tag{2.75}$$

2. Backward difference approximations of the first and second derivatives:
$$\left.\frac{\partial w}{\partial x}\right|_k = \frac{3w_k - 4w_{k-1} + w_{k-2}}{2\Delta x}. \tag{2.76}$$

$$\left.\frac{\partial^2 w}{\partial x^2}\right|_k = \frac{2w_k - 5w_{k-1} + 4w_{k-2} - w_{k-3}}{(\Delta x)^2}. \tag{2.77}$$

The finite difference method is a simple approach to approximate the derivatives. Moreover, it can treat different initial conditions and boundary conditions. As a result, we use the finite difference method to derive the following semi-discrete model and the discrete model for analysis.

2.4.2 Semi-discrete beam model

We recall the beam model without external excitation

$$(\rho A + m_a)\frac{\partial^2 w}{\partial t^2} + EI\frac{\partial^4 w}{\partial x^4} + CI\frac{\partial^5 w}{\partial t \partial x^4} + \frac{\partial^2 M_a}{\partial x^2} + b_s\frac{\partial w}{\partial t} = 0. \tag{2.78}$$

Ideally, the PDE model (2.78) has infinite spacial nodes. However, in practice, we can only address finite spatial nodes. Therefore, we can discretize spacial domain to reserve finite number of nodes. For the time domain, we will not make the discretization in this section.

Using finite difference method, we obtain a semi-discrete approximation model by spacial discretization. The continuous model (2.78) can be reconstructed along with (2.73) as

$$\begin{aligned}\frac{d^2 w_k}{dt^2} =& r_k(w_{k-2} - 4w_{k-1} + 6w_k - 4w_{k+1} + w_{k+2}) + r_c\frac{d(w_{k-2} - 4w_{k-1} + 6w_k - 4w_{k+1} + w_{k+2})}{dt} \\ &+ r_u(M_{k+1} - 2M_k + M_{k-1}),\end{aligned} \tag{2.79}$$

where $r_k = -EI/((\rho A + m_a)(\Delta x)^4)$, $r_c = -CI/((\rho A + m_a)(\Delta x)^4) - b_s/(\rho A + m_a)$ and $r_u = -1/((\rho A + m_a)(\Delta x)^2)$.

For the finite difference scheme, we let $f_k = w_{k-2} - 4w_{k-1} + 6w_k - 4w_{k+1} + w_{k+2}, 1 \le k \le K$. Then we have

$$f_k = \begin{cases} w_{-1} - 4w_0 + 6w_1 - 4w_2 + w_3 & k = 1 \\ w_0 - 4w_1 + 6w_2 - 4w_3 + w_4 & k = 2 \\ w_{k-2} - 4w_{k-1} + 6w_k - 4w_{k+1} + w_{k+2} & 3 \le k \le K-2 \\ w_{k-3} - 4w_{k-2} + 6w_{k-1} - 4w_k + w_{k+1} & k = K-1 \\ w_{k-2} - 4w_{k-1} + 6w_k - 4w_{k+1} + w_{k+2} & k = K \end{cases}. \tag{2.80}$$

Note that in (2.80) there are four virtual points w_0, w_{-1}, w_{K+1} and w_{K+2} are used. It is necessary to represent these points with real points of the beam. This can be achieved by using the boundary conditions (2.17) and the finite difference equations (2.70)-(2.72)

$$\begin{aligned} &w_0 = 0; \\ &w_{-1} = w_1; \\ &w_{K+1} = 2w_K - w_{K-1}; \\ &w_{K+2} = 2w_{K+1} - 2w_{K-1} + w_{K-2} = 4w_K - 4w_{K-1} + w_{K-2}. \end{aligned} \tag{2.81}$$

Substituting (2.81) into (2.80), we obtain

$$f_k = \begin{cases} 7w_1 - 4w_2 + w_3 & k = 1 \\ -4w_1 + 6w_2 - 4w_3 + w_4 & k = 2 \\ w_{k-2} - 4w_{k-1} + 6w_k - 4w_{k+1} + w_{k+2} & 3 \le k \le K-2 \\ w_{k-3} - 4w_{k-2} + 5w_{k-1} - 2w_k & k = K-1 \\ 2w_{k-2} - 4w_{k-1} + 2w_k & k = K \end{cases}. \tag{2.82}$$

Then, the matrix form of f_k can be written as

$$f_k = \begin{bmatrix} 7 & -4 & 1 & 0 & \cdots & \cdots & \cdots & 0 \\ -4 & 6 & -4 & 1 & \ddots & \ddots & \ddots & \vdots \\ 1 & -4 & 6 & -4 & 1 & \ddots & \ddots & \vdots \\ 0 & 1 & -4 & 6 & -4 & 1 & \ddots & \vdots \\ \vdots & \ddots & \ddots & \ddots & \ddots & \ddots & \ddots & 0 \\ \vdots & \ddots & \ddots & 1 & -4 & 6 & -4 & 1 \\ \vdots & \ddots & \ddots & \ddots & 1 & -4 & 5 & -2 \\ 0 & \cdots & \cdots & \cdots & 0 & 2 & -4 & 2 \end{bmatrix} \begin{bmatrix} w_1 \\ w_2 \\ w_k \\ \vdots \\ \vdots \\ \vdots \\ w_k \\ w_{K-1} \\ w_K \end{bmatrix} = \mathbf{A_f} \begin{bmatrix} w_1 \cdots w_K \end{bmatrix}^T. \tag{2.83}$$

We choose the system state vector as $\mathbf{x} = [\mathbf{x_1}, \mathbf{x_2}]^\top$, then the state-space model of the beam system can be given as

$$\begin{aligned} \begin{bmatrix} \dot{\mathbf{x}}_\mathbf{1} \\ \dot{\mathbf{x}}_\mathbf{2} \end{bmatrix} &= \begin{bmatrix} \mathbf{0} & \mathbf{I} \\ r_k\mathbf{A_f} & r_c\mathbf{A_f} \end{bmatrix} \begin{bmatrix} \mathbf{x_1} \\ \mathbf{x_2} \end{bmatrix} + \begin{bmatrix} \mathbf{0} \\ \mathbf{B_u} \end{bmatrix} u \\ y &= \begin{bmatrix} \mathbf{I} & \mathbf{0} \end{bmatrix} \begin{bmatrix} \mathbf{x_1} \\ \mathbf{x_2} \end{bmatrix} \end{aligned} \tag{2.84}$$

with $\mathbf{x_1} = [w_1 \cdots w_K]^T$, $\mathbf{x_2} = [\dot{w}_1 \cdots \dot{w}_K]^T$, $u = U^a(t)$ and $\mathbf{B_u} = -3r_u[M_{a1} \cdots M_{aK}]$. Note that $\mathbf{B_u}$ depends on the location of the piezoelectric actuator.

The state space model (2.84) can be then written as

$$\begin{aligned} \dot{\mathbf{x}} &= A\mathbf{x} + B\mathbf{u} \\ y &= C\mathbf{x}, \end{aligned} \tag{2.85}$$

where

$$A = \begin{bmatrix} \mathbf{0} & \mathbf{I} \\ r_k\mathbf{A_f} & r_c\mathbf{A_f} \end{bmatrix}, B = \begin{bmatrix} \mathbf{0} \\ \mathbf{B_u} \end{bmatrix}, C = \begin{bmatrix} \mathbf{I} & \mathbf{0} \end{bmatrix}.$$

We set the number of nodes of the beam model (2.85) as $K = 8$. The parameters r_k, r_c and r_u can be theoretically computed by using the material properties in Table 1.1 and Table 1.2. At the free end of the beam, we can obtain the following transfer function of (2.85)

$$\begin{aligned} G(s) = \frac{\begin{array}{l} -113.2s^{11} - 6.555e07s^{10} - 1.265e13s^9 - 8.14e17s^8 - 1.123e19s^7 - 5.41e23s^6 \\ +1.336e26s^5 + 5.159e30s^4 + 2.212e31s^3 + 7.117e35s^2 - 1.125e36s - 3.101e40 \end{array}}{\begin{array}{l} s^{16} + 75.96s^{15} + 1.466e07s^{14} + 8.376e08s^{13} + 8.084e13s^{12} + 3.239e15s^{11} \\ +2.084e20s^{10} + 5.27e21s^9 + 2.543e26s^8 + 3.42e27s^7 + 1.32e32s^6 + 6.923e32s^5 \\ +2.227e37s^4 + 2.329e37s^3 + 6.421e41s^2 + 2.519e40s + 6.078e44 \end{array}} \end{aligned} \tag{2.86}$$

The frequency response is shown in Figure 2.9. We can see that eight vibration modes are kept because the number of nodes is selected as $K = 8$. The beam dynamics can be better described with increasing number of nodes. However, the system order and computational load will be higher with increasing nodes. Therefore, appropriate trade-off should be made between the accuracy and flexibility.

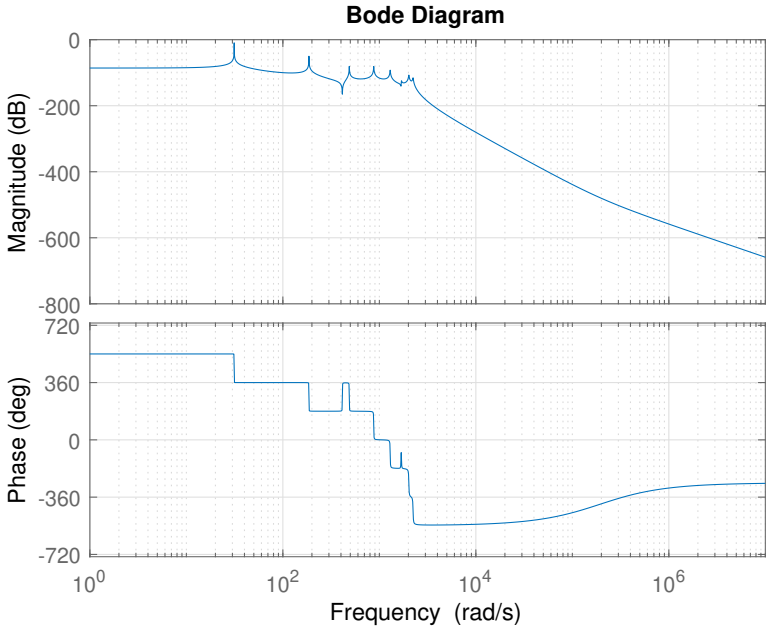

Figure 2.9: Frequency response of system (2.84)

2.4.3 Discrete beam model

We first discrete the beam equation

$$(\rho A + m_a)\frac{\partial^2 w}{\partial t^2} + EI\frac{\partial^4 w}{\partial x^4} + CI\frac{\partial^5 w}{\partial t \partial x^4} + \frac{\partial^2 M_a}{\partial x^2} + b_s\frac{\partial w}{\partial t} = 0 \tag{2.87}$$

as

$$\begin{aligned}(\rho A + m_a)&\frac{w_k^{n+1} - 2w_k^n + w_k^{n-1}}{\Delta t^2} + EI\frac{w_{k+2}^n - 4w_{k+1}^n + 6w_k^n - 4w_{k-1}^n + w_{k-2}^n}{\Delta x^4} \\ &+ CI\frac{\frac{w_{k+2}^n - 4w_{k+1}^n + 6w_k^n - 4w_{k-1}^n + w_{k-2}^n}{\Delta x^4} - \frac{w_{k+2}^{n-1} - 4w_{k+1}^{n-1} + 6w_k^{n-1} - 4w_{k-1}^{n-1} + w_{k-2}^{n-1}}{\Delta x^4}}{\Delta t} \\ &+ \frac{M_{ak+1}^n - 2M_{ak}^n + M_{ak-1}^n}{\Delta x^2} + b_s\frac{w_k^n - w_k^{n-1}}{\Delta t} = 0\end{aligned} \tag{2.88}$$

where n and k represent time and spacial node respectively.

Reorganizing (2.88), one have

$$\begin{aligned}w_k^{n+1} = -\frac{\Delta t^2}{(\rho A + m_a)}\Bigg(&EI\frac{w_{k+2}^n - 4w_{k+1}^n + 6w_k^n - 4w_{k-1}^n + w_{k-2}^n}{\Delta x^4} \\ &+ CI\frac{\frac{w_{k+2}^n - 4w_{k+1}^n + 6w_k^n - 4w_{k-1}^n + w_{k-2}^n}{\Delta x^4} - \frac{w_{k+2}^{n-1} - 4w_{k+1}^{n-1} + 6w_k^{n-1} - 4w_{k-1}^{n-1} + w_{k-2}^{n-1}}{\Delta x^4}}{\Delta t} \\ &+ \frac{M_{k+1}^n - 2M_k^n + M_{k-1}^n}{\Delta x^2} + b_s\frac{w_k^n - w_k^{n-1}}{\Delta t}\Bigg) + 2w_k^n - w_k^{n-1}.\end{aligned} \tag{2.89}$$

Theoretically, the unknown parameters estimation and the controller design can be realised based on the discrete model (2.89) or the semi-discrete model (2.85). In practice, there are still challenging issues that are not fully addressed. Although the PDE model can be implemented by using the finite difference method, a critical issue lies in these models is that estimating the unknown parameters is time consuming and sometimes impossible to complete in practice [76].

2.5 Beam model simplification

To estimate the unknown system parameters and design controllers, the PDE model (2.69) is desired to be simplified due to the complexity on designing and the time-consuming feature on realizing.

In the literature, plenty of simplification methods can be find to simplify the PDE models. For example, the Galerkin's summation method was proposed and its convergence properties were studied under different boundary conditions in [77]. In [78], a specific procedure for implementing the Galerkin's method was provided and illustrated with numerical examples. In [79], a reduced-order model was introduced by using the truncated set of linear mode shapes, where different vibration modes of the elastic beams were studied. Another approach named differential quadrature method that can simplify the PDE model in an approximate form was proposed in [49]. The effect of different varying parameters was discussed based on the simplified form. In [80], the balanced model reduction method was proposed to simplify the high-order model. However, the states information is replaced by the new states that have no physical meanings. Although the modelling of the beam and the simplification of several PDE models have been studied in the above-mentioned literatures, a model that is suitable for online estimating the parameters of the beam by using the piezoelectric actuator and strain gauge was not developed yet.

Before going into the specific methodologies, we show the idea of modelling with different methods in Figure 2.10. The semi-discrete model and the discrete model make it possible to implement the PDE model by using finite difference method. However, these two system models are described by infinite spatial nodes, which lead to high-order systems. With less nodes, the accuracy will not be guaranteed. For the balanced model order reduction method, the states of the system are completely changed. Overall, the Galerkin's model shows a best flexibility for real plant compared with other models. Therefore, we will use this method to construct the model for parameter estimation and control.

2.5.1 Model simplification with balanced model order reduction method

Since the system model (2.85) is derived by finite difference method as shown in Section 2.4.2, the model will be more accurate with an increasing number of nodes. However, the order will increase along with the node numbers. It is numerically difficult to operate with high-order systems even if no controller included. As a result, model order reduction is very important for such scenarios.

Balanced model order reduction is a method that can neglect the low effect states to represent the system model by using a lower-order model [81, 82]. In (2.85), we set the number of nodes as 500 to make a trade-off between the accuracy and the complexity. For comparison purpose, we name the beam system with 500 nodes as full-order system. The model is reduced to a fourth-order system by balanced model reduction method as

$$\begin{aligned} \dot{\mathbf{x}}_\mathbf{r} &= \mathbf{A}_\mathbf{r}\mathbf{x}_\mathbf{r} + \mathbf{B}_\mathbf{r}u \\ y &= \mathbf{C}_\mathbf{r}\mathbf{x}_\mathbf{r} + \mathbf{D}_\mathbf{r}u. \end{aligned} \tag{2.90}$$

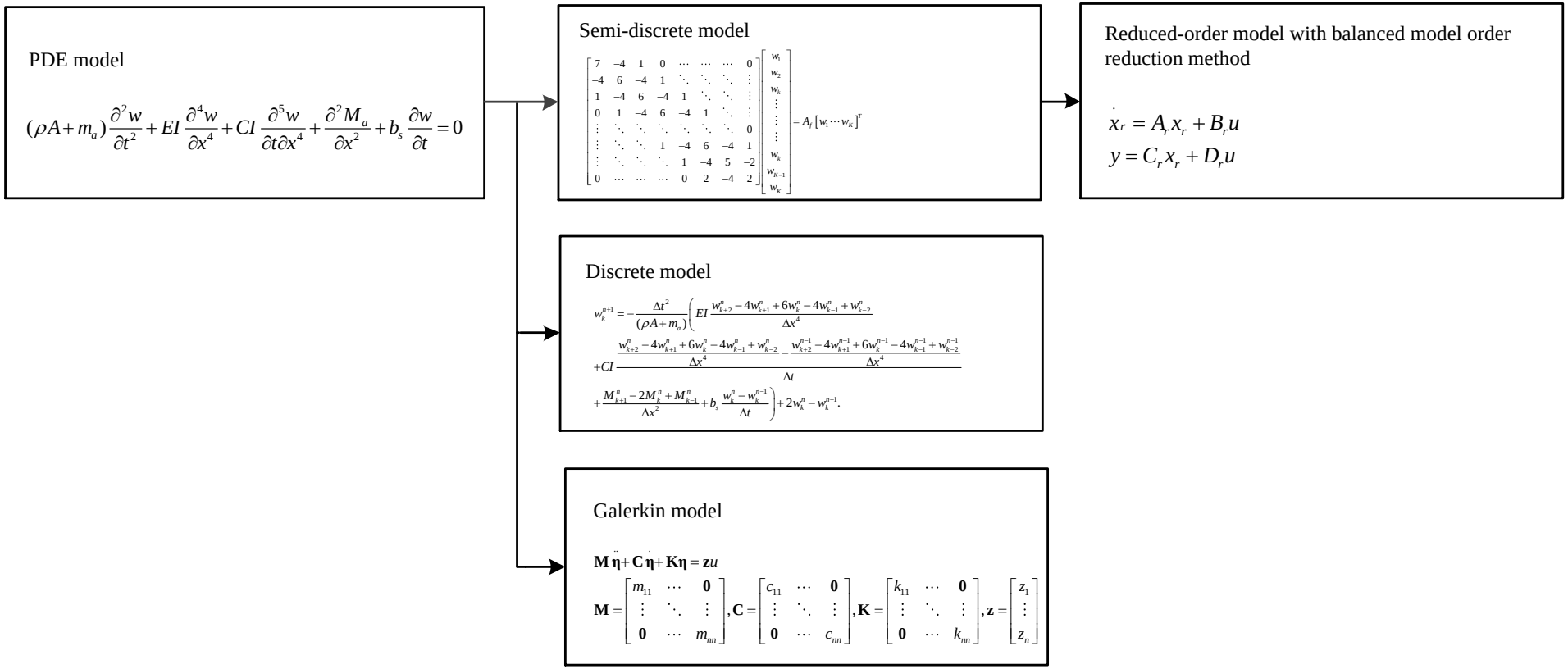

Figure 2.10: Modelling of the beam with different methods

The Bode Diagram of the high-order system and the reduced-order system is shown in Figure 2.11. We can see that the first two modes are reserved to represent the system.

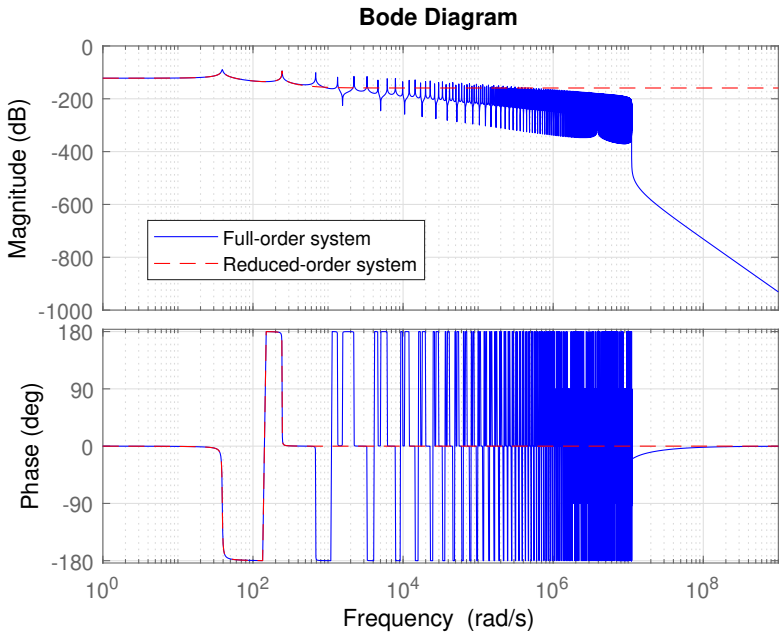

Figure 2.11: Bode diagram of the full-order system and reduced-order system

2.5.2 Model simplification with the Galerkin's method

Although the model can be reduced by the balanced model order reduction method, the reduced system (2.90) is not straightforward to represent the original system (2.85) because the information in the states are not retained. It is desired to have a simplified model that describes the characteristics of the system. Therefore, we investigated another method named Galerkin's method for a better representation. In this section, we use Galerkin method to simplify the model of the system (2.90).

The model of vertically placed beam with the effect of fluid can be written as

$$(\rho A + m_a)\frac{\partial^2 w}{\partial t^2} + EI\frac{\partial^4 w}{\partial x^4} + CI\frac{\partial w}{\partial t} + \frac{\partial^2 M_a}{\partial x^2} + b_s\frac{\partial w}{\partial t} = 0 \tag{2.91}$$

The Galerkin's method is adopted to convert the PDE to an ODE. It is shown that the Galerkin method is valid for such a transformation [83]. The displacement of the beam can be written as a summation of different oscillation modes as

$$w(x,t) = \sum_{i=1}^{n} W_i(x)\eta_i(t) \tag{2.92}$$

where $W_i(x)$ are the mode shape functions and $\eta_i(t)$ are the corresponding modal coefficients. By substituting (2.92) into (2.91) one have the residual

$$\begin{aligned} R =&(\rho A + m_a)\sum_{i=1}^{n} W_i(x)\frac{d^2\eta_i(t)}{dt^2} + EI\sum_{i=1}^{n}\frac{d^4 W_i(x)}{dx^4}\eta_i(t) + CI\sum_{i=1}^{n}\frac{d^4 W_i(x)}{dx^4}\frac{d\eta_i(t)}{dt} \\ &+ \frac{d^2 M_a}{dx^2} + b_s\sum_{i=1}^{n} W_i(x)\frac{d\eta_i(t)}{dt}. \end{aligned} \tag{2.93}$$

The Galerkin method gives

$$\int_0^L RW_j(x)dx = 0. \tag{2.94}$$

Then, we have

$$\begin{aligned}&\int_0^L (\rho A + m_a)\sum_{i=1}^{n} W_i(x)\frac{d^2\eta_i(t)}{dt^2}W_j(x)dx + \int_0^L EI\sum_{i=1}^{n}\frac{d^4W_i(x)}{dx^4}\eta_i(t)W_j(x)dx \\ &+ \int_0^L CI\sum_{i=1}^{n}\frac{d^4W_i(x)}{dx^4}\frac{d\eta_i(t)}{dt}W_j(x)dx + \int_0^L \frac{d^2M_a}{dx^2}W_j(x)dx \\ &+ \int_0^L b_s\sum_{i=1}^{n} W_i(x)\frac{d\eta_i(t)}{dt}W_j(x)dx = 0.\end{aligned} \tag{2.95}$$

Equation (2.95) becomes

$$\begin{aligned}&\sum_{i=1}^{n}\left\{m_{ij}\frac{d^2\eta_i(t)}{dt^2} + c_{ij}\frac{d\eta_i(t)}{dt} + k_{ij}\eta_i(t) + z_i u(t)\right\} = 0, \\ &j = 1, 2, \ldots, n\end{aligned} \tag{2.96}$$

where

$$m_{ij} = \int_0^L (\rho A + m_a)W_i(x)W_j(x)dx \tag{2.97}$$

$$c_{ij} = \int_0^L CI\frac{d^4W_i(x)}{dx^4}W_j(x)dx + \int_0^L b_s\sum_{i=1}^{n} W_i(x)W_j(x)dx. \tag{2.98}$$

$$k_{ij} = \int_0^L EI\frac{d^4W_i(x)}{dx^4}W_j(x)dx. \tag{2.99}$$

$$\begin{aligned}z_i &= r_a d_{31} E_p\left[\frac{d}{dx}W_i(x_1) - \frac{d}{dx}W_i(x_2)\right] \\ &= r_a d_{31} E_p\int_0^L W_j(x)\frac{d^2}{dx^2}\left[H(x - x_1) - H(x - x_2)\right]dx.\end{aligned} \tag{2.100}$$

$$u(t) = U_a(t) \tag{2.101}$$

Using the orthogonality principle of the modes shapes [56], one have

$$\int_0^L W_i(x)W_j(x)dx = 0, \quad i \neq j. \tag{2.102}$$

i.e.

$$m_{ij} = 0, \quad i \neq j. \tag{2.103}$$

$$c_{ij} = 0, \quad i \neq j. \tag{2.104}$$

$$k_{ij} = 0, \quad i \neq j. \tag{2.105}$$

We can then rewrite the motion equation (2.96) as a matrix-vector form

$$\mathbf{M}\ddot{\eta} + \mathbf{C}\dot{\eta} + \mathbf{K}\eta = \mathbf{z}u \tag{2.106}$$

where

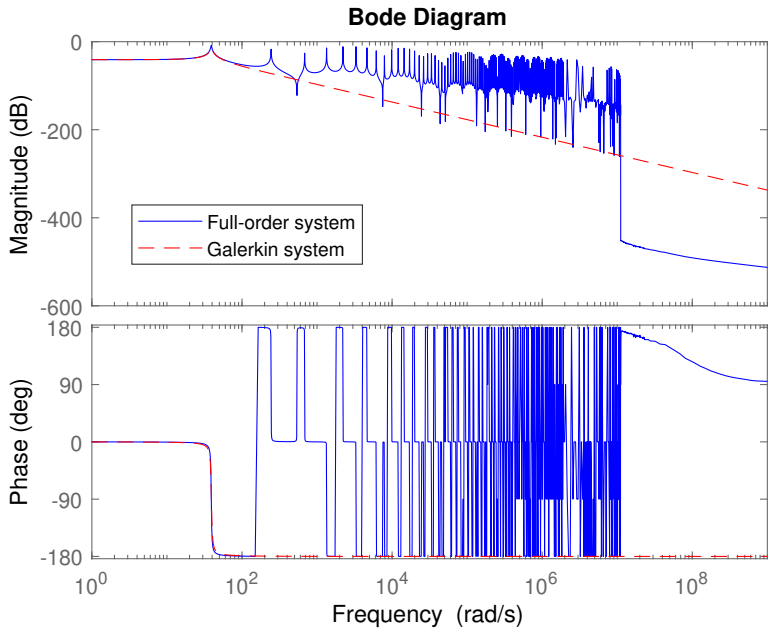

Figure 2.12: Bode plot of the full order model and first mode Galerkin model

$$\mathbf{M} = \begin{bmatrix} m_{11} & \cdots & \mathbf{0} \\ \vdots & \ddots & \vdots \\ \mathbf{0} & \cdots & m_{nn} \end{bmatrix}, \mathbf{C} = \begin{bmatrix} c_{11} & \cdots & \mathbf{0} \\ \vdots & \ddots & \vdots \\ \mathbf{0} & \cdots & c_{nn} \end{bmatrix},$$
$$\mathbf{K} = \begin{bmatrix} k_{11} & \cdots & \mathbf{0} \\ \vdots & \ddots & \vdots \\ \mathbf{0} & \cdots & k_{nn} \end{bmatrix}, \mathbf{z} = \begin{bmatrix} z_1 \\ \vdots \\ z_n \end{bmatrix}.$$

Theoretical values of m_{ij}, c_{ij}, k_{ij} of the dry beam can be computed by using (2.96) along with the mode shape function [56]

$$W_i(x) = C_i \left[(\cos \beta_i x - \cosh \beta_i x) - \frac{\cos \beta_i L + \cosh \beta_i L}{\sin \beta_i L + \sinh \beta_i L} (\sin \beta_i x - \sinh \beta_i x) \right]. \tag{2.107}$$

2.5.3 Comparison of the simplified Galerkin model and the full order model

To compare the simplified Galerkin model with the full order model, we take first three modes for illustration. For the full order model, we refer to the semi-discrete model (2.85). The number of nodes are set as $K = 500$ to achieve a trade-off between the accuracy and the computation cost. A 1000th-order model is constructed to represent the full order model. The derived values m_{ij}, c_{ij}, k_{ij} in the simplified Galerkin model (2.106) are computed based on (2.96) and (2.107). Material properties of a steel beam is given in Table 1.1.

Take m_{11} for example, we have

$$\begin{aligned} m_{11} &= \int_0^L (\rho A + m_a) W_1(x) W_1(x) dx \\ &= (\rho A + m_a) \int_0^L (\cos \beta_1 x - \cosh \beta_1 x) - \frac{\cos \beta_1 L + \cosh \beta_1 L}{\sin \beta_1 L + \sinh \beta_1 L} (\sin \beta_1 x - \sinh \beta_1 x) \\ &= 0.2224 \end{aligned} \tag{2.108}$$

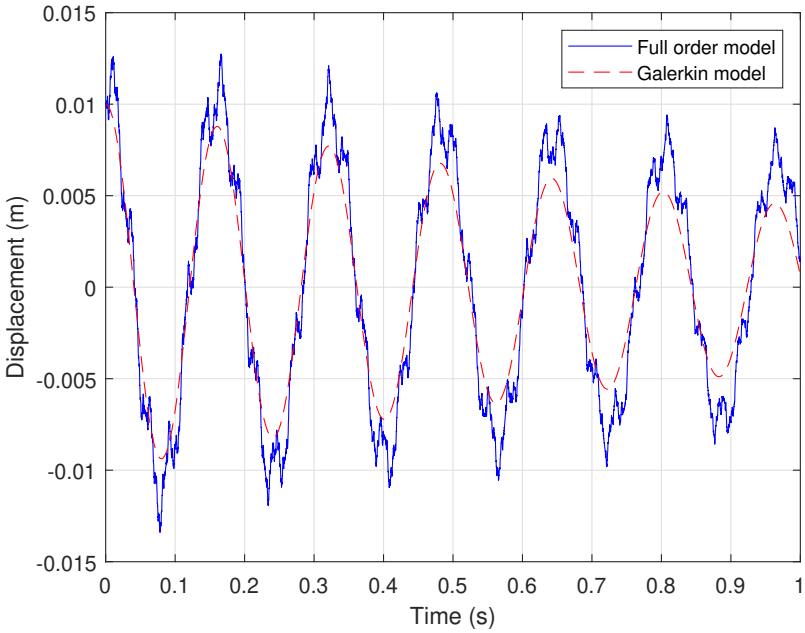

Figure 2.13: Displacement of the tip of the beam by using the full order model and first mode Galerkin model

Similarly, we can compute

$$\begin{aligned} m_{22} &= 0.2224, m_{33} = 0.2224 \\ c_{11} &= 0.36, c_{22} = 0.36, c_{33} = 0.36 \\ k_{11} &= 340.9348, k_{22} = 13390, k_{33} = 104978 \\ z_1 &= -2.1435, z_2 = -4.8029 \end{aligned} \tag{2.109}$$

We firstly consider the Galerkin model (2.106) with the first vibration mode, the beam model can be written as a second-order model as

$$\begin{aligned} \begin{bmatrix} \dot{x}_1 \\ \dot{x}_2 \end{bmatrix} &= \begin{bmatrix} 0 & 1 \\ -1532.98 & -1.62 \end{bmatrix} \begin{bmatrix} x_1 \\ x_2 \end{bmatrix} + \begin{bmatrix} 0 \\ 9.64 \end{bmatrix} u \\ y &= \begin{bmatrix} -2 & 0 \end{bmatrix} \begin{bmatrix} x_1 \\ x_2 \end{bmatrix} \end{aligned} \tag{2.110}$$

where $x_2 = \dot{x}_1$.

We release the beam at a distance of $0.01m$ (i.e., set the initial condition of (2.110) as $x(0) = [-0.005, 0]$). The initial condition is computed by

$$\begin{aligned} W_1(L)x_1(0) &= 0.01 \\ -2x_1(0) &= 0.01 \\ x_1(0) &= -0.005. \end{aligned} \tag{2.111}$$

Comparison results are shown in Figure 2.12 and Figure 2.13. From Figure 2.12 we can see the first vibration mode (the first peak in Figure 2.12) is reserved and the higher modes are truncated. Figure 2.13 shows the results of the simplification for the full order model by using the Galerkin's method.

We can then consider the first two oscillation modes using the Galerkin model. By computing the values m_{ij}, c_{ij}, k_{ij} in the simplified Galerkin model (2.106), a fourth-order model can be obtained as

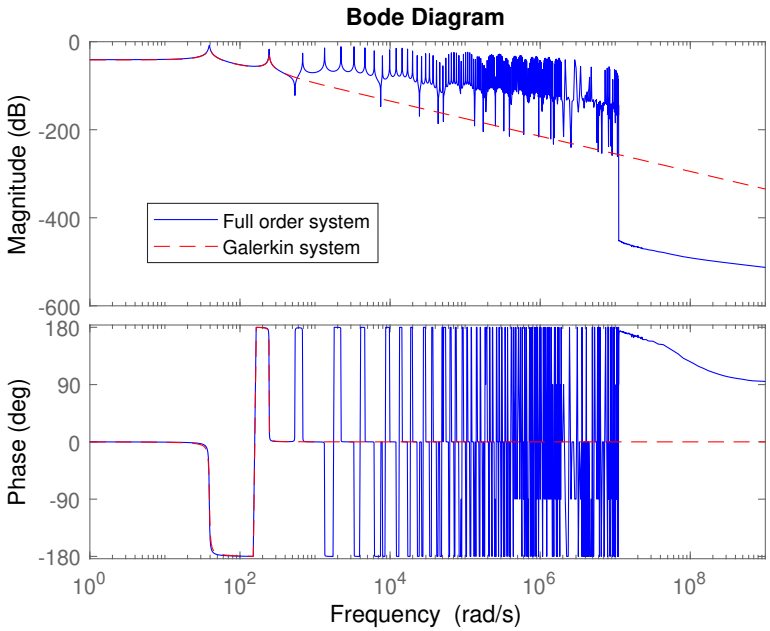

Figure 2.14: Bode plot of the full order model and first two modes Galerkin model

$$\begin{bmatrix} \dot{x}_1 \\ \dot{x}_2 \\ \dot{x}_3 \\ \dot{x}_4 \end{bmatrix} = \begin{bmatrix} 0 & 0 & 1 & 0 \\ 0 & 0 & 0 & 1 \\ -1532.98 & 0 & -1.62 & 0 \\ 0 & -60207 & 0 & -1.62 \end{bmatrix} \begin{bmatrix} x_1 \\ x_2 \\ x_3 \\ x_4 \end{bmatrix} + \begin{bmatrix} 0 \\ 0 \\ 9.64 \\ 16.1493 \end{bmatrix} u$$
$$y = \begin{bmatrix} -2 & 2 & 0 & 0 \end{bmatrix} \begin{bmatrix} x_1 \\ x_2 \\ x_3 \\ x_4 \end{bmatrix} \tag{2.112}$$

where $x_3 = \dot{x}_1$ and $x_4 = \dot{x}_2$.

We release the beam at a distance of $0.01m$ (i.e., set the initial condition of (2.112) as $x(0) = [-0.0058, -0.0008, 0, 0]$). The initial condition is computed by

$$\begin{aligned} W_1(L)x_1(0) + W_2(L)x_2(0) &= 0.01 \\ W_1(L/2)x_1(0) + W_2(L/2)x_2(0) &= 0.005 \end{aligned} \tag{2.113}$$

i.e.

$$\begin{aligned} -2x_1(0) + 2x_2(0) &= 0.01 \\ -0.6767x_1(0) - 1.4282x_2(0) &= 0.005 \end{aligned} \tag{2.114}$$

i.e.

$$\begin{aligned} x_1(0) &= -0.0058 \\ x_2(0) &= -0.0008. \end{aligned} \tag{2.115}$$

Comparison results are shown in Figure 2.14-Figure 2.15. From Figure 2.14 we can see the first vibration mode and the second vibration mode are reserved and the higher modes are truncated. Figure 2.15 shows the first two modes Galerkin model (2.112) is a better simplification of the full order model compared with the first mode Galerkin model (2.110) in Figure 2.13.

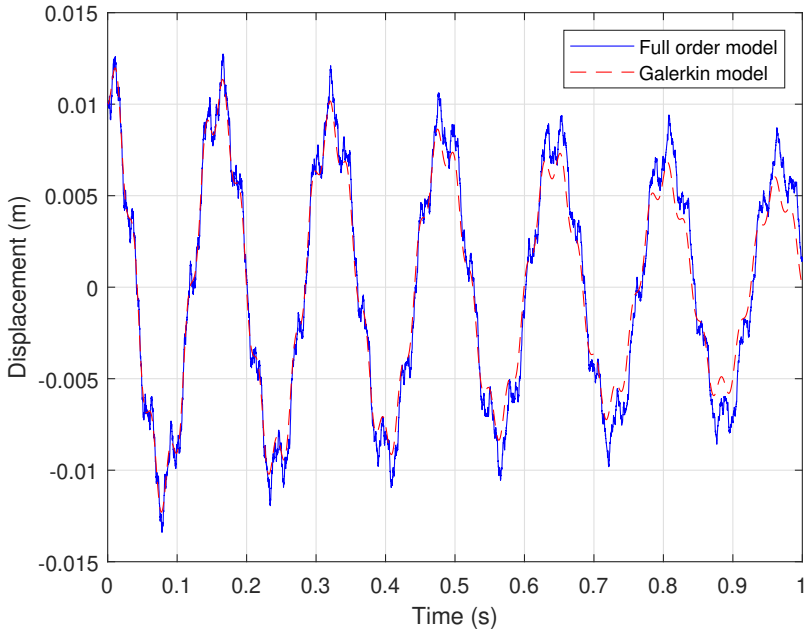

Figure 2.15: Displacement of the tip of the beam by using the full order model and first two modes Galerkin model

To further see the influence of the higher modes of the beam, we then consider the first three oscillation modes of the Galerkin model. By computing the values m_{ij}, c_{ij}, k_{ij} in the simplified Galerkin model (2.106), a sixth-order model can be obtained as

$$\begin{bmatrix} \dot{x}_1 \\ \dot{x}_2 \\ \dot{x}_3 \\ \dot{x}_4 \\ \dot{x}_5 \\ \dot{x}_6 \end{bmatrix} = \begin{bmatrix} 0 & 0 & 0 & 1 & 0 & 0 \\ 0 & 0 & 0 & 0 & 1 & 0 \\ 0 & 0 & 0 & 0 & 0 & 1 \\ -1532.98 & 0 & 0 & -1.62 & 0 & 0 \\ 0 & -60207 & 0 & 0 & -1.62 & 0 \\ 0 & 0 & -472020 & 0 & 0 & -1.62 \end{bmatrix} \begin{bmatrix} x_1 \\ x_2 \\ x_3 \\ x_4 \\ x_5 \\ x_6 \end{bmatrix} + \begin{bmatrix} 0 \\ 0 \\ 0 \\ 9.64 \\ 16.1493 \\ -16.1722 \end{bmatrix} u$$

$$y = \begin{bmatrix} -2 & 2 & -2 & 0 & 0 & 0 \end{bmatrix} \begin{bmatrix} x_1 \\ x_2 \\ x_3 \\ x_4 \\ x_5 \\ x_6 \end{bmatrix} \tag{2.116}$$

where $x_4 = \dot{x}_1, x_5 = \dot{x}_2$ and $x_6 = \dot{x}_3$.

We release the beam at a distance of $0.01m$ (i.e., set the initial condition of (2.116) as $x(0) = [-0.0057, -0.0009, -0.0002, 0, 0, 0]$). The initial condition is computed by

$$\begin{aligned} W_1(L)x_1(0) + W_2(L)x_2(0) + W_3(L)x_3(0) &= 0.01 \\ W_1(2L/3)x_1(0) + W_2(2L/3)x_2(0) + W_3(2L/3)x_3(0) &= 0.0067 \\ W_1(L/3)x_1(0) + W_2(L/3)x_2(0) + W_3(L/3)x_3(0) &= 0.0033 \end{aligned} \tag{2.117}$$

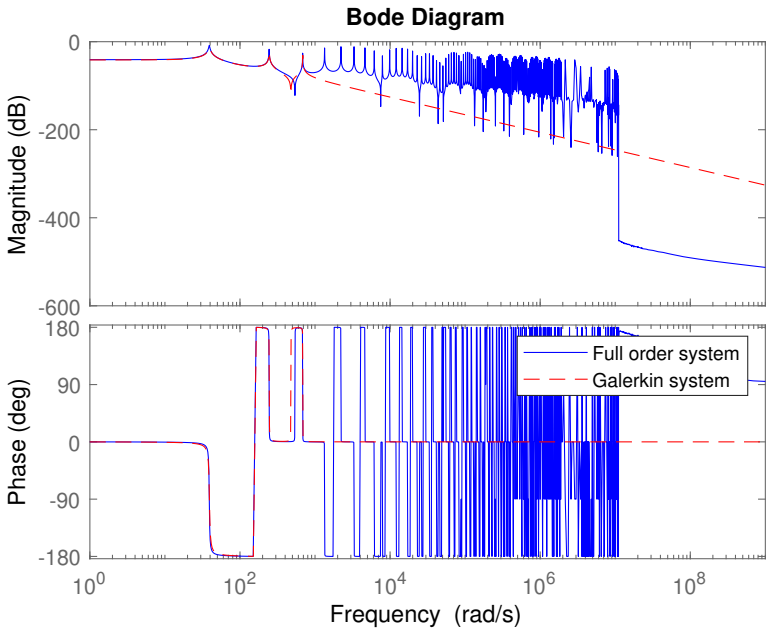

Figure 2.16: Bode plot of the full order model and first three modes Galerkin model

i.e.

$$\begin{aligned} -2x_1(0) + 2x_2(0) - 2x_3(0) &= 0.01 \\ -1.0904x_1(0) - 0.8533x_2(0) + 1.2841x_3(0) &= 0.0067 \\ -0.3299x_1(0) - 1.1769x_2(0) - 1.4460x_3(0) &= 0.0033 \end{aligned} \tag{2.118}$$

i.e.

$$\begin{aligned} x_1(0) &= -0.0057 \\ x_2(0) &= -0.0009 \\ x_3(0) &= -0.0002. \end{aligned} \tag{2.119}$$

Comparison results are shown in Figure 2.16-Figure 2.17. From Figure 2.16 we can see the first three vibration modes are reserved and the higher modes are truncated. Figure 2.17 shows the first three modes Galerkin model (2.116) is slightly different with the first two modes Galerkin model (2.112) presented in Figure 2.15.

From the above comparisons we can see the vibration of the beam is dominated by the first mode and the second mode. Although higher modes can be further considered without much difficulty, the improvement is slight. Moreover, including higher modes make the model more complex which is not desired in practice. Therefore, we mainly deal with the first mode vibration and the second mode vibration for illustration in the following chapters.

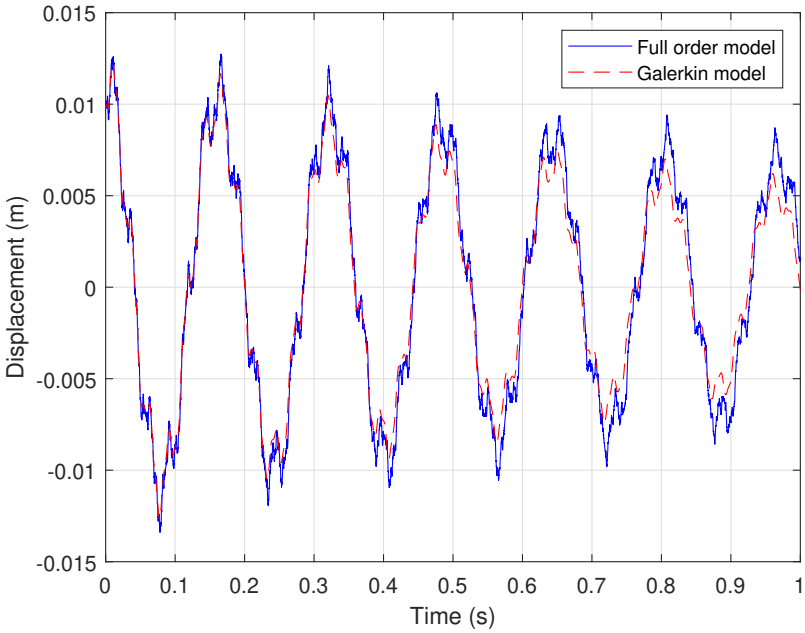

Figure 2.17: Displacement of the tip of the beam by using the full order model and first three modes Galerkin model

2.6 Conclusions

In this chapter, a PDE based model is provided including the beam motion equation and the piezoelectric actuator sub-model. The Kelvin-Voigt damping is considered in the modelling procedure and the deflection-strain relationship is presented for the purpose of experimental validation. Moreover, the fluid dynamics are described by a combination of fluid forces. The model is then described by a semi-discrete model and a discrete model. To implement and analysis the proposed model, finite difference method is adopted to discrete the beam model. In addition, the model is simplified with balanced model order reduction method and Galerkin's method respectively. Since the Galerkin's method can retain the physical information of the states compared with the balanced model order reduction method, it is more flexible for parameter estimation and control.

Part III

Parameter Estimation for the Beam System

Chapter 3

Adaptive Parameter Estimation for One Mode Beam System

3.1 Introduction

For a wide class of dynamics systems, the structure of the system model may be known. The problem is that the parameters are usually unknown or partly known. Some of the parameters can be determined by the physical laws or the characteristics of materials, many other parameters are not possible to be directly measured or computed [9, 84]. In some applications, the parameters are fixed constants which can be determined by using off-line parameter estimation methods. However, in many applications, the parameters may be changing with time due to different operating scenarios. In such cases, off-line parameter estimation methods may be not capable to determine these time varying parameters.

To estimate the parameters during the process of dynamics systems, on-line parameter estimation methods have been widely studied in the past decades. The main idea behind on-line parameter estimation methods is to minimize the output error by using optimization algorithms. The well known parameter estimation methods that can be found in the literature are gradient algorithm based methods [85] and least-squares based methods [84]. A general description of both gradient method and least-squares are presented in [84]. Because of the simple structure of the gradient method, a wide class of adaptive laws are designed based on the success of gradient method and these methods have been widely used in industry in the early 1960s. In the 1970s, it was found the gradient method is not stable in the global sense. Since then, the gradient algorithm based parameter estimation methods have been replaced by Lyapunov theory based gradient methods which are proved global stable [84]. The least-squares is another classical method used for parameter estimation with recursive form or nonrecursive form [84]. In [86], a variable forgetting factor recursive least-squares is proposed for system identification. The forgetting factor leads to a compromise between the tracking capabilities and the stability. To avoid using the prediction error, [87] proposed an estimation error based adaptive parameter estimation method. The persistent excitation condition can be online verified.

For the beam parameters, a least squares formulation is introduced considering different boundary conditions in [88]. In [89], a real-time parameter estimation strategy is presented to determine the unknown stiffness, damping and a voltage/force conversion constant. The dynamic system is defined and augmented by these parameters which is estimated in real time. In [90], uncertain parameters of a moving-mass and beam system are estimated by the subspace-based algorithm both in numerical simu-

lation and experiments.

In this chapter, the parameter estimation problem of the beam system with the first oscillation mode is addressed. The states of the system are estimated by using the Levant exact differentiator via sliding mode technique. To online estimate the parameters, the parameter estimation error is extracted by introducing an auxiliary filter. A new adaptive parameter updating law is then derived based on the estimation error. By using Lyapunov theory, the stability of the system is proved. Simulation and experimental results show the effectiveness of the proposed estimation method.

3.2 Adaptive parameter estimation for the beam system with first mode

We can write the Galerkin model (2.106) with the first oscillation mode as

$$m_{11}\ddot{\eta} + c_{11}\dot{\eta} + k_{11}\eta = z_1 u. \tag{3.1}$$

We choose the system state vector as $x = [x_1, x_2]^T = [\eta, \dot{\eta}]^T$, then the state-space formulation of the system (3.1) can be given as

$$\begin{cases} \dot{x}_1 = x_2 \\ \dot{x}_2 = -\Theta_1 x_2 - \Theta_2 x_1 + b_{11} u \\ y = x_1 \end{cases} \tag{3.2}$$

where $\Theta_1 = \frac{c_{11}}{m_{11}}, \Theta_2 = \frac{k_{11}}{m_{11}}$ are the unknown system parameters, $b_{11} = \frac{z_1}{m_{11}}$ is supposed to be a known parameter.

To estimate the unknown system parameters Θ_1 and Θ_2, we will propose a new parameter estimation method in this section. Figure 3.1 shows the structure of the proposed parameter estimation method.

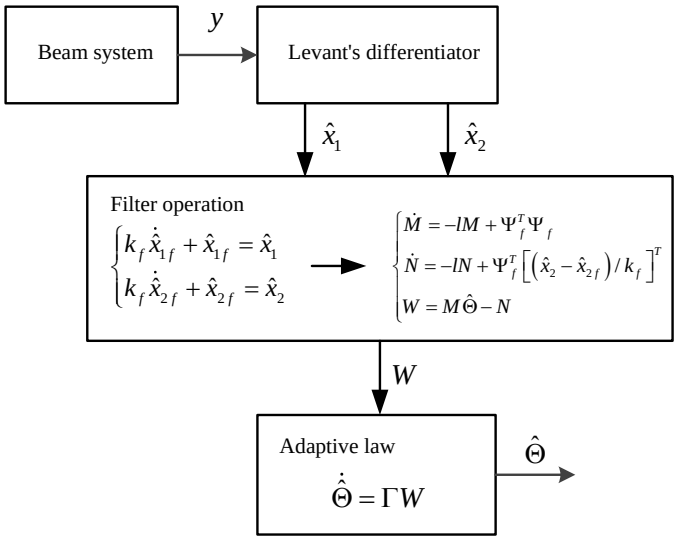

Figure 3.1: Structure of the proposed parameter estimation method

3.2.1 State Estimation

In order to estimate the coefficients of (3.1), we measure the output (displacement information) from the strain gauge. Although the system output $y = x_1$ can can be measured, the other state variable x_2 is unknown. In such a case, we use Levant exact differentiator [91] to estimate the state x_2 via sliding mode technique. The Levant's differentiator is constructed as

$$\begin{cases} \dot{\hat{x}}_1 = -\alpha_1 \left|\hat{x}_1 - x_1\right|^{1/2} \operatorname{sign}\left(\hat{x}_1 - x_1\right) + \hat{x}_2 \\ \dot{\hat{x}}_2 = -\alpha_2 \operatorname{sign}\left(\hat{x}_2 - \dot{\hat{x}}_1\right) \end{cases} \tag{3.3}$$

where α_1, α_2 are positive constants and $\hat{x}_1, \hat{x}_2$ are observed states of x_1, x_2.

Based on the developments in [91], the following theorem holds:

Theorem 3.1. *[91] For an input signal x_1 consisting of a base signal x_0 and a bounded noise that fulfills $|x_1 - x_0| \leq \epsilon$, the following inequalities establish in finite time*

$$\begin{aligned} |x_1 - \hat{x}_1| &\leq \mu_1 \epsilon \\ |x_2 - \hat{x}_2| &\leq \mu_2 \epsilon^{1/2} \end{aligned} \tag{3.4}$$

where μ_1, μ_2 depend exclusively on the parameters α_1, α_2 of the differentiator (3.3).

Proof. We refer to [91] for detailed proof. □

From the analysis in [91] and [92], the exact derivatives can be by calculated by using the robust exact differentiator with finite-time convergence. The differentiator is proved to feature the best possible asymptotics in the presence of infinitesimal Lebesgue-measurable measurement noises, if the second time derivative of the unknown base signal is bounded. Therefore, with the help of the robust exact differentiator (3.3), it is acceptable to use the estimated states in the parameter estimation algorithms.

To ensure the convergence of parameter estimation, the following definition of regressor should be used:

Definition 3.1. *[93] A vector Ψ is persistently excited if there exist $T_1 > 0, \varsigma > 0$, such that $\int_t^{t+T_1} \Psi(r)\Psi^T(r)dr \geq \varsigma I, \forall t \geq 0$ is true.*

The above condition implies that sufficiently rich information should be involved in the regressor, which has been recognized as a mandatory condition for parameter estimation [93]. This condition can usually be fulfilled in the beam system.

3.2.2 Adaptive parameter estimation and stability analysis

In this section, we will introduce a new adaptive algorithm to estimate the parameters in the Galerkin model (3.1). For this purpose, we first define a set of filtered variables as [87]

$$\begin{cases} k_f \dot{\hat{x}}_{1f} + \hat{x}_{1f} = \hat{x}_1, \quad \hat{x}_{1f}(0) = 0 \\ k_f \dot{\hat{x}}_{2f} + \hat{x}_{2f} = \hat{x}_2, \quad \hat{x}_{2f}(0) = 0. \end{cases} \tag{3.5}$$

where k_f is a designing filter coefficient. In order to focus on the parameter estimation and their applications on the beam system, the effects of nonzero initial conditions are ignored.

To facilitate the parameter estimation, we reconstruct the second equation in (3.2) as

$$\dot{\hat{x}}_{2f} = \Psi_f \Theta + \zeta_1, \tag{3.6}$$

where $\Psi_f = [-\hat{x}_{2f} \quad -\hat{x}_{1f}]$ is known regressor and $\Theta = [\Theta_1 \quad \Theta_2]^T$ is the unknown parameter vector to be estimated. ζ_1 is the lumped state observer error. From Theorem 3.1 we know that ζ_1 is a small bounded error.

To avoid using the prediction error as in the classical method (e.g. gradient method), we define the auxiliary variables as follows [94]

$$\begin{cases} \dot{M} = -lM + \Psi_f^T \Psi_f \\ \dot{N} = -lN + \Psi_f^T \left[(\hat{x}_2 - \hat{x}_{2f}) / k_f \right]^T \\ W = M\hat{\Theta} - N \end{cases} \tag{3.7}$$

where $l > 0$ is a positive constant. $\hat{\Theta}$ is the estimated parameter defined by $\hat{\Theta} = \Theta - \tilde{\Theta}$ with $\tilde{\Theta}$ being the parameter estimation error.

By integrating both sides of (3.7), the solution of M and N can be derived as

$$\begin{cases} M = \int_0^t e^{-l(t-r)} \Psi_f^T(r) \Psi_f(r) dr \\ N = \int_0^t e^{-l(t-r)} \Psi_f^T(r) \left[(\hat{x}_2 - \hat{x}_{2f}) / k_f \right]^T dr \end{cases} \tag{3.8}$$

Remark 3.1. *From (3.8) we can deduce that $N = M\Theta + \zeta_2$ with $\zeta_2 = \int_0^t e^{-l(t-r)} \Psi_f^T(r) \zeta_1 dr$ being the bounded residual error fulfills $||\zeta_2|| \leq \varpi$. Thus we can represent the auxiliary variable W as $W = M\hat{\Theta} - N = -M\tilde{\Theta} - \zeta_2$. Since W contains the information of the estimation error $\tilde{\Theta}$, an adaptive law can be designed based on W.*

We design the parameter updating law as

$$\dot{\hat{\Theta}} = \Gamma W. \tag{3.9}$$

Remark 3.2. *Compared to the traditional parameter estimation methods (e.g. gradient method), the proposed adaptive law (3.9) is driven by the parameter estimation error rather than the prediction error. Thus the convergence of the parameter estimation error can be guaranteed.*

The main results of this chapter can be summarized as follows:

Theorem 3.2. *Consider system (3.1) with the parameter updating law (3.9), if the regressor matrix Ψ is persistently excited, the filtered regressor matrix M satisfies $\lambda_{min}(M) > \sigma > 0$ and the parameter error $\tilde{\Theta}$ exponentially converge to a small set around zero [94].*

Proof. We select the Lyapunov function as

$$V_1 = \frac{1}{2} tr(\tilde{\Theta}^T \Gamma^{-1} \tilde{\Theta}). \tag{3.10}$$

One can obtain the time derivative of V_1 as

$$\begin{aligned} \dot{V}_1 &= tr(\tilde{\Theta}^T \Gamma^{-1} \dot{\tilde{\Theta}}) = tr(\tilde{\Theta}^T W) = tr(-\tilde{\Theta}^T M \tilde{\Theta} - \tilde{\Theta}^T \zeta_2) \\ &\leq -\sigma ||\tilde{\Theta}||^2 - tr(\tilde{\Theta}^T \zeta_2) \end{aligned} \tag{3.11}$$

By using Young's inequality, we have

$$tr(\tilde{\Theta}^T \zeta_2) \leq \frac{1}{2} ||\tilde{\Theta}||^2 + \frac{1}{2} ||\zeta_2||^2 \tag{3.12}$$

Substituting (3.12) into (3.11) yields

$$\dot{V}_1 \leq -(\sigma - \frac{1}{2}) ||\tilde{\Theta}||^2 - \frac{1}{2} \varpi^2 \leq -\tau_1 V_1 + \tau_2 \tag{3.13}$$

where $\tau_1 = \sigma - 1/2$ is a positive constant for all $t > 0$ since σ can be designed as $\sigma > 1/2$, $\tau_2 = -1/2\varpi^2$ is an small residual error. Based on Lyapunov's Theorem and Theorem 1, the parameter error $\tilde{\Theta}$ exponentially converge to a small set around zero. □

3.3 Simulations and Experiments

3.3.1 Simulations

3.3.1.1 Simulations with the simplified system model

In this simulation, the beam system is described by the simplified Galerkin model (3.1). The system parameters are set as $\Theta_1 = 0.83, \Theta_2 = 1600$. In the adaptive estimation scheme, the same model is used. The parameters of the adaptive law (3.9) are set as $\Gamma = 1 \cdot \text{diag}(1 \cdot 10^{11}, 1 \cdot 10^{8})$, $k_f = 0.001$, $l = 1 \cdot \text{diag}(0.1, 0.1)$. For the tuning of these parameters, large learning gain Γ can increase the convergence rate while may cause parameter shifting at the transient response. The filter coefficient k_f and the forgetting factor l should be chosen by making a trade-off between the estimation performance and the robustness.

We release the tip of the beam at a distance of 0.01m to show the effectiveness of the proposed adaptive parameter estimation method. This is a regular case in the turbine system encountering flows. The vibration of the beam makes the system fulfills the persistent excitation condition. Therefore, the unknown system parameters can be estimated as mentioned in Theorem 3.2.

Simulation results are shown in Figure 3.2- Figure 3.4. We can see from Figure 3.2 the displacement and the velocity can be exactly observed by using the robust sliding mode observer (3.3). Figure 3.3 shows the result of parameter estimation with the help of the proposed adaptive parameter updating law (3.9). With the estimated parameters, we collected the output data from the estimated model. The estimated output match well with the system output as shown in Figure 3.4.

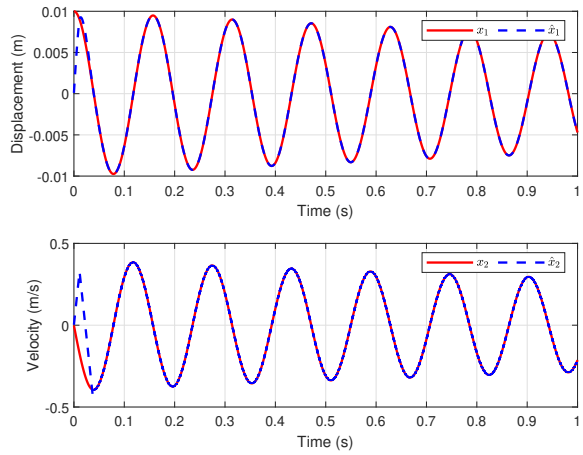

Figure 3.2: Observed states by using the robust sliding mode observer (3.3)

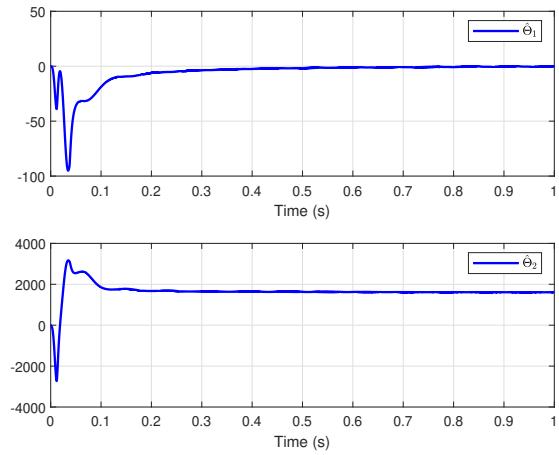

Figure 3.3: Estimated parameters by using the proposed adaptive law (3.9)

3.3.1.2 Simulations with the high-order (20th-order) system model

In this simulation, the system model is described by using the high-order model (2.85) with 10 spacial nodes. System parameters are set following Table 1.1. In the adaptive parameter estimation scheme, the simplified Galerkin model (3.1) is used. The parameters of the adaptive law (3.9) are set as $\Gamma = 1 \cdot \text{diag}(1 \cdot 10^{7}, 1 \cdot 10^{10})$, $k_f = 0.001$, $l = 1 \cdot \text{diag}(0.1, 0.1)$.

Simulation results are shown in Figure 3.5- Figure 3.7. We can see from Figure 3.5 the displacement and the velocity can be estimated using the robust sliding mode observer (3.3). Figure 3.6 shows the

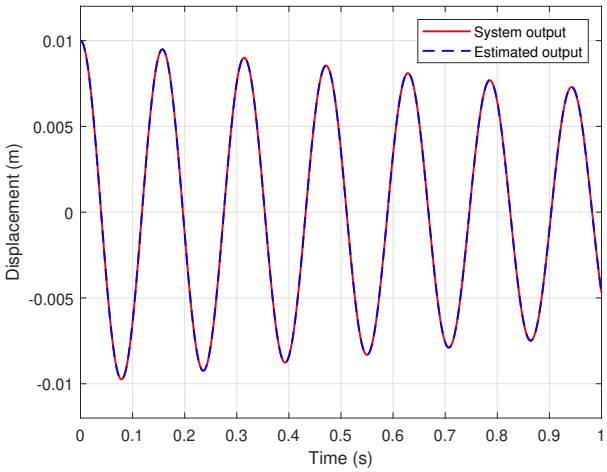

Figure 3.4: Comparison of system output and estimated output

result of parameter estimation with the help of the proposed adaptive parameter updating law (3.9). With the estimated parameters, we collected the output data from the estimated model. The estimated output match well with the high-order (20th-order) system output as shown in Figure 3.7.

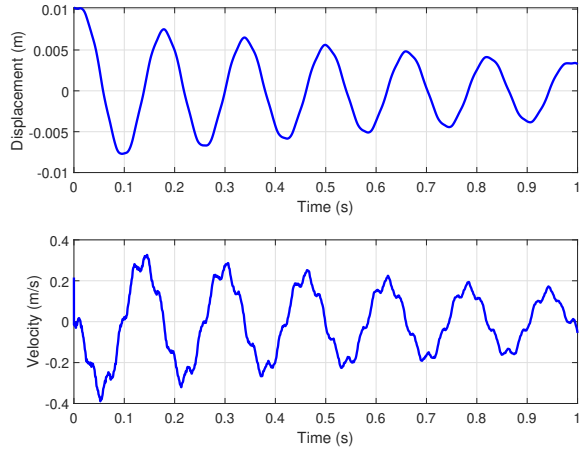

Figure 3.5: Observed states by using the robust sliding mode observer (3.3)

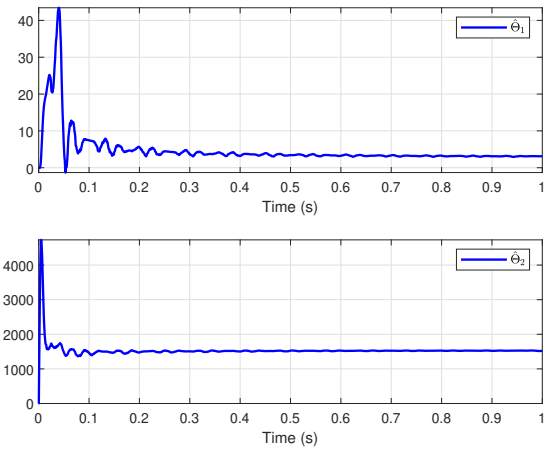

Figure 3.6: Estimated parameters by using the proposed adaptive law (3.9)

3.3.2 Practical Experiments

In the experiment, we use a waterproof strain gauge (type number: WFLA-6-11-3LDBTB) from Tokyo Measuring Instruments Laboratory to measure the strain of the beam. NI 9235 quarter-bridge strain gauge module from National Instruments is used to collect the signal of the strain gauge. A bridge offset nulling calibration is introduced to eliminate the offset of the strain gauge. The overall experiment configuration is shown in Figure 3.8.

We firstly estimate the parameters of the dry beam. The experimental results are shown in Figure 3.9- Figure 3.11. The state estimation results and the parameter estimation results are depicted in Figure 3.9 and Figure 3.10. Figure 3.11 shows the vibration of the first mode are correctly estimated.

To show the estimation performance of the submerged beam, we further estimated the parameters of the beam submerged in water. Because the piezoelectric actuator is not waterproof, we submerged 24cm

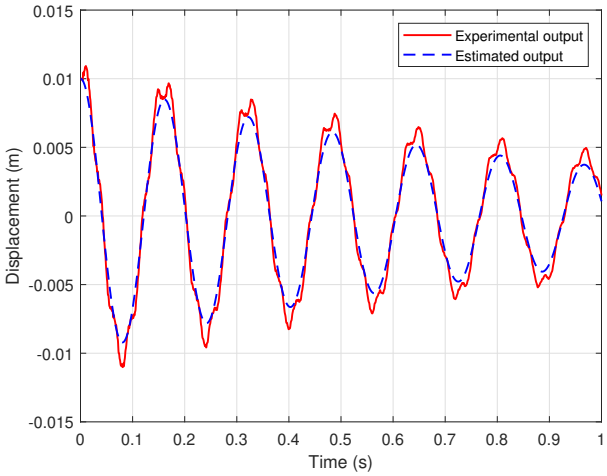

Figure 3.7: Comparison of system output and estimated output

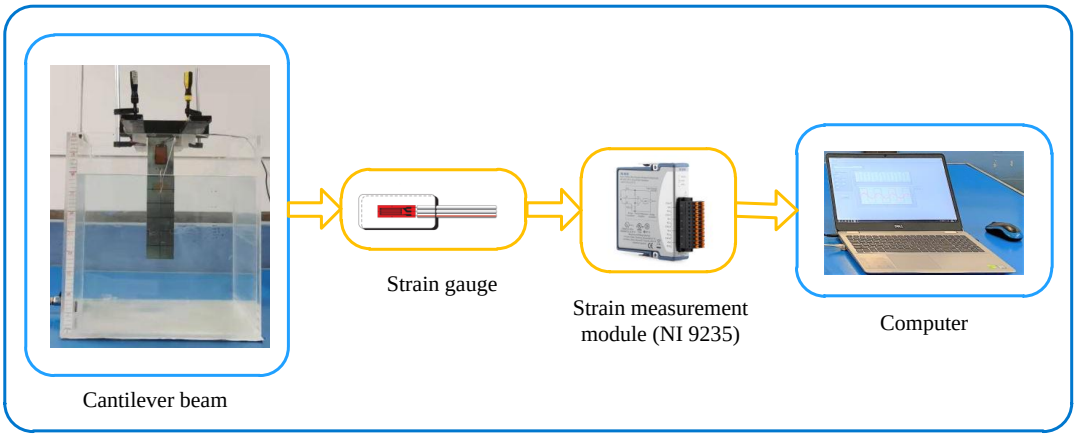

Figure 3.8: Overall experiment configuration for parameter estimation of the beam system

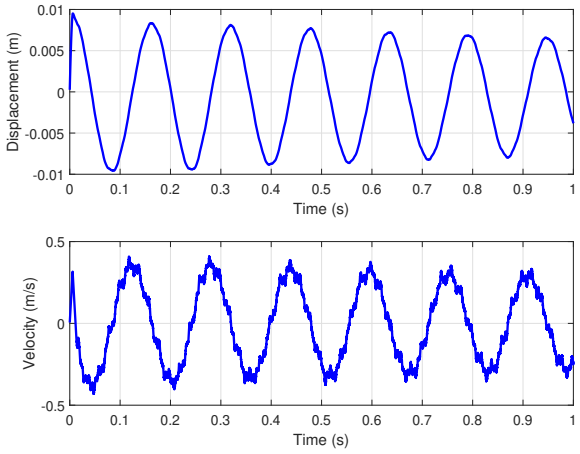

Figure 3.9: Observed states of the dry beam

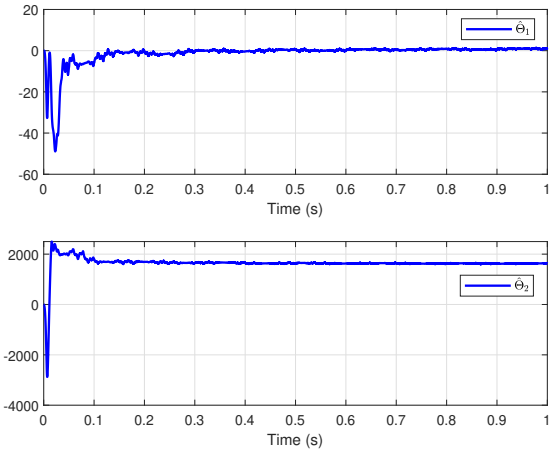

Figure 3.10: Estimated parameters of the dry beam

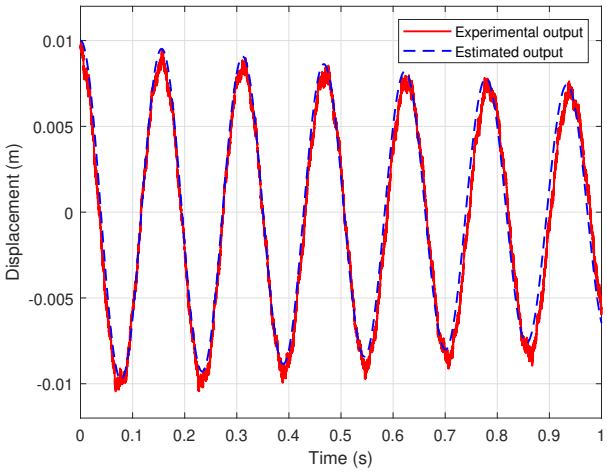

Figure 3.11: Comparison of experimental output and estimated output of the dry beam

of the beam in the water tank. We then release the beam at a distance of 1cm. The experiment results are given in Figure 3.12- Figure 3.14. From Figure 3.12 we can see the states of the system can be estimated. The estimation performance of the system parameters are presented in Figure 3.13. Figure 3.14 shows the comparison of experimental output and estimated output of the submerged beam. It can be seen the system response of the model with estimated parameters fits well with the experimental output.

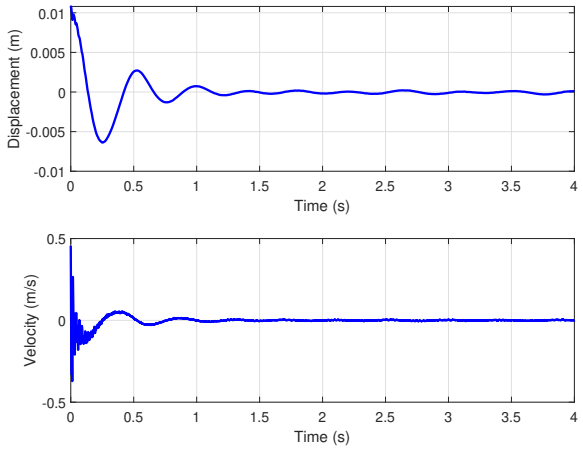

Figure 3.12: Observed states of the submerged beam

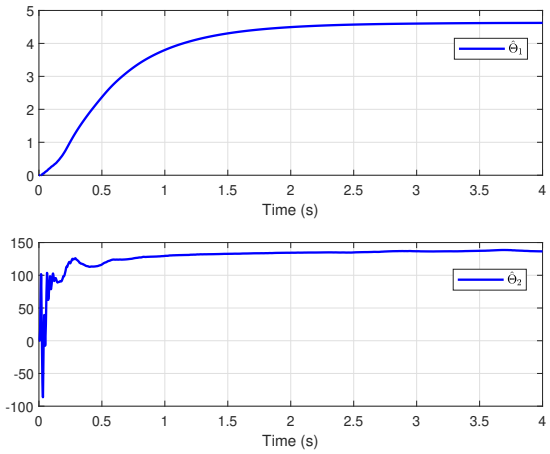

Figure 3.13: Estimated parameters of the submerged beam

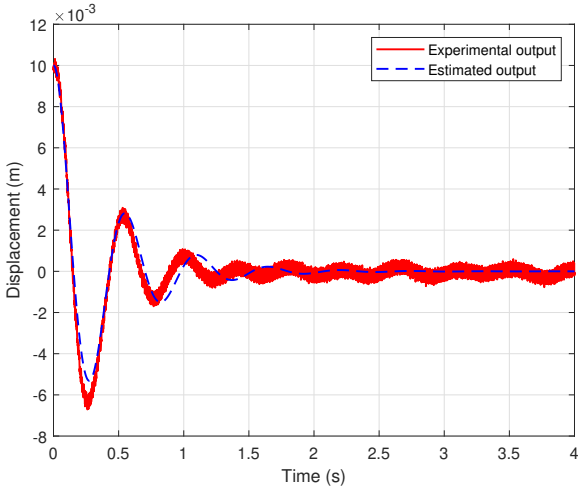

Figure 3.14: Comparison of experimental output and estimated output of the submerged beam

3.4 Conclusions

In this chapter, we mainly addressed the parameter estimation problem of the beam system with the first oscillation mode. The states of the system are estimated by using the Levant exact differentiator via sliding mode technique. To online estimate the parameters, the parameter estimation error is extracted by introducing an auxiliary filter. A new adaptive parameter updating law is then derived based on the estimation error. By using Lyapunov theory, the stability of the system is proved. Simulation and experimental results show the effectiveness of the proposed estimation method.

Chapter 4

Adaptive Parameter Estimation for Multi-modes Beam System

4.1 Introduction

For the vibrating systems like the beam, system parameters may be unknown and varying under different operating conditions [95, 96]. For example, the frequency and damping of the beam in different liquids are not the same [97]. It is highly desired to design parameter estimation strategies to online estimate the unknown varying model parameters, which in turn contributes to the precise modeling and control synthesis. For parameter estimation techniques of the PDE models, many challenging mathematical problems (e.g. the uniqueness and stability) remain to be addressed. In [98], a high-gain adaptive regulator was introduced to stabilize and estimate the unknown parameters of a PDE based beam model. Although the uniqueness of the classical solution is justified, the computational load is high for solving the PDE numerically. Hence, in practice, it is preferable to construct the ordinary differential equation (ODE) based models. In [80], an offline identification approach was adopted to estimate the parameters of the discrete-time beam model. In [99], an online estimator was proposed to estimate the frequencies of the two main vibration modes of a cantilever beam. The work was done in the frequency domain based on the algebraic derivative approach.

For parameter estimation of ODE-based systems, many researchers have been working on adaptive parameter estimation techniques [93]. In [77], a two-stage gradient based method was proposed by means of iterative algorithms for autoregressive systems. In [100], an online optimization algorithm based on the gradient method together with an extended Kalman filter was investigated. Another well-known parameter estimation technique is the least-squares method or recursive least-squares method [84, 101]. Although the convergence of these algorithms can be proved under the persistent excitation condition, there are still challenging issues accounting for measurement noises for the beam systems and the verification of the required excitation condition.

Moreover, for parameter estimation, it is more convenient to parameterize the system model to separate the lumped parameters from signals [87]. In this procedure, the use of differentiation (or system states) is not desirable because of the amplification of the noises, which would even be worse for the plants that contain high-frequency modes [84]. To address this problem, in our previous work [94], a stable filter is applied to derive a new parameterized formula without using the derivatives. Then the unknown parameters are estimated by using the input and output signals only. In addition, the convergence

of parameter estimation error is proved under the persistent excitation (PE) condition. However, with respect to the vibration problem in the beam system, there are multiple oscillation modes with higher frequencies. In such cases, the estimation algorithm in [94] may not retain its performance since only a constant gain set by the designer is adopted.

In this chapter, we will estimate the system parameters for multi-modes beam system with only input and output information due to the fact that the states of the system can not be measured or estimated. A new adaptive parameter estimation approach will be proposed to online estimate the parameters of a cantilever beam modeled with Euler-Bernoulli theory. To illustrate the proposed adaptive algorithm for estimating the system parameters with multiple oscillation modes, we will select the first mode and the second mode to construct the model. The model with two oscillation modes will be then written as a compact parameterized form. Based on the parameterized model, a new adaptive parameter updating law will be proposed. The convergence of the parameter estimation error is proved by using Lyapunov theory. Compared to conventional gradient method and least-squares method, the proposed adaptive estimation method can achieve improved performance. Comparative simulations and experiments will be carried out to verify the effectiveness of the proposed method.

4.2 Model description

Based on the definition of natural frequency and damping ratio [56], equation (2.106) together with (2.92) can be further written as the following state-space model

$$\begin{cases} \dot{X} = AX + Bu \\ y = CX \end{cases} \tag{4.1}$$

where the system state vector is chosen as $X = [\eta_1, \eta_2, \cdots, \eta_{n-1}, \eta_n, \dot{\eta}_1, \dot{\eta}_2, \cdots, \dot{\eta}_{n-1}, \dot{\eta}_n]^T$ and

$$\begin{aligned}
A &= \begin{bmatrix} \mathbf{0}_{n\times n} & \boldsymbol{I}_{n\times n} \\ -\boldsymbol{\Omega}^2 & -2\boldsymbol{\zeta}\boldsymbol{\Omega} \end{bmatrix}, B = \begin{bmatrix} 0_{n\times 1} \\ \boldsymbol{B}_w \end{bmatrix}, \\
C &= \begin{bmatrix} \boldsymbol{C}_w & \mathbf{0}_{1\times n} \end{bmatrix} \\
\boldsymbol{\Omega} &= \begin{bmatrix} \omega_1 & \cdots & \mathbf{0} \\ \vdots & \ddots & \vdots \\ \mathbf{0} & \cdots & \omega_n \end{bmatrix}, \boldsymbol{\zeta} = \begin{bmatrix} \zeta_1 & \cdots & \mathbf{0} \\ \vdots & \ddots & \vdots \\ \mathbf{0} & \cdots & \zeta_n \end{bmatrix}, \\
\boldsymbol{B}_w &= \begin{bmatrix} \frac{z_1}{m_{11}} & \cdots & \frac{z_n}{m_{nn}} \end{bmatrix}, \\
\boldsymbol{C}_w &= \begin{bmatrix} W_1 & \cdots & W_n \end{bmatrix}
\end{aligned}$$

where ω_i and ζ_i are the natural frequency and damping ratio of $i_{th}(i = 1, 2, \ldots, n)$ oscillation mode.

In the system model (4.1), the unknown parameters ω_i and ζ_i are essential for modeling and subsequent control synthesis. Hence, the aim of this study is to introduce a constructive estimation scheme to derive the values of ω_i and ζ_i by using the input and output measurement.

Remark 4.1. *System (4.1) describes the piezoelectric cantilever beam behavior with multiple oscillation modes. Theoretically, the system model will be more accurate with more oscillation modes. However, this will lead to a high order system model, which is more complicated to implement in practice. As a result, a trade-off should be made between the accuracy and the practicability. In this paper, we take two major oscillation modes into consideration to demonstrate the effectiveness of the proposed adaptive parameter estimation method.*

4.3 Adaptive Parameter Estimation

This section will introduce a real-time parameter estimation scheme for the above ODE based model (4.1) with two main vibration modes. After parameterizing the system model, an adaptive law with a time-varying gain will be proposed. Without loss of generality, we assume the input u and output y are bounded. For the unbounded cases, the normalization operation [102] can be applied to fulfill this condition.

4.3.1 Model Parameterization

Considering the first and second oscillation modes, the model (4.1) can be rewritten as

$$\begin{cases} \dot{\bar{X}} = \bar{A}\bar{X} + \bar{B}u \\ y = \bar{C}\bar{X} \end{cases} \tag{4.2}$$

where the system states are chosen as $\bar{X} = [\eta_1, \eta_2, \dot{\eta}_1, \dot{\eta}_2]^T$ and

$$\begin{aligned} \bar{A} &= \begin{bmatrix} 0 & 0 & 1 & 0 \\ 0 & 0 & 0 & 1 \\ \bar{k}_1 & 0 & \bar{c}_1 & 0 \\ 0 & \bar{k}_2 & 0 & \bar{c}_2 \end{bmatrix}, \bar{B} = \begin{bmatrix} 0 \\ 0 \\ \bar{b}_1 \\ \bar{b}_2 \end{bmatrix}, \\ \bar{C} &= \begin{bmatrix} -2 & 2 & 0 & 0 \end{bmatrix} \end{aligned} \tag{4.3}$$

with $\bar{k}_1 = -\omega_1^2, \bar{k}_2 = -\omega_2^2, \bar{c}_1 = -2\zeta_1\omega_1, \bar{c}_2 = -2\zeta_2\omega_2, \bar{b}_1 = z_1/m_{11}$ and $\bar{b}_2 = z_2/m_{22}$.

As shown in the above model (4.2), the parameters $\bar{k}_1, \bar{k}_2, \bar{c}_1, \bar{c}_2, \bar{b}_1, \bar{b}_2$ involving ω_i and ζ_i are essential for modeling the beam system, which will be estimated in this study. However, one difficulty for using model (4.2) is that the states $\bar{X}$ cannot be directly measured. In practice, only the input voltage $u = U_a(t)$ and the output displacement $y = 2L^3\varepsilon/(3L_1h)$ can be measured. Hence, an alternative model that is described by the input and output is desirable for parameter estimation. To address this issue, we can obtain the transfer function of model (4.2) as

$$G(s) = \bar{C}(sI - \bar{A})^{-1}\bar{B} = \frac{b_2s^2 + b_1s + b_0}{s^4 + a_3s^3 + a_2s^2 + a_1s + a_0} \tag{4.4}$$

where

$$\begin{cases} b_2 = 2\bar{b}_2 - 2\bar{b}_1 \\ b_1 = 2\bar{b}_1\bar{c}_2 - 2\bar{b}_2\bar{c}_1 \\ b_0 = 2\bar{b}_1\bar{k}_2 - 2\bar{b}_2\bar{k}_1 \\ a_3 = -\bar{c}_1 - \bar{c}_2 \\ a_2 = -\bar{k}_1 - \bar{k}_2 + \bar{c}_1\bar{c}_2 \\ a_1 = \bar{c}_1\bar{k}_2 + \bar{k}_1\bar{c}_2 \\ a_0 = \bar{k}_1\bar{k}_2 \end{cases} \tag{4.5}$$

are unknown parameters including ω_i and ζ_i as shown in (4.3).

To accomplish the parameter estimation in the time-domain, the model (4.4) can be further expressed as an ODE as

$$y^{(4)} + a_3y^{(3)} + a_2y^{(2)} + a_1y^{(1)} + a_0y = b_2u^{(2)} + b_1u^{(1)} + b_0u \tag{4.6}$$

To avoid using derivatives of output y as [94], i.e. $y^{(4)}, y^{(3)}, y^{(2)}, y^{(1)}$, we filter each side of (4.6) with a fourth-order filter $1/\Lambda(s)$, where $\Lambda(s) = (s+\lambda)^4 = s^4 + k_3 s^3 + k_2 s^2 + k_1 s + k_0$, and then have

$$\begin{aligned} &\frac{s^4}{\Lambda(s)}y + a_3\frac{s^3}{\Lambda(s)}y + a_2\frac{s^2}{\Lambda(s)}y + a_1\frac{s}{\Lambda(s)}y + a_0\frac{1}{\Lambda(s)}y \\ &= b_2\frac{s^2}{\Lambda(s)}u + b_1\frac{s}{\Lambda(s)}u + b_0\frac{1}{\Lambda(s)}u. \end{aligned} \tag{4.7}$$

Then, equation (4.7) can be rewritten as a parameterized form

$$\begin{aligned} y =& b_2\frac{s^2}{\Lambda(s)}u + b_1\frac{s}{\Lambda(s)}u + b_0\frac{1}{\Lambda(s)}u + (k_3 - a_3)\frac{s^3}{\Lambda(s)}y \\ &+ (k_2 - a_2)\frac{s^2}{\Lambda(s)}y + (k_1 - a_1)\frac{s}{\Lambda(s)}y + (k_0 - a_0)\frac{1}{\Lambda(s)}y \\ =& \Theta^T \Psi \end{aligned} \tag{4.8}$$

where

$$\begin{aligned} \Theta &= [b_2, b_1, b_0, k_3 - a_3, k_2 - a_2, k_1 - a_1, k_0 - a_0]^T, \\ \Psi &= \left[\frac{s^2}{\Lambda(s)}u, \frac{s}{\Lambda(s)}u, \frac{1}{\Lambda(s)}u, \frac{s^3}{\Lambda(s)}y, \frac{s^2}{\Lambda(s)}y, \frac{s}{\Lambda(s)}y, \frac{1}{\Lambda(s)}y\right]^T. \end{aligned}$$

The values of frequencies ω_1, ω_2 and damping ratios ζ_1, ζ_2 to be online estimated are determined by $\bar{k}_1, \bar{k}_2, \bar{c}_1, \bar{c}_2$, which can be obtained by using (4.3) and (4.4). One can obtain the eigenvalues of $\bar{A}$ in (4.3) as

$$\begin{cases} p_1 = \frac{\bar{c}_2}{2} + \frac{\sqrt{\bar{c}_2^2 + 4\bar{k}_2}}{2} \\ p_2 = \frac{\bar{c}_2}{2} - \frac{\sqrt{\bar{c}_2^2 + 4\bar{k}_2}}{2} \\ p_3 = \frac{\bar{c}_1}{2} + \frac{\sqrt{\bar{c}_1^2 + 4\bar{k}_1}}{2} \\ p_4 = \frac{\bar{c}_1}{2} - \frac{\sqrt{\bar{c}_1^2 + 4\bar{k}_1}}{2} \end{cases} \tag{4.9}$$

From (4.4), one can obtain the eigenvalues p_1, p_2, p_3, p_4 by computing the roots of the characteristic polynomial $s^4 + a_3 s^3 + a_2 s^2 + a_1 s + a_0$. Substituting p_1, p_2, p_3, p_4 into (4.9), we can solve (4.9) and obtain $\bar{k}_1, \bar{k}_2, \bar{c}_1, \bar{c}_2$. Then the frequencies ω_1, ω_2 and damping ratios ζ_1, ζ_2 can be computed.

For the other two parameters $\bar{b}_1$ and $\bar{b}_2$ in (4.3), one can obtain the values with the help of (4.5). We can rewrite the first three equations of (4.5) as

$$\begin{bmatrix} -2 & 2 \\ 2\bar{c}_2 & -2\bar{c}_1 \\ 2\bar{k}_2 & -2\bar{k}_1 \end{bmatrix} \begin{bmatrix} \bar{b}_1 \\ \bar{b}_2 \end{bmatrix} = \begin{bmatrix} b_2 \\ b_1 \\ b_0 \end{bmatrix}. \tag{4.10}$$

Since (4.10) is over-constrained, we can obtain the approximate solution of (4.10) by introducing Moore–Penrose inverse. Then $\bar{b}_1$ and $\bar{b}_2$ can be obtained as

$$\begin{bmatrix} \bar{b}_1 \\ \bar{b}_2 \end{bmatrix} = \begin{bmatrix} -2 & 2 \\ 2\bar{c}_2 & -2\bar{c}_1 \\ 2\bar{k}_2 & -2\bar{k}_1 \end{bmatrix}^+ \begin{bmatrix} b_2 \\ b_1 \\ b_0 \end{bmatrix} \tag{4.11}$$

where $[\cdot]^+$ is the Moore–Penrose inverse. Another way to compute $\bar{b}_1$ and $\bar{b}_2$ is to use only two equations of (4.10). The computational burden will be less and the differences will be only in transient.

Clearly, the system parameters $\bar{k}_1, \bar{k}_2, \bar{c}_1, \bar{c}_2, \bar{b}_1, \bar{b}_2$ in (4.3) can be obtained as long as the parameters $a_i, i = 0, 1, 2, 3$ and $b_j, j = 0, 1, 2$ in (4.5) are estimated online. Hence, the problem now is to online estimate the unknown model parameters Θ based on the measured input u and output y.

To ensure the convergence of parameter estimation, the persistent excitation condition should be fulfilled. This condition can usually be fulfilled in the beam system. However, the verification of this condition is not a trivial task. This will be studied in the following subsection.

4.3.2 Adaptive Parameter Estimation

Although the classical gradient algorithm has been applied for system (4.8), the tuning of learning gain that affects the performance is generally difficult, since it is also sensitive to measurement noise. In this subsection, we introduce an alternative adaptive parameter estimation algorithm to estimate the unknown parameter Θ of parameterized model (4.8), and allow verifying the required excitation condition.

To eliminate the influence of noise, we first define the auxiliary regressor matrix P and vector Q as

$$\begin{cases} \dot{P} = -lP + \Psi\Psi^T, P(0) = 0 \\ \dot{Q} = -lQ + \Psi y, Q(0) = 0 \end{cases} \tag{4.12}$$

where $l > 0$ is a forgetting factor set as a small constant.

One can obtain the solution of (4.12) as

$$\begin{cases} P = \int_0^t e^{-l(t-r)}\Psi(r)\Psi^T(r)dr \\ Q = \int_0^t e^{-l(t-r)}\Psi(r)y(r)dr \end{cases} \tag{4.13}$$

which are bounded for any bounded Ψ and y.

To obtain the estimation error $\tilde{\Theta} = \Theta - \hat{\Theta}$ to design an adaptive law, we define another auxiliary vector W as

$$W = P\hat{\Theta} - Q \tag{4.14}$$

where $\hat{\Theta}$ is the estimated parameter.

Combining (4.13) and (4.14), the vector W can be further reformulated as

$$W = -P\tilde{\Theta}. \tag{4.15}$$

Hence, the parameter estimation error $\tilde{\Theta}$ can be explicitly calculated online based on the measured input u and output y, which can be used to design the adaptive laws [87] to obtain better performance than the classical gradient algorithm. Moreover, the purpose of introducing the above filtered matrix P is to provide a feasible approach to verify the required excitation condition, which can be summarized as the following lemma:

Lemma 4.1. *If the regressor Ψ defined in (4.8) is persistently excited, the matrix P is positively definite (i.e., $\lambda_{\min}(P(t)) > \sigma > 0$ for a positive constant σ), and vice versa.*

We refer to [94] for a similar proof of the above lemma. The value of this lemma lies in that one can calculate the minimum eigenvalue of matrix P to evaluate if the required excitation condition of regressor Ψ is fulfilled.

Since W is a function of parameter estimation error $\tilde{\Theta}$, one can use it to design the adaptive laws as shown in [94], where the adopted constant learning gain should be carefully set by the designers. However, from (4.12) and (4.15), we can see that the regressor Ψ is involved in the vector W, which may influence the convergence response of the estimated parameters [103]. Hence, we will introduce a new adaptive law with a time-varying gain to handle effects of regressor so as to simplify the tuning of learning gains. Taking the effect of the regressor Ψ into consideration, we define a time-varying gain H

as

$$\dot{H} = \gamma H - H\Psi\Psi^T H \tag{4.16}$$

where $\gamma > 0$ is a design constant and $H(0) = H_0 > 0$ is the initial condition.

Using the matrix identity

$$\frac{d}{dt}HH^{-1} = \dot{H}H^{-1} + H\frac{d}{dt}H^{-1} = 0 \tag{4.17}$$

we have its solution

$$H(t) = \left[e^{-\gamma t}H_0^{-1} + \int_0^t e^{-\gamma(t-r)}\Psi(r)\Psi^T(r)dr\right]^{-1}. \tag{4.18}$$

Now, the boundedness of matrix H is shown as [103]:

Lemma 4.2. *If the regressor Ψ is persistently excited, the matrix H^{-1} defined in (4.17) is bounded by*

$$\beta I \leq H^{-1}(t) \leq \alpha I \tag{4.19}$$

where $\beta = e^{-\gamma T_1}\varsigma$ and $\alpha = \lambda_{min}(H_0^{-1}) + \varpi^2, \varpi \geq \|\Psi\|$.

The proof of the above claims can be inspired by [103], which is not presented here due to the page limit.

As shown in (4.13) and (4.18), the matrix H converges to the inverse of auxiliary matrix P. Hence, it can be used to compensate the effect of regressor in the variable W. We can use W and H together to design the following adaptive parameter updating law

$$\dot{\hat{\Theta}} = -\Gamma HW \tag{4.20}$$

where $\Gamma > 0$ is a positive constant.

The main results of this paper can be given as the following Theorem:

Theorem 4.1. *Consider system (4.6) with the parameter updating law (4.20), if the regressor Ψ is persistently excited, the estimation error $\tilde{\Theta}$ exponentially converges to zero.*

Proof. We choose the Lyapunov candidate function as

$$V = \frac{1}{2\Gamma}\tilde{\Theta}^T H^{-1}\tilde{\Theta}. \tag{4.21}$$

One can obtain the time derivative of V along with (4.20) as

$$\begin{aligned}\dot{V} &= \frac{1}{2\Gamma}\left(\dot{\tilde{\Theta}}^T H^{-1}\tilde{\Theta} + \tilde{\Theta}^T\dot{H}^{-1}\tilde{\Theta} + \tilde{\Theta}^T H^{-1}\dot{\tilde{\Theta}}\right)\\ &= \frac{1}{\Gamma}\tilde{\Theta}^T H^{-1}\dot{\tilde{\Theta}} + \frac{1}{2\Gamma}\tilde{\Theta}^T\dot{H}^{-1}\tilde{\Theta}\\ &= -\tilde{\Theta}^T P\tilde{\Theta} + \frac{1}{2\Gamma}\tilde{\Theta}^T\dot{H}^{-1}\tilde{\Theta}.\end{aligned} \tag{4.22}$$

From (4.18), we have

$$\dot{H}^{-1} = -\gamma H^{-1} + \Psi\Psi^T. \tag{4.23}$$

Then, equation (4.22) can be further written as

$$\begin{aligned}\dot{V} &= -\tilde{\Theta}^T P\tilde{\Theta} + \frac{1}{2\Gamma}\tilde{\Theta}^T\left(-\gamma H^{-1} + \Psi\Psi^T\right)\tilde{\Theta}\\ &\leq -\frac{\sigma}{\alpha}\tilde{\Theta}^T H^{-1}\tilde{\Theta} - \frac{\gamma}{2\Gamma}\tilde{\Theta}^T H^{-1}\tilde{\Theta} + \frac{\varpi^2}{2\Gamma\beta}\tilde{\Theta}^T H^{-1}\tilde{\Theta}\\ &\leq -\left(\frac{2\Gamma\sigma}{\alpha} + \gamma - \frac{\varpi^2}{\beta}\right)\frac{1}{2\Gamma}\tilde{\Theta}^T H^{-1}\tilde{\Theta}\\ &\leq -\mu V\end{aligned} \tag{4.24}$$

where $\mu = 2\Gamma\sigma/\alpha + \gamma - \varpi^2/\beta$ is a positive constant for large gains Γ, γ. Based on the Lyapunov's Theorem, the estimation error $\tilde{\Theta}$ exponentially converges to zero. □

Remark 4.2. *One can find that the adaptive law (4.20) is constructed based on the derived variable W, which is driven by the parameter estimation error $\tilde{\Theta}$ as shown in (4.15). Therefore, the convergence of this algorithm can be rigorously proved. Clearly, the proposed adaptive estimation method avoids using any predictor/observer, which is different from the gradient algorithms and least-squares methods driven by the observer error (as shown in [84]). Besides, a time-varying gain H is adopted to compensate the effect of regressor Ψ in the adaptive law to enhance the convergence over that given in [94]. In this line, as shown in the proof of Theorem 1, the learning gain Γ can be trivially selected compared with the gradient counterparts. Moreover, online validation of the persistent excitation can be achieved by testing the positive definiteness of P according to Lemma 4.1.*

4.4 Simulations and Experiments

4.4.1 Simulations

In the simulations, the beam system model (4.6) can be written as

$$\begin{aligned} &y^{(4)} + 65.42y^{(3)} + 6.18 \cdot 10^4 y^{(2)} + 1.95 \cdot 10^5 y^{(1)} \\ &+ 9.23 \cdot 10^7 y = 13.02u^{(2)} - 1.18 \cdot 10^3 u^{(1)} - 1.11 \cdot 10^6 u \end{aligned} \tag{4.25}$$

where $a_3 = 65.42, a_2 = 6.18 \cdot 10^4, a_1 = 1.95 \cdot 10^5, a_0 = 9.23 \cdot 10^7, b_2 = 13.02, b_1 = -1.18 \cdot 10^3, b_0 = -1.11 \cdot 10^6$ are the model parameters to be estimated. These nominal values are computed from the material properties given in Table 1.1 together with the procedure described in Section 2.5.3 and Section 4.3. The input signal is a square wave with amplitude 0.1 and frequency 7 Hz to ensure the required excitation condition given in Lemma 1. The polynomial used to derive the parameterized form is chosen as $\Lambda(s) = (s + 100)^4$. The other parameters of the proposed adaptive law are $\Gamma = 80 \cdot \text{diag}(1, 1, 1, 1, 1, 1, 1), H(0) = 1 \cdot 10^{22} \cdot \text{diag}(1, 1, 10, 10, 10, 10, 10)$ and $l = 0.01, \gamma = 0.1$.

For comparison, the gradient-based method and least-squares method [84] are used to estimate the unknown system parameters under the same operation condition. The gradient-based adaptive law is designed as [84]

$$\dot{\hat{\Theta}} = \Gamma_1 e\Psi, \quad e = y - \hat{\Theta}^T\Psi \tag{4.26}$$

and the least-squares algorithm as

$$\dot{\hat{\Theta}} = \Gamma_2 e\Psi, \quad e = y - \hat{\Theta}^T\Psi, \quad \dot{\Gamma}_2 = -\Gamma_2\Psi\Psi^T\Gamma_2. \tag{4.27}$$

The learning gain of the gradient-based method in (4.26) is $\Gamma_1 = 1 \cdot \text{diag}(2 \cdot 10^{11}, 2 \cdot 10^{15}, 6 \cdot 10^{19}, 3 \cdot 10^{12}, 2 \cdot 10^{17}, 7 \cdot 10^{18}, 4 \cdot 10^{23})$. The initial value of the covariance matrix Z in the least-squares method (4.27) is $\Gamma_2(0) = 1 \cdot 10^{23} \cdot \text{diag}(1, 1, 1, 10, 10, 10, 10)$.

Clearly, the tuning of these gains for the gradient-based method and least-squares method should consider the effect of regressor Ψ (e.g. the amplitude of each component), and thus it is a time-consuming phase, requiring preliminary information of the plant. In contrast, for the proposed estimation algorithm, since the effect of regressor Ψ on the convergence is handled by introducing the time-varying gain H, such that the tuning of the learning constant Γ is more straightforward, i.e. all components in the gain Γ can be set as a constant.

Simulation results are depicted in Figure 4.1 and Figure 4.2. Figure 4.1 shows the profile of the input and output signal of the system (4.25). Figure 4.2 provides the estimation of the parameters a_i, b_j. We can see that the proposed adaptive estimation method has a smoother and faster response compared with the gradient method and least-squares method. Hence, the proposed adaptive method can accurately estimate the unknown model parameters. This is because the adaptive law (4.20) is designed by using the extracted parameter estimation error instead of the predictor/observer error in the conventional methods. The gradient method achieves larger overshoots and slower convergence performance. Moreover, the least-squares method suffers from a windup problem in the gain Γ_2 given in (4.27).

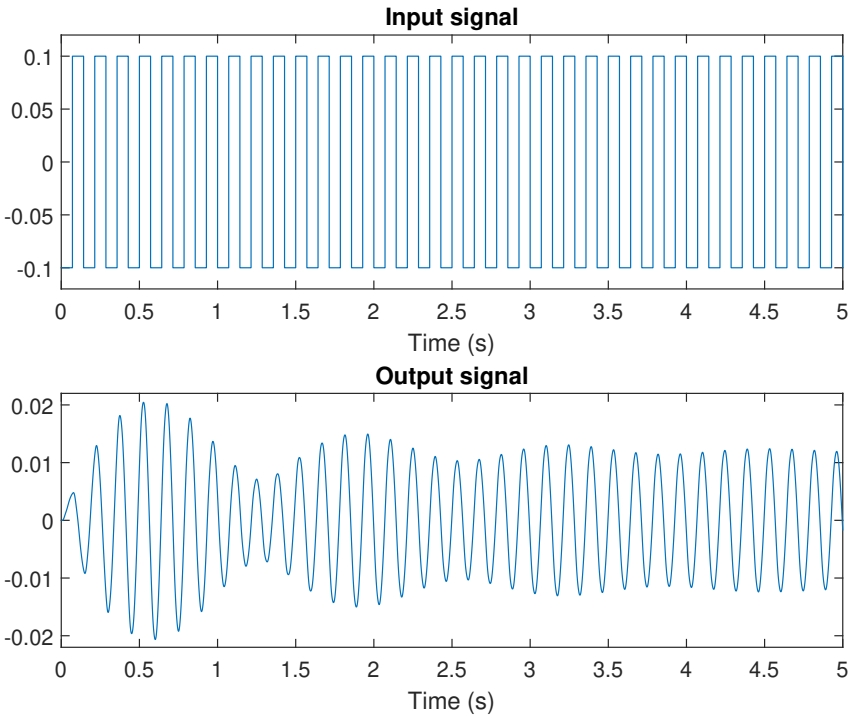

Figure 4.1: Input and output signals (simulation results)

According to (4.2) and (4.4), we can obtain the first mode frequency ω_1, the second mode frequency ω_2, the first mode damping ratio ζ_1 and the second mode damping ratio ζ_2. Comparative values are shown in Table 4.1. It is shown that the proposed adaptive method has better estimation results than the other two methods.

Table 4.1: Comparison of frequencies and damping ratios with gradient method, least-squares and the proposed adaptive method

	$\omega_1(rad/s)$	$\omega_2(rad/s)$	ζ_1	ζ_2
True value	39.1533	245.3711	0.0207	0.13
Gradient	38.8304	245.0479	0.0216	0.1374
least-squares	39.1339	231.6241	0.02	0.1205
Adaptive	39.1682	245.3184	0.0207	0.13

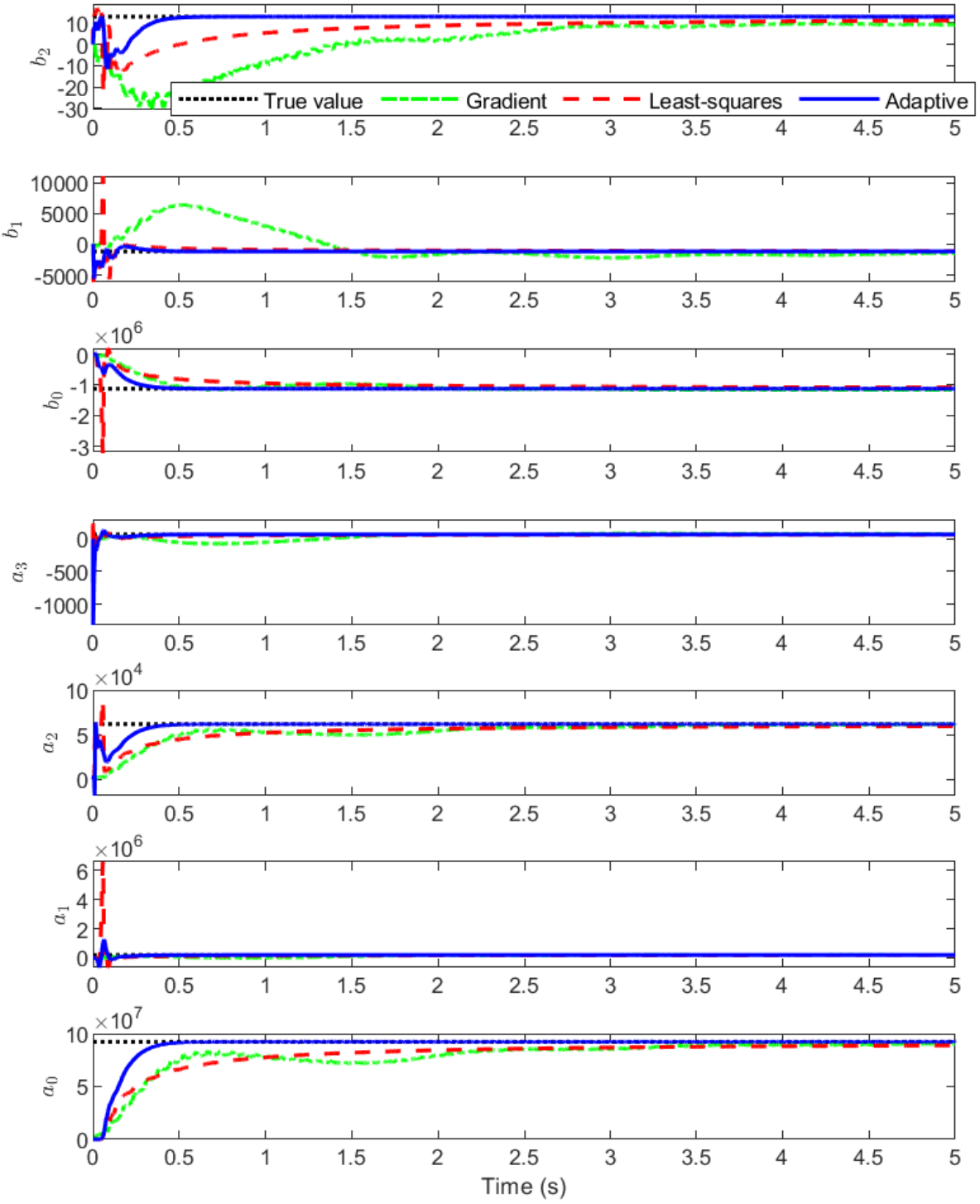

Figure 4.2: Comparative convergence performance of gradient method, least-squares method and the proposed adaptive method (simulation results)

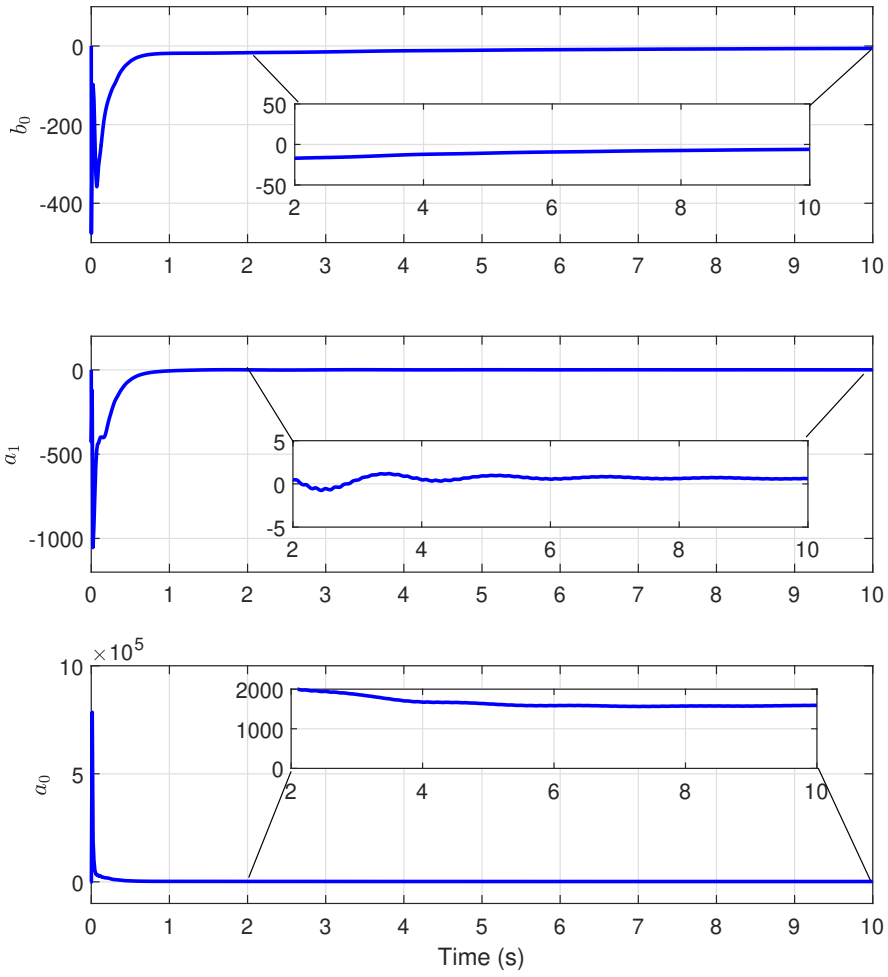

Figure 4.3: Estimation results of the first mode system

4.4.2 Practical Experiments

Before performing the estimation of the two modes system, we firstly consider the system with only the first mode. Following the procedure in Section 4.3, we can obtain the parameterized system as

$$y = \Theta^T \Psi \tag{4.28}$$

where

$$\Theta = [b_0, k_1 - a_1, k_0 - a_0]^T, \Psi = \left[\frac{1}{\Lambda(s)}u, \frac{s}{\Lambda(s)}y, \frac{1}{\Lambda(s)}y\right]^T.$$

The polynomial is chosen as $\Lambda(s) = (s+2)^2$. The parameters of the adaptive law (4.20) used in the experiments are $\Gamma = 10 \cdot \text{diag}(1,1,10), H(0) = 1 \cdot \text{diag}(1 \cdot 10^{21}, 1 \cdot 10^{21}, 1 \cdot 10^{23}), l = 0.01, \gamma = 0.1$. The estimation results are given in Figure 4.3 and the reconstructed output is shown in Figure 4.4. From Figure 4.4 we can see that the dynamics of the system output can be partly reconstructed considering the first mode while there are discrepancies between the experiment output and the reconstructed output.

Following the analysis given in the simulations, we conduct the experiments for the two modes system.The parameters of the adaptive law (4.20) used in the experiments are $\Gamma = 10 \cdot \text{diag}(1,1,1,1,1,1,1), H(0) = 1 \cdot \text{diag}(1 \cdot 10^{23}, 1 \cdot 10^{15}, 1 \cdot 10^{24}, 1 \cdot 10^{21}, 1 \cdot 10^{22}, 1 \cdot 10^{24}, 1 \cdot 10^{25}), l = 0.01, \gamma = 0.1$. The learn-

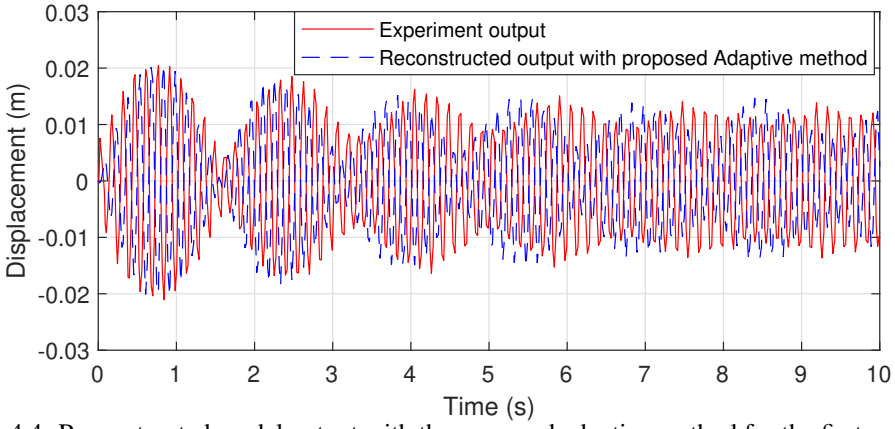

Figure 4.4: Reconstructed model output with the proposed adaptive method for the first mode system

ing gain of the gradient-based method in (4.26) is $\Gamma_1 = 1 \cdot \text{diag}(1 \cdot 10^{11}, 1 \cdot 10^{10}, 1 \cdot 10^{19}, 1 \cdot 10^{16}, 1 \cdot 10^{17}, 1 \cdot 10^{19}, 1 \cdot 10^{21})$. The initial value of the covariance matrix Γ_2 in the least-squares method (4.27) is $\Gamma_2(0) = 1 \cdot \text{diag}(1 \cdot 10^{10}, 1 \cdot 10^{16}, 1 \cdot 10^{17}, 1 \cdot 10^{21}, 1 \cdot 10^{24}, 1 \cdot 10^{23}, 1 \cdot 10^{27})$. Clearly, since a time-varying gain H is used to handle the effect of regressor, the tuning of learning gain for the proposed algorithm is easier than the gradient algorithm.

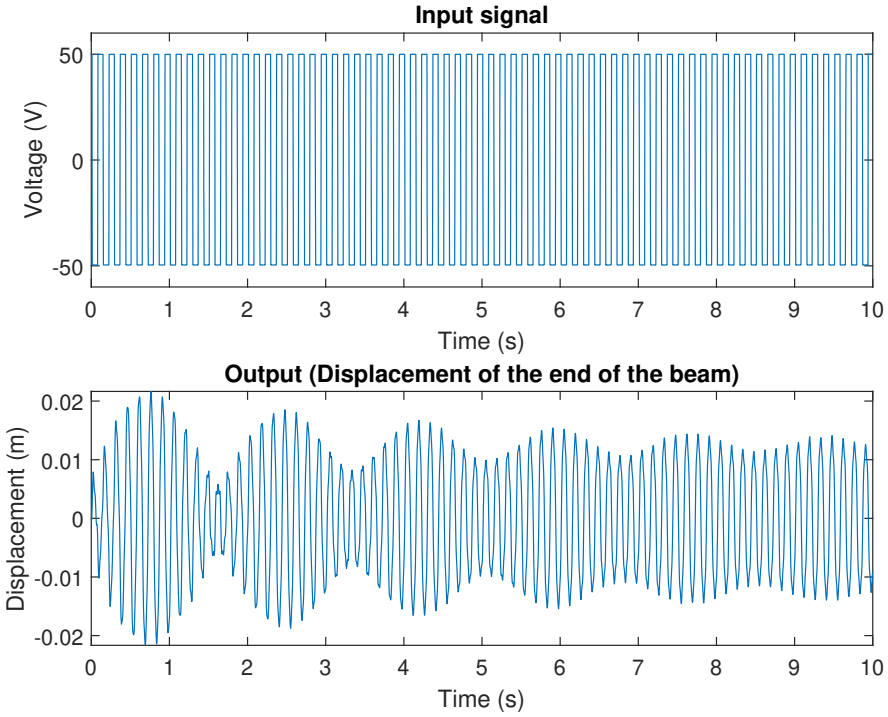

Figure 4.5: Input and output signals (experiment results)

Experimental results are given in Figure 4.5-Figure 4.7. Figure 4.5 describes the profile of the input and output signal collected from the test bench. The input signal is a square wave with amplitude 50 V and frequency 7 Hz. To alleviate the effect of the high-frequency electrical noises, a low-pass filter is applied before feeding into the estimation algorithm. The parameter estimation results of gradient method, least-squares method and the proposed adaptive method are shown in Figure 4.6. We can see that the proposed adaptive method (4.20) has an overall better performance compared to the gradient-based method

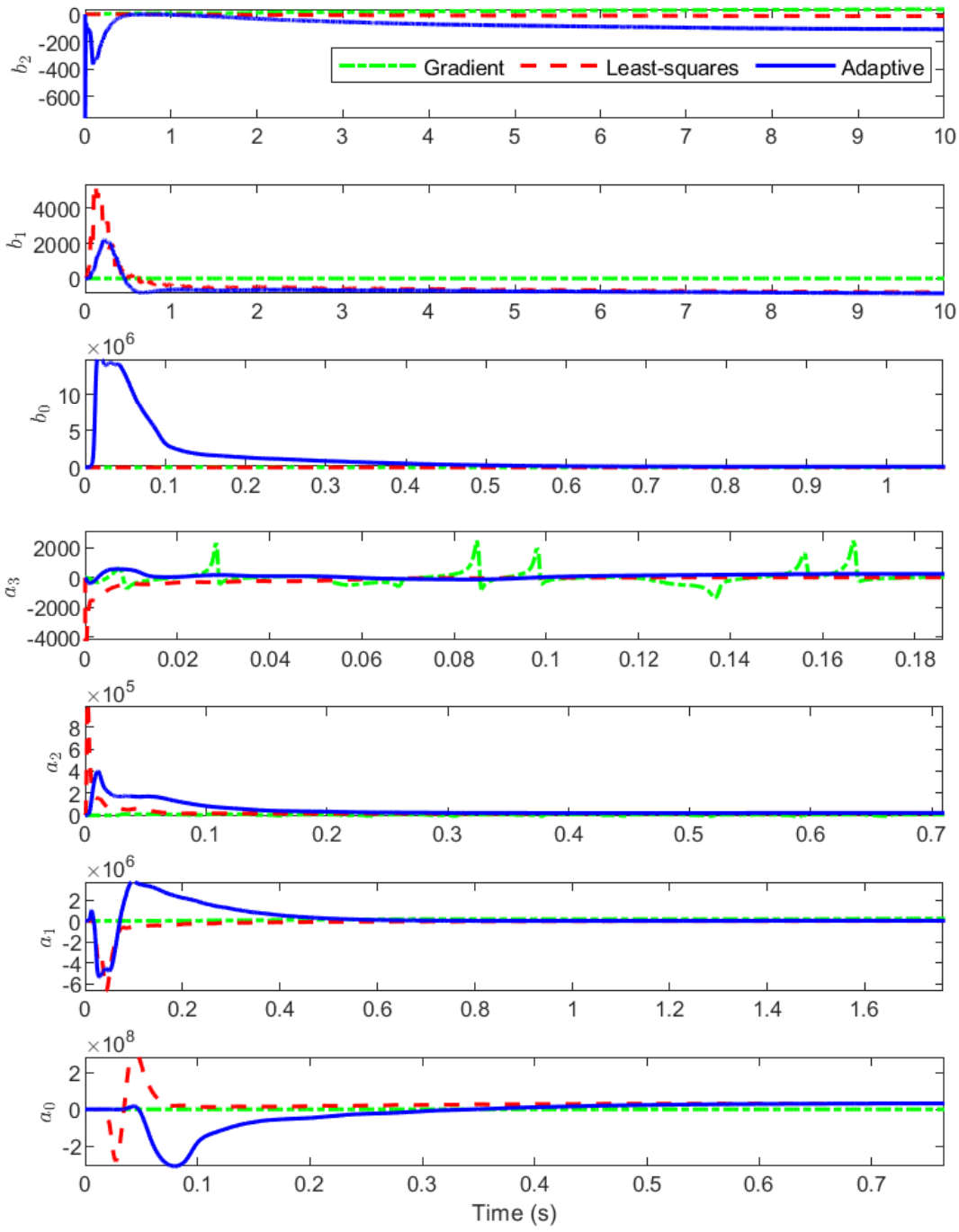

Figure 4.6: Comparative convergence performance of gradient method, least-squares method and the proposed adaptive method (experiment results)

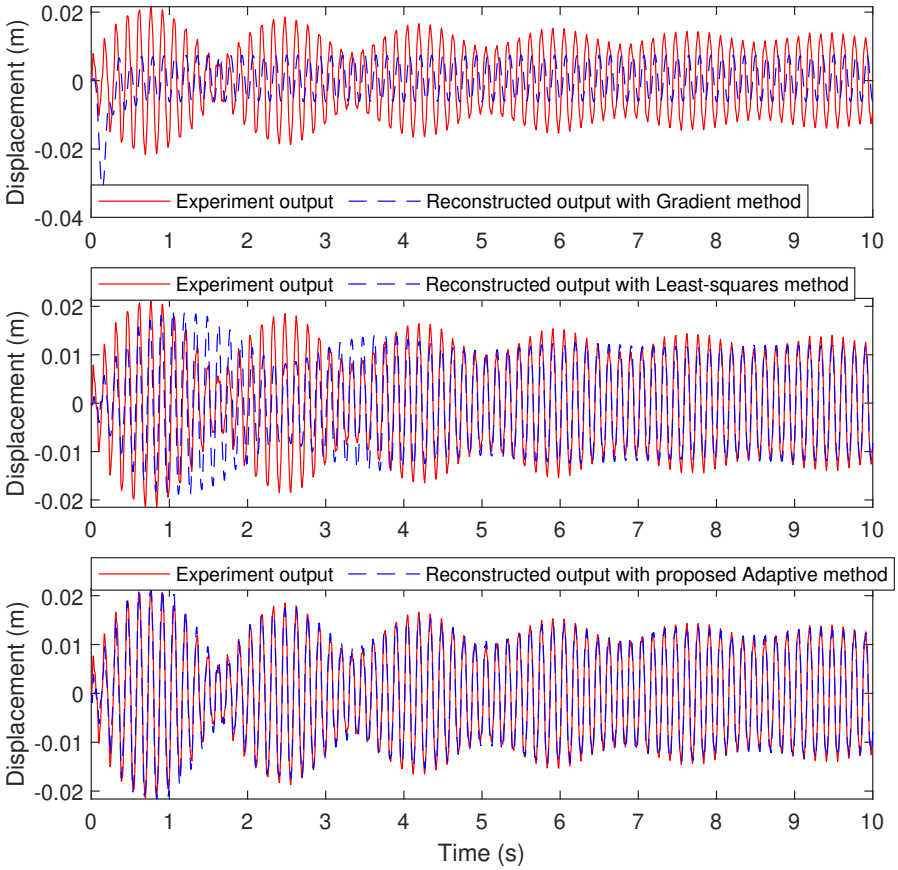

Figure 4.7: Reconstructed model output with gradient method, least-squares method and the proposed adaptive method

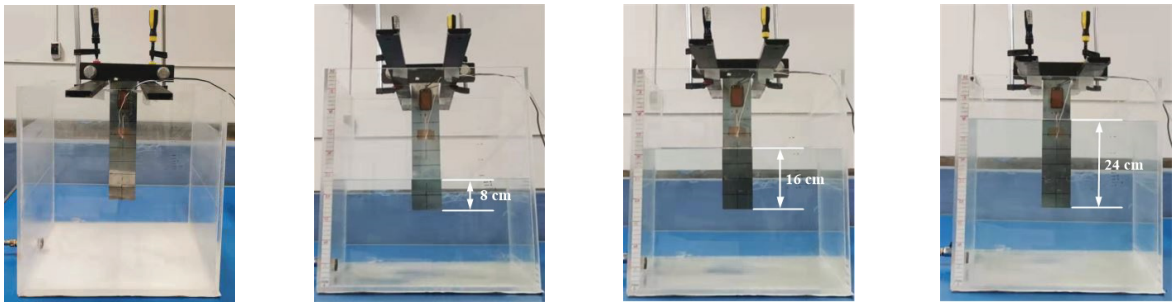

(a) Case 1: In air (b) Case 2: 8cm submerged (c) Case 3: 16cm submerged (d) Case 4: 24cm submerged

Figure 4.8: The beam submerged in different level of water

Table 4.2: Frequencies and damping ratios for the beam submerged in different level of water

	$\omega_1(rad/s)$	$\omega_2(rad/s)$	ζ_1	ζ_2
Case 1: In air	39.6432	197.0857	0.0155	0.2099
Case 2: 8cm submerged	20.4028	180.0480	0.1117	0.2723
Case 3: 16cm submerged	16.2501	123.4138	0.2442	0.3914
Case 4: 24cm submerged	14.4084	112.3138	0.3483	0.4825

(4.26) and the least-squares method (4.27). In particular, smaller oscillations of the parameters can be achieved with the proposed adaptive method. However, the gradient algorithm has a slow convergence rate and more oscillations or even steady-state errors in the estimated parameters. To illustrate the accuracy of the proposed approach, we further reconstruct and compare the output of the model using the estimated parameters with these three different methods. The measured output and model output with the estimated parameters are shown in Figure 4.7, from which we can see that the proposed method can accurately estimate the unknown model parameters and thus approximate the output dynamics of the real beam system. In contrast, the gradient method and the least-squares method can not achieve such a good performance. The gradient algorithm leads to steady-state errors in the model output, implying unprecise parameter estimation, while the least-squares method has a transient error during the first 3 sec, indicating a sluggish convergence for parameter estimation. These experimental results showcase the advantages of the proposed learning algorithm with the introduced time-varying gains.

To show the effectiveness of the proposed method for the beam submerged in fluid. Different level of water is filled in the box as shown in Figure 4.8. Comparative results for the beam submerged in different level of water are given in Table 4.2. From Table 4.2 we can see both of the first mode frequency and the second mode frequency of the submerged beam are less than the frequencies of the dry beam. For each mode of the submerged beam, the frequency decreases as the water level increases. Moreover, the damping of the submerged beam is larger than the dry beam. For the submerged beam, the damping increases as the water level increases.

4.5 Conclusion

This chapter developed a new adaptive parameter estimation approach for a cantilever beam modeled based on the Euler-Bernoulli theory. Taking into consideration of the first mode and second mode, the beam model is finally reduced to a fourth-order ODE. Then the adaptive parameter estimation method is proposed to estimate the unknown parameters. The estimation can be online achieved and only input and output signal is needed. Differentiation of the signals are avoided in the estimation procedure which is preferable in practice. At last, the convergence of the parameter estimation error is proved by suing Lyapunov theory. Simulation and experiment results show the effectiveness of the proposed method.

Part IV

Vibration Control of the Beam System

Chapter 5

Unknown System Dynamics Estimator based Vibration Control for the Beam System

5.1 Introduction

Unknown system dynamics (e.g. unmodelled dynamics, parameter perturbations and external disturbances) are unavoidable in the beam system. The disturbance observer based methods [25, 104–106] provide an effective way to address the lumped unknown dynamics. The vibration control performance for the beam system can be enhanced by including the estimated unknown dynamics because the lumped unknown dynamics can be compensated by the controller. In this chapter, we will take all the unmodelled dynamics, uncertainties, parameter perturbations and unknown disturbances as lumped unknown dynamics, an unknown system dynamics estimator will be proposed to cope with the lumped unknown dynamics of the beam system. To suppress the vibration of the beam, a feedback control law including the estimated dynamics will be developed.

5.2 State of art

In many applications that can be described by beams (e.g. turbine blades), different forces (e.g. flow forces) are imposed on the flexible beams. Control strategies play important roles on rejecting these external forces. If no control strategy is used, the vibration of the beam will last for a very long time once the beam is exerted by an external force. The vibration not only affects the performance of the applications, but also damages the structure and reduces the service life. In recent years, vibration suppression of the beam has been a research area of great interest.

In this section, we will review control strategies for the beam and beam in the fluid. In addition, unknown parameters estimation methods will be introduced when the accurate model can not be obtained in practice.

5.2.1 Classification of beam control

In order to control the beam, the control force can be applied at different position with different characteristics. In this regard, the control can be mainly divided into two types, i.e. boundary control and distributed control [107]. The main difference between boundary control and distributed control is the control force applied on the beam.

Boundary control is a method that applies control force at the boundary of the beam. It requires only a few actuators and sensors, and this feature makes it simple to implement in practical engineering. The idea of boundary control was firstly utilised on the systems described by the wave equations like strings [108], and then extended to other systems. In [109], the boundary control was introduced for the Timoshenko beam. For Euler-Bernoulli beam, a dynamic boundary force control and a dynamic boundary torque control are applied at the end of the clamped-free beam in [110]. For rotating beam problems, a rotating Timoshenko beam was investigated by using boundary control [111]; a shear beam was studied under boundary control by combining a decoupled controller and an observer [112]. For beams with input delay in boundary control, [113] introduced a feedback control law that makes the system exponentially stabilisation; [114] provided an observer-predictor based scheme to track and estimate the state in the stabilisation procedure of the system.

Compared with boundary control, distributed control increases the number of sensors and actuators in different points. With more feedback signals, distributed control can obtain a better performance. However, it will be more difficult to implement in practice. In [115], distributed control was used to design the control strategy for the active damper. The distributed control allows to control all the modes of vibration at once. Hence, one may avoid the spillover problems of the uncontrolled modes. In [116], the optimally controlled distributed forces effectively damps out the transient vibration of the beam. For the Euler–Bernoulli beam model with the tip payload, [117] proposed a distributed control in order to track a desired reference signal of the motion of the beam. It is proved that the tracking error is exponentially stable in a constrained space.

5.2.2 Classical beam control strategies

For the control strategies for the vibration suppression of the flexible beams, the most widely studied control methods of the beam can be summarized as follows.

5.2.2.1 PID control

Proportional, integral and derivative (PID) control is a well-known practical controller widely used in many industrial equipment. It has a simple structure and is easy to implement. A salient feature of PID control is it does not need the precise model of the system. Although PID control can deal well with simple linear systems, it is difficult for it to get a good control performance for high-order systems and nonlinear systems. PID control algorithm is described as

$$u = K_p e + K_i \int_0^t e dt + K_d \frac{d}{dt} e \tag{5.1}$$

where u is the control action, e is the error, K_p is proportional gain, K_i is integral gain and K_d is derivative gain.

For beam control problem, [118] provided an experimental result of PID control for flexible steel can-

tilever beam by using piezoelectric actuators. In [119], a mathematical beam model was introduced and corresponding PID control is designed. Similar modelling procedure and PID-based control algorithm can also be found in [120] and [24].

5.2.2.2 Optimal control

Optimal control deals with finding a control law for the dynamic system over a period time such that the cost function is optimized. The cost function is generally defined as

$$J = \int_0^T \left(\mathbf{x}^T \mathbf{Q} \mathbf{x} + u^T \mathbf{R} u\right) dt \tag{5.2}$$

where $\mathbf{x}$ is the state vector of the system, u is the control action. $\mathbf{Q}$ and $\mathbf{R}$ are positive matrices.

Optimal control strategies are investigated for the vibration control of different beams in many literature. In [26], a minimax linear–quadratic–Gaussian (LQG) optimal control was proposed which minimizes the total vibration energy in the beam. A digital regulator is designed and experimentally implemented for a flexible beam type structure containing piezoelectric sensors and actuators by using optimal control design techniques in [121]. For beams controls considering time delay, a discrete optimal control algorithm [122] was designed based on the augmented state system. [123] addressed the issue of the active vibration control of the transverse modes in a flexible elastic systems by applying the optimal forces on a sets of piezoelectric actuators.

5.2.2.3 Robust control

In order to address the uncertainties and unknown dynamics, robust control is introduced to control flexible beams. In [124], a distributed parameter H_∞ method is proposed for an Euler-Bernoulli beam with Kelvin-Voigt damping. Finite dimensional suboptimal controllers are derived and show robust stabilization in the presence of unmodelled time delays. In [125], a mixed H_2/H_∞ control is presented for the purpose of vibration suppression of a clamped-free smart beam with piezoelectric actuator and vibrometer sensor in the linear matrix inequality (LMI) framework. The robust controller with a regional pole placement constraint is designed based on the augmented plant composed of the nominal model and its accompanied uncertainty by solving a convex optimization problem.

There are also several other control methods that can be suitable on the beam control problems. For the Euler-Bernoulli beam, [126] introduced active disturbance rejection and sliding mode control approach to attenuate the external disturbances and stabilize the beam. In [127], an adaptive boundary iterative learning control was proposed based on a time-weighted Lyapunov-Krasovskii-like composite energy function. To deal with the uncertainty, three adaptive laws are designed and learned in the iteration domain. In [27], a semi-active control method was proposed for the vibration control of a sandwich beam.

Although there are many control strategies proposed for various beams, very few control methods are focusing on the beams immersed in fluid. However, the beam-fluid interaction problem is increasingly getting attention in hydrodynamic applications [50]. In [128], vibration amplitude of a cantilever beam immersed in fluid was controlled according to a closed-loop velocity proportional feedback control approach. The equation of motion of coupled fluid-structure system was solved by Galerkin methods. For different flows contacting with beams, there are still many problems (e.g. parametric perturbations, unmodelled dynamics and time delays) need to be further investigated. To control the beam submerged

in fluid, new control strategies and disturbance rejection techniques are required to conduct further investigations.

5.2.3 Disturbance observer based methods

In real applications, it is unavoidable to cope with the unknown dynamics (e.g. unmodelled dynamics and unknown disturbances) which may deteriorate the control performance. In recent years, lots of attentions have been attracted on this problem. For the elastic structures, it is nearly impossible to have the complete system description for the control purpose. In such cases, unknown system dynamics estimator plays an important role on addressing the unknown dynamics.

Vibration control is commonly applied on the flexible systems to suppress the vibration. The problem in the vibration control is that the unknown forces or torques can not be directly measured. These forces can only be computed indirectly by the resulting vibrations. As a result, apart from the control of vibration, it is essential to compensate the unknown forces which lead to the vibration. In [25], a disturbance observer (DO) is designed for a Timoshenko beam under distributed disturbances. DO-based boundary control is introduced to stabilize vibrations of the beam. In [129], a proportional integral observer (PIO) is proposed to estimate the unknown inputs for the flexible beam. As a special modification of DO, the PIO is mainly designed for detection of faults and estimation of nonlinear affects (e.g. fraction and backlash). This work show the effectiveness of the estimation of the force in practice. In [130], a modified PIO is further developed for the estimation of the unknown forces of the elastic structure. Improved robustness is achieved accounting for the measurement noise.

Taking the lumped unknown dynamics as an extra state, extended state observer (ESO) provides another scheme to estimate the unknown terms [104, 105]. In [131], an ESO-based LQR control is designed for the ball and beam system with disturbances and uncertainties. To avoid accurate high-order model of the system, a simpler model is used in the controller. An ESO-based controller is designed which shows good robustness to the disturbances. In [132], a high-gain ESO is proposed to compensate the unknown dynamics of the flexible beam. Based on the high-gian ESO, the ADRC is presented to supress the vibration of the beam. The boundedness of the closed-loop system is proved by a frequency domain method. For the Euler-Bernoulli beam, an ESO is proposed to estimate the disturbance and canceled online in [126], where ADRC and SMC are constructed respectively.

For distributed systems, an infinite dimensional disturbance estimator is proposed to determine the unknown dynamics for the Euler-Bernoulli beam in [133]. Based on the estimator, a state observer and two tyeps of velocity feedback controllers are constructed. In [134], the distributed disturbance estimator is proposed for the wave equation described by PDE. It is proved that the estimator is capable to estimate the unknown dynamics.

Along with the rapidly growth of the artificial intelligence, neural network estimators are of great interests in recent years. In [135], a flexible spacecraft is investigated which uses NN to estimate the nonlinearities and uncertainties. The estimated terms are then incorporated into the adaptive control. In [106], the NN is constructed to estimate the natural frequencies of a steel beam. For the beam with a surface crack, a NN-based identification method is proposed to identify the crack locations and depth. Compared with the multi-layer perceptron network, the proposed RBFNN takes less computational time at the training procedure.

Although the above-mentioned estimation methods can satisfy certain applications, tuning of the

parameters is still not trivial. For the NN-based estimation approaches, it is time consuming to online estimate the unavoidable unknown system dynamics. In real applications, a simple structure of the estimator is preferable.

In this chapter, we will take all the unmodelled dynamics, uncertainties, parameter perturbations and unknown disturbances as lumped unknown dynamics, a new unknown system dynamics estimator (USDE) will be proposed to estimate the unknown dynamics. An USDE-based controller will be designed to suppress the vibration of the beam.

5.3 Unknown system dynamics estimation

In this section, we will propose an estimator to capture the unknown dynamics of the beam system. In addition, radial basis function neural network (RBFNN) and the extended state observer (ESO) will be presented for comparison.

5.3.1 Design of the unknown system dynamics estimator

We recall the Galerkin model (2.106) with unknown system dynamics F_w as

$$\begin{cases} \dot{x}_1 = x_2 \\ \dot{x}_2 = -k_1 x_1 - c_1 x_2 + b_1 u + F_w \\ y = x_1 \end{cases} \tag{5.3}$$

In this subsection, we mainly focus on the estimation of the lumped unknown system dynamics F_w. We assume F_w and its derivative are bounded, i.e., $\sup_{t>0} |\dot{F}_w| \leq \bar{F}_w$ holds for a constant $\bar{F}_w > 0$. To reconstruct the unknown dynamics F_w, we first define a set of filtered variables as

$$\begin{cases} k_f \dot{x}_{1f} + x_{1f} = x_1, & x_{1f}(0) = 0 \\ k_f \dot{x}_{2f} + x_{2f} = x_2, & x_{2f}(0) = 0 \\ k_f \dot{u}_f + u_f = u, & u_f(0) = 0 \end{cases} \tag{5.4}$$

where $k_f > 0$ is a positive filter parameter.

The USDE can be designed as

$$\hat{F}_w = \frac{x_2 - x_{2f}}{k_f} + k_1 x_{1f} + c_1 x_{2f} - b_1 u_f \tag{5.5}$$

The convergence property of the USDE can be given as

Lemma 5.1. *For system (5.3) with the USDE (5.5), the estimation error $\tilde{F}_w = F_w - \hat{F}_w$ is bounded as*

$$\|\tilde{F}_w\| \leq \sqrt{\tilde{F}_w^2(0) e^{-\frac{t}{k_f}} + k_f^2 \bar{F}_w^2} \tag{5.6}$$

and thus $\hat{F}_w \to F_w$ holds for any $k_f \to 0$ and/or $\bar{F}_w \to 0$.

Proof. We apply a low-pass filter on both sides of the second equation in (5.3), one can obtain

$$\dot{x}_{2f} = -k_1 x_{1f} - c_1 x_{2f} + b_1 u_f + F_{wf} \tag{5.7}$$

where F_{wf} given by $k_f \dot{F}_{wf} + F_{wf} = F_w$ is the filtered variable of F_w.

To avoid using the filtered acceleration signal $\dot{x}_{2f}$, one can rewrite the second equation of (5.4) as

$$\dot{x}_{2f} = \frac{x_2 - x_{2f}}{k_f} \tag{5.8}$$

By substituting (5.8) into (5.7) along with (5.5), one can obtain $\hat{F}_w = F_{wf}$. This means the USDE (5.5) deduces the filtered version of the lumped unknown dynamics.

From the definition $\tilde{F}_w = F_w - \hat{F}_w$ and the fact $\dot{F}_{wf} = -\frac{1}{k_f}F_{wf} + \frac{1}{k_f}F_w = \frac{1}{k_f}\tilde{F}_w$, one can obtain the derivative $\dot{\tilde{F}}_w$ as

$$\dot{\tilde{F}}_w = \dot{F}_w - \dot{F}_{wf} = \dot{F}_w + \frac{1}{k_f}F_{wf} - \frac{1}{k_f}F_w = -\frac{1}{k_f}\tilde{F}_w + \dot{F}_w \tag{5.9}$$

We choose a Lyapunov candidate function as

$$V = \frac{1}{2}\tilde{F}_w^T\tilde{F}_w \tag{5.10}$$

The time derivative of (5.10) can be calculated along with (5.9) as

$$\dot{V} = \tilde{F}_w^T\dot{\tilde{F}}_w \leq -\frac{1}{k_f}\tilde{F}_w^T\tilde{F}_w + \tilde{F}_w^T\dot{F}_w \tag{5.11}$$

By using the Young's inequality $\tilde{F}_w^T\dot{F}_w = \frac{\tilde{F}_w^T\tilde{F}_w}{2k_f} + \frac{k_f}{2}\dot{F}_w^T\dot{F}_w$, (5.11) can be further written as

$$\dot{V} \leq -\frac{1}{k_f}\tilde{F}_w^T\tilde{F}_w + \frac{\tilde{F}_w^T\tilde{F}_w}{2k_f} + \frac{k_f}{2}\dot{F}_w^T\dot{F}_w \leq -\frac{1}{k_f}V + \frac{k_f}{2}\bar{F}_w^2 \tag{5.12}$$

Then we can deduce that the estimation error $\tilde{F}_w$ is bounded by $\|\tilde{F}_w\| \leq \sqrt{\tilde{F}_w^2(0)e^{-\frac{t}{k_f}} + k_f^2\bar{F}_w^2}$. Hence, we can conclude that $\tilde{F}_w$ can exponentially converge to zero as $k_f \to 0$ and/or $\bar{F}_w \to 0$. □

Remark 5.1. *To implement the proposed USDE (5.5), the designing parameter k_f in the filter (5.4) needs to be determined appropriately. The parameter k_f can not be chosen too large due to the phase lag. A small k_f can reduce the ultimate estimation error, while a too small one may make the system sensitive to noise. As a result, a trade-off between the estimation performance and the robustness should be appropriately made.*

5.3.2 Comparison to other estimators

In order to show the advantages of the proposed USDE, we compare with some other estimators. One is the radial basis function neural network (RBFNN), which is a function approximator. Another estimator selected is the extended state observer (ESO).

5.3.2.1 Radial basis function neural network (RBFNN)

For the unknown function approximation, radial basis function (RBF)NN is distinguished from other networks because of its universal approximation and fast learning speed [136]. In control engineering, RBFNN can be used to modelling unknown system dynamics due to its good capability on unknown function approximation [137]. Any function can be approximated within an arbitrary small error by using an RBFNN provided there are enough neurons [138]. The RBFNN has one input layer, one hidden layer and one output layer. The number of neurons in the input layer is related to the number of inputs. The input neurons normalise the inputs and feed them into the hidden layer. The hidden layer conducts a nonlinear transformation commonly by using Gaussian activation functions to obtain a variable number of neurons. The output layer generates the prediction which is a linear summation of the hidden layer's outputs multiplied by the corresponding NN weights. In this this layer, the NN weights need to be online updated. In this chapter, the following linearly parameterized RBFNN is used to approximate the

unknown danamics $F_w(\mathbf{u_w})$

$$F_w(\mathbf{u_w}) = \Psi_w^T(\mathbf{u_w})W \tag{5.13}$$

where $W = [w_1, w_2, \ldots, w_n]^T \in R^n$ is the NN weight vector and n is the neuron number; $\Psi_w(\mathbf{u_w}) = [\Psi_{w1}(\mathbf{u_w}), \Psi_{w2}(\mathbf{u_w}), \ldots, \Psi_{wq}(\mathbf{u_w})]^T$ is the regressor vector with $\Psi_{wi}(\mathbf{u_w})$ being chosen as the following Gaussian functions

$$\Psi_{wi}(\mathbf{u_w}) = \exp\left[\frac{-(\mathbf{u_w} - \mu_i)^T(\mathbf{u_w} - \mu_i)}{\varsigma_i^2}\right], \quad i = 1, 2, \ldots, q \tag{5.14}$$

where $\mathbf{u_w} = [u_{w1}, u_{w2}, \ldots, u_{wj}]^T$ is the input vector, μ_i are the neuron's centers and ς_i are the width of the Gaussian functions. The overall structure of the RBFNN is shown in Figure. 5.1.

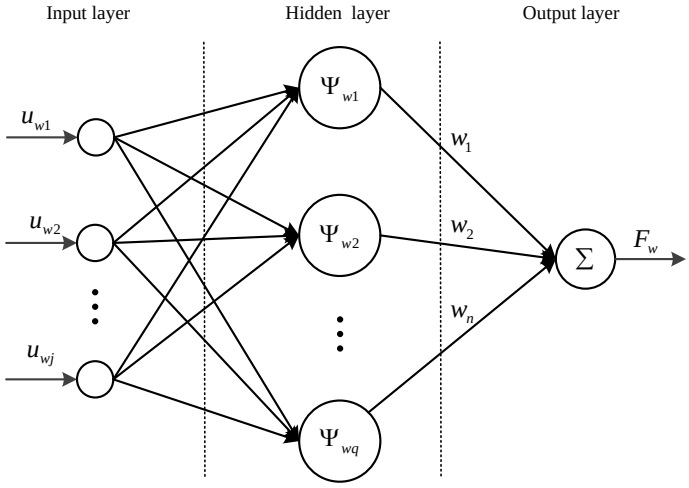

Figure 5.1: Overall structure of RBFNN

It has been proved that the RBFNN (5.13) is capable to approximate any continuous function to an arbitrary accuracy given enough neurons. The approximation can be written as

$$F_{ww}(\mathbf{u_w}) = \Psi_w^T(\mathbf{u_w})W^* + \xi \tag{5.15}$$

where W^* are the ideal NN weights and ξ is the NN approximation error.

Note that the ideal NN weights W^* presented in (5.15) is only for analytical purpose. W^* is defined as follows [137]

$$W^* \triangleq \arg\min_{W \in R^n} \left\{ \sup_{\mathbf{u_w} \in R^q} \left| F_{ww}(\mathbf{u_w}) - \Psi_w^T(\mathbf{u_w})W \right| \right\}. \tag{5.16}$$

The following assumption is widely accepted and applied for the RBFNN:

Assumption 5.1. *The ideal NN weights exist and the approximation error ξ is bounded by $\|\xi\| \leq \xi^*$ with constant $\xi^* > 0$.*

Remark 5.2. *Compared to other NN approximations (e.g. multi-layer neural network), the RBFNN has a linear parameterized form which is much easier to design and implement. Another salient feature in the RBFNN structure is only one NN weight vector requires to be online updated. A wide class of adaptive law can be tailored to drive the RBFNN approximator.*

For the beam system (5.3), the lumped unknown dynamics including parameter uncertainties and unknown disturbances $\hat{F}_w$ can be estimated by using the RBFNN as

$$\hat{F}_w = \Psi_w^T(\mathbf{u_w})W \tag{5.17}$$

By defining auxiliary variables P, Q and M as

$$\begin{cases} \dot{P} = -lP + \Psi_w^T \Psi_w \\ \dot{Q} = -lQ + \Psi_w^T \left[(x_2 - x_{2f}) / k_f + k_1 x_1 + c_1 x_2 - b_1 u \right]^T \\ M = P\hat{W} - Q \end{cases} \tag{5.18}$$

the weighted parameter updating law can be designed as

$$\dot{\hat{W}} = \Gamma_w M \tag{5.19}$$

where $\Gamma > 0$ is a designed diagonal matrix.

5.3.2.2 Extended state observer (ESO)

As stated in [104], ESO takes the lumped unknown dynamics as a new state variable. We define $x_3 = F_w$ and denote $\dot{x}_3 = h(t)$, then the beam system (5.3) can be rearranged as

$$\begin{cases} \dot{x}_1 = x_2 \\ \dot{x}_2 = -k_1 x_1 - c_1 x_2 + b_1 u + x_3 \\ \dot{x}_3 = h(t) \\ y = x_1 \end{cases} \tag{5.20}$$

A high-gain observer can be designed to estimate the states of the extended system (5.20) as [104]

$$\begin{cases} \dot{\hat{x}}_1 = \hat{x}_2 - \lambda_a (\hat{x}_1 - x_1) \\ \dot{\hat{x}}_2 = -k_1 x_1 - c_1 x_2 + b_1 u + \hat{x}_3 - \lambda_b (\hat{x}_1 - x_1) \\ \dot{\hat{x}}_3 = -\lambda_c (\hat{x}_1 - x_1) \end{cases} \tag{5.21}$$

where λ_a, λ_b and λ_c are the feedback gains of the observer. $\hat{x}_3$ is the estimation of the unknown dynamics F_w. The explanation of choosing observer gains λ_a, λ_b and λ_c can be found in [104].

Remark 5.3. *Compared to the RBFNN (5.17), ESO (5.21) and the proposed USDE (5.5) have simpler structures which are easier to realize and tune for designers. A salient feature of the proposed USDE (5.5) is only one designing parameter need to be adjusted while the ESO and RBFNN have more coefficients have to be determined.*

5.4 USDE-based controller design

After obtaining the estimation of the unknown system dynamics $\hat{F}_w$ in (5.5), we introduce a composite control for the beam system (5.3) in this section.

To achieve the goal of vibration suppression, we define an auxiliary variable including the control error x_1 and its derivative x_2 as

$$z = \alpha_2 x_1 + x_2 \tag{5.22}$$

where $\alpha_2 > 0$ is a positive constant. As noted in [139], x_1 is bounded as long as z is bounded. For real-time control, we use Euler method to obtain x_2 from x_1. The error deduced from Euler method is ignored in the controller design.

Then we can design the USDE based controller as

$$u = \frac{1}{b_1} \left(-\beta_2 z + k_1 x_1 + c_1 x_2 - \alpha_2 x_2 - \hat{F}_w \right). \tag{5.23}$$

The closed-loop system stability with the controller (5.23) and the USDE (5.5) is shown in the following theorem.

Theorem 5.1. *Consider the beam system (5.3), the controller (5.23) and the USDE (5.5), the error variable z and the estimation error $\tilde{F}_w$ will converge to a small region around zero.*

Proof. We select a Lyapunov function as

$$V = \frac{1}{2}z^2 + \frac{1}{2}\tilde{F}_w^2. \tag{5.24}$$

The time derivative of V can be calculated as

$$\begin{aligned}
\dot{V} &= z \cdot \dot{z} + \tilde{F}_w \cdot \dot{\tilde{F}}_w \\
&= z \cdot (\alpha_2 x_2 + \dot{x}_2) + \tilde{F}_w \cdot \dot{\tilde{F}}_w \\
&= z(\alpha_2 x_2 - k_1 x_1 - c_1 x_2 + b_1 u + \hat{F}_w + \tilde{F}_w) + \tilde{F}_w \cdot \dot{\tilde{F}}_w \\
&= z(-\beta_2 z + \tilde{F}_w) + \tilde{F}_w \cdot \dot{\tilde{F}}_w \\
&= -\beta_2 z^2 + z \cdot \tilde{F}_w + \tilde{F}_w \cdot \dot{\tilde{F}}_w \\
&= -\beta_2 z^2 + z \cdot \tilde{F}_w + \tilde{F}_w \cdot (-\frac{1}{k_f}\tilde{F}_w + \dot{F}_w) \\
&= -\beta_2 z^2 \phi - \frac{1}{k_f}\tilde{F}_w^2 + z \cdot \tilde{F}_w + \tilde{F}_w \cdot \dot{F}_w \\
&\leq -\beta_2 z^2 \phi - \frac{1}{k_f}\tilde{F}_w^2 + \frac{1}{2}z^2 + \frac{1}{2}\tilde{F}_w^2 + \frac{1}{2}\tilde{F}_w^2 + \frac{1}{2}\dot{F}_w^2 \\
&\leq -(\beta_2 - \frac{1}{2})z^2 - (\frac{1}{k_f} - 1)\tilde{F}^2 + \frac{1}{2}\bar{F}_w^2 \\
&\leq -\tau_3 V + \xi_3
\end{aligned} \tag{5.25}$$

where $\tau_3 = \min\{\beta_2 - 1/2, 1/k_f - 1\}$ is a positive constant as long as $\beta_2 > 1/2$ and $0 < k_f < 1$, $\xi_3 = 1/2\bar{F}_w^2$. Then the ultimate bounds of z and $\tilde{F}_w$ can be obtained by solving the inequality (5.25) as $V(t) \leq e^{-\tau_3 t}V(0) + \xi_3/\tau_3$. This implies z and $\tilde{F}_w$ all exponentially converge to a small region defined by $\Omega := \left\{z, \tilde{F}_w \mid \|z\| \leq \sqrt{2\xi_3/\tau_3}, \|\tilde{F}_w\| \leq \sqrt{2\xi_3/\tau_3}\right\}$. Then we can conclude that the errors z and $\tilde{F}_w$ are bounded and the ultimate bounds are determined by the variation rate of the lumped unknown dynamics $\sup_{t>0}|\dot{F}_w| \leq \bar{F}_w$. This further implies the control error x_1 converge to zero. □

5.5 Simulations

In this section, we will provide comparative results to illustrate the effectiveness of the proposed USDE (5.5) and the USDE-based controller (5.23). We let the tip of the beam release at a distance at 0.01m, then we compare the estimation results during the vibration and the control performance with PD control and USDE-based control.

The filter coefficient of (5.4) is chosen as $k_f = 0.001$, the feedback gains in the controller (5.23) are set as $\alpha_2 = 20, \beta_2 = 100$. We let $\hat{F}_w = 0$ in (5.23) and a PD controller is formed.

From Figure 5.2 we can see the estimation of the unknown dynamics with the proposed USDE (5.5) has a fairly good estimation performance. We release the tip of the beam at a distance of 0.01m, the vibration control results are shown in Figure 5.3. Both the PD control and the USDE-based control can

suppress the vibration of the beam. The USDE-based control has a faster response compared with the PD control. In addition, the steady-state error can reach to zero with the proposed USDE-based control in a short time. This is because the lumped unknown dynamics can be estimated with the help of (5.5) and then compensated into the USDE-based controller (5.23).

To show the advantage of the proposed USDE, we will compare the USDE with the RBFNN approximation approach and the ESO method. The parameters of the RBFNN are chosen as $u_w = [x_1, x_2]^{\mathrm{T}}$, $\mu_{j,i} = \begin{bmatrix} -10 & -5 & 0 & 5 & 10 \\ -10 & -5 & 0 & 5 & 10 \end{bmatrix}$ and $\varsigma_i = 5$, $i = 1, 2, 3, 4, 5$. The parameters of the adaptive law (5.19) are set as $\Gamma_w = 1 \cdot \mathrm{diag}(1 \times 10^4, 1 \times 10^4, 1 \times 10^4, 1 \times 10^4, 1 \times 10^4)$, $l = 1 \cdot \mathrm{diag}(800, 800, 800, 800, 800)$. The parameters of ESO are selected as $s^3 + \lambda_a s^2 + \lambda_b s + \lambda_c = (s + 1000)^3$ for the trade-off between robustness and the estimation performance. The comparative results are given in Figure 5.4 and Figure 5.5. It is shown that the three estimators can all have a good estimation after a short time. However, the ESO has a large overshoot at the transient state which is not desired. One may see from Figure 5.5 the proposed USDE has a better estimation accuracy compared with the RBFNN and the ESO. Although the RBFNN can achieve better performance by increasing the number of neurons, the computational cost would be increased at the same time. For the ESO, a larger observer gain can improve the estimation performance. However, a very large gain will make the system sensitive to noise.

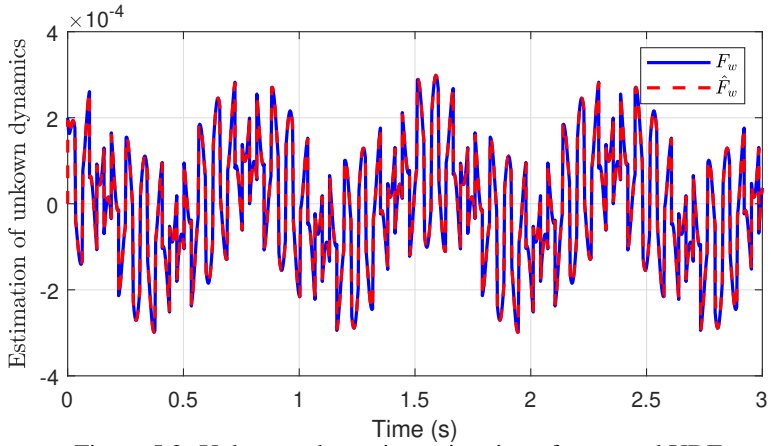

Figure 5.2: Unknown dynamics estimation of proposed UDE

To further illustrate the effectiveness of the proposed USDE-based control, a higher order (20th-order) model will be used to simulate the system dynamics which is more close to the reality. We select the number of nodes in (2.85) as $K = 10$. Then a twentieth-order model is constructed to describe the system dynamics. In the controller design, the second order model (5.3) is retained. Comparative results are shown in Figure 5.6 - Figure 5.8. We can see both the PD control and the USDE-based control can suppress the vibration. The advantage of the USDE-based control is a smoother response can be achieved without any overshoot. This lies in the compensation of the proposed estimator (5.5).

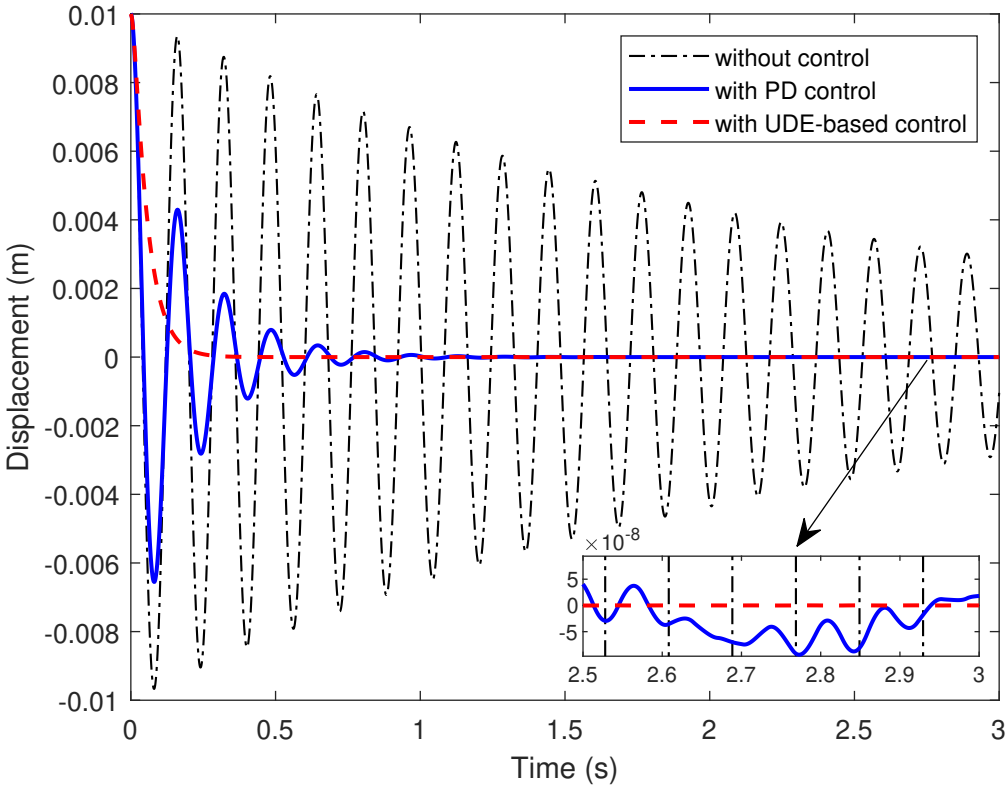

Figure 5.3: Vibration control performance with PD control and the proposed UDE-based control

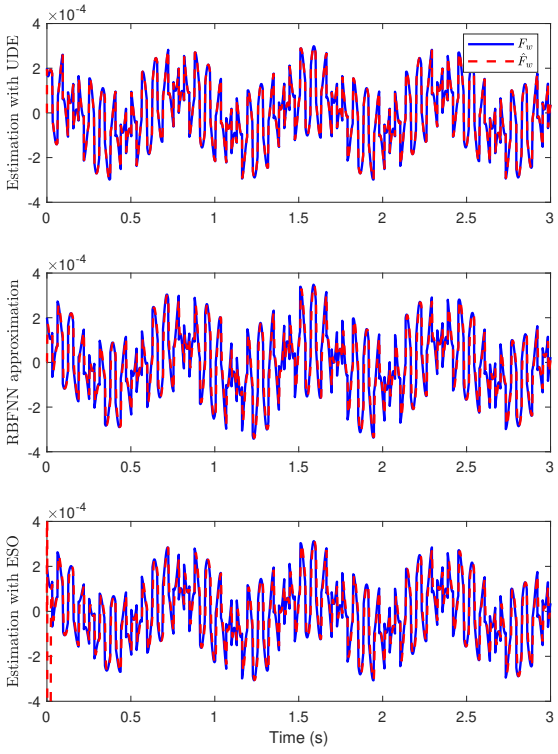

Figure 5.4: Estimation performance with the proposed UDE, RBFNN approximation and ESO

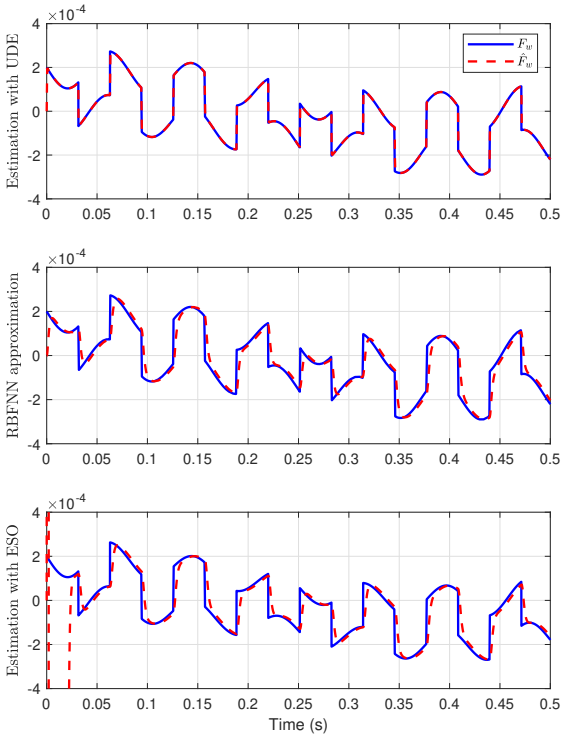

Figure 5.5: The room-in plot of Figure 5.4

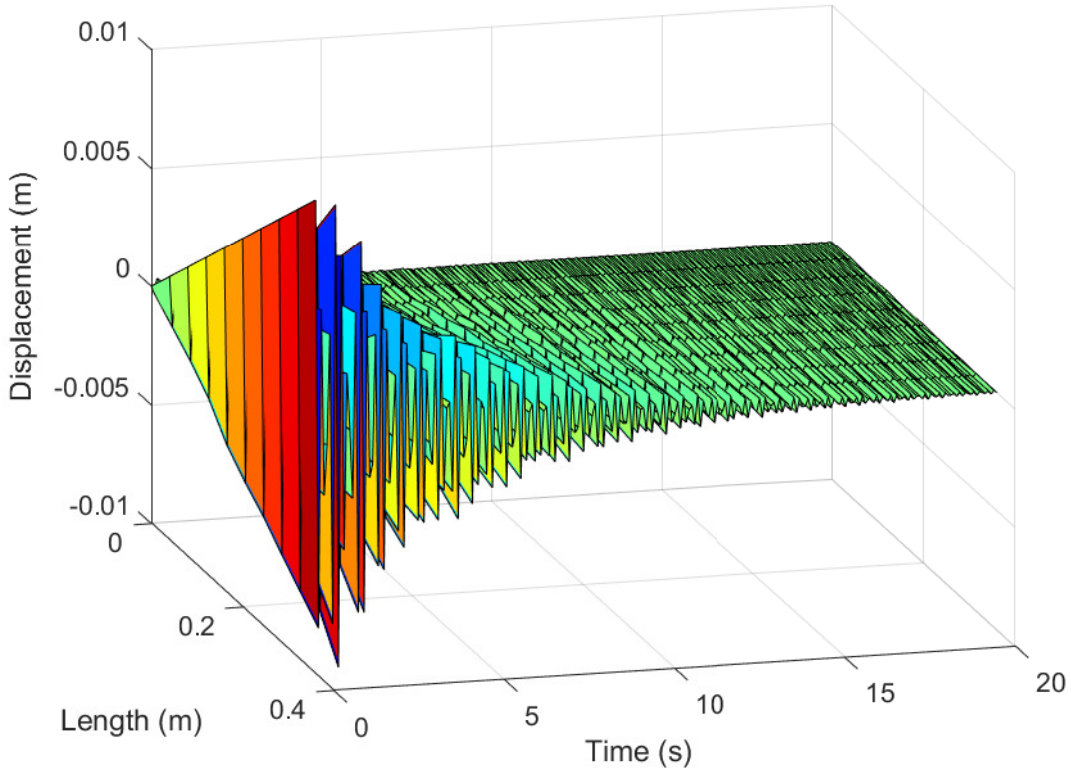

Figure 5.6: Vibration of the beam without control

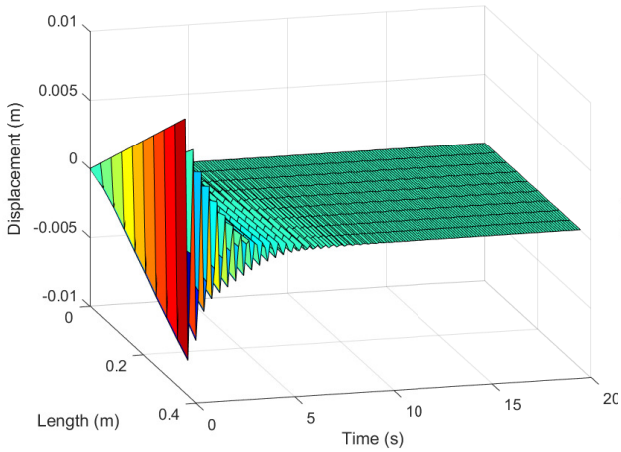

Figure 5.7: Vibration control of the beam with PD control

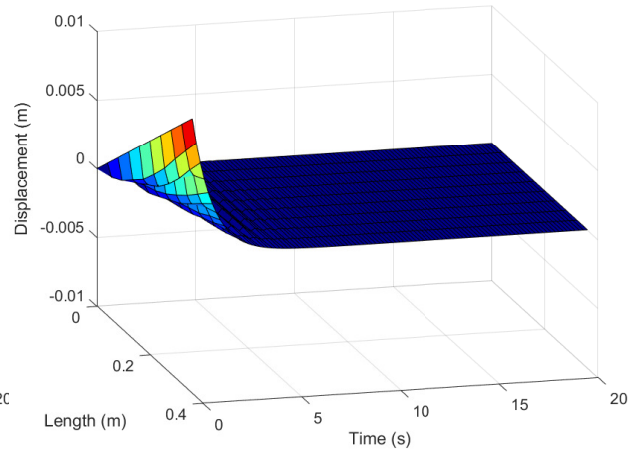

Figure 5.8: Vibration control of the beam with proposed UDE-based control

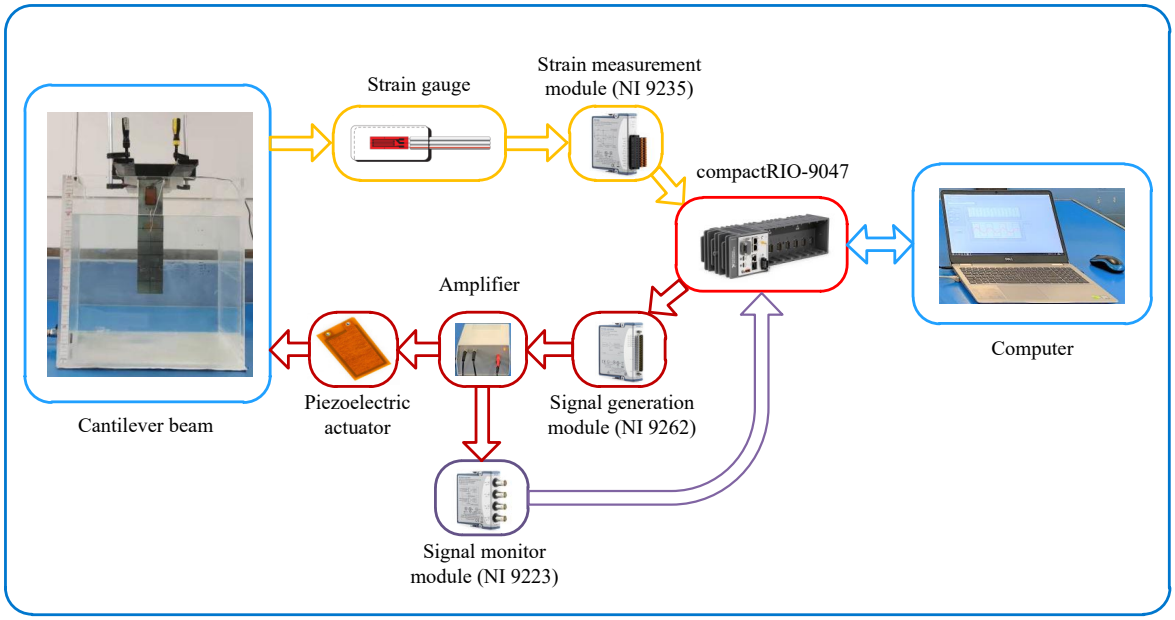

Figure 5.9: Overall hardware configuration of the beam system

5.6 Experiments

The overall hardware configuration for the control of the beam is given in Figure 5.9.

In the experiments, the sampling rate of the compactRIO-9047 is set as $fs = 800Hz$. The parameters of the PD control is set as $k_p = 200000, k_d = 0.15$. The filter parameter in (5.5) is chosen as $k_f = 0.002$. The parameters in the USDE-based control (5.23) are selected as $\alpha = 540, \beta = 1500$.

We release the tip of the beam at a distance at 0.01m, the experimental results are given in Figure 5.10 and Figure 5.11. It is shown both the PD control and the USDE-based control can suppress the vibration. Clearly, the proposed USDE-based control has a better control performance compared with the PD control. With the proposed USDE-based control, the beam can be stabilized within a very short time (roughly 2 seconds). In contrast, the PD control need a longer time to achieve the same performance.

To show the effectiveness of the vibration suppression for the submerged beam, we submerged 1cm of the beam in water. Because the damping of the submerged beam is much larger than the dry beam. We release the submerged beam at a distance of 2cm, the results are described in Figure 5.12. It is shown the vibration of the submerged beam can be reduced with the USDE-based control. However, the control signal is not large enough to impose a larger force on the beam. As shown in Figure 5.13, The control signal is saturated at $-100V$ and $250V$ due to the limit of the hardware.

5.7 Conclusions

In this chapter, an alternative estimator based vibration control strategy is proposed to both suppress the vibration and estimate the unknown system dynamics. Different to the function approximation based methods, the proposed control has a simple structure which is more realistic to implement in practice. In the proposed estimator, only one parameter need to be tuned depends on the bandwidth of the filter. The estimated unknown dynamics is compensated into the controller and thus makes the system more robust

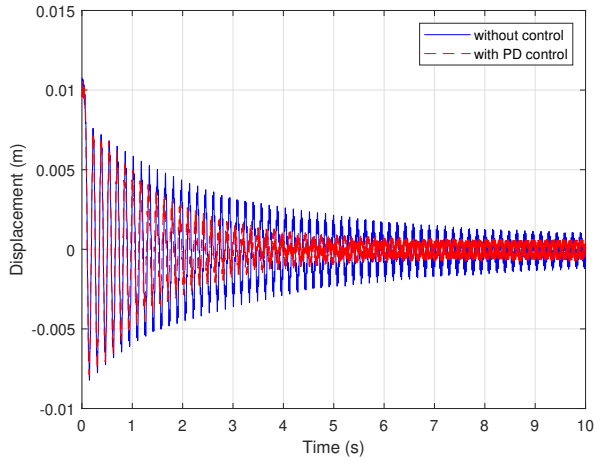

Figure 5.10: Tip displacement of the beam with and without PD control (experiment results)

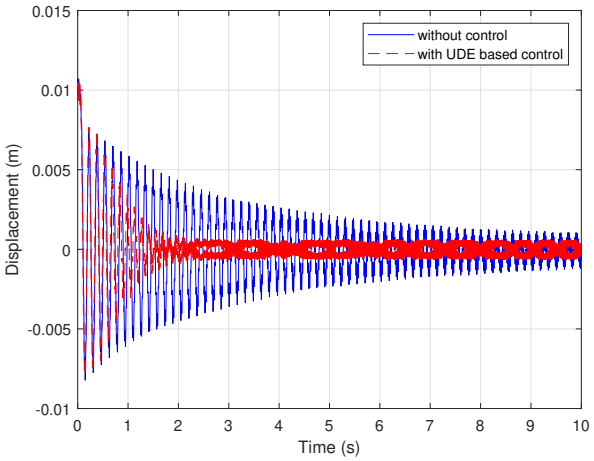

Figure 5.11: Tip displacement of the submerged beam with and without USDE based control (experiment results)

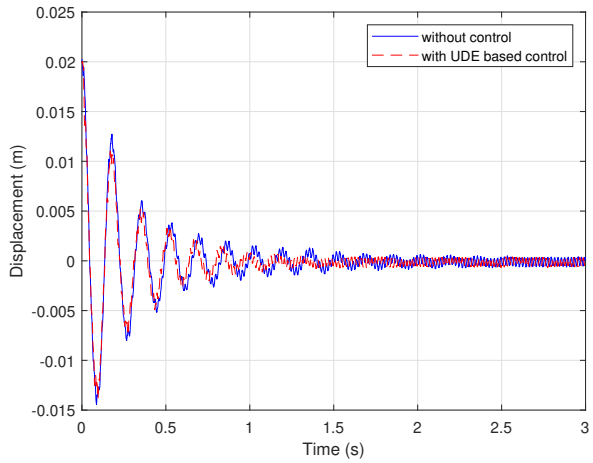

Figure 5.12: Tip displacement of the submerged beam with and without USDE based control (experiment results)

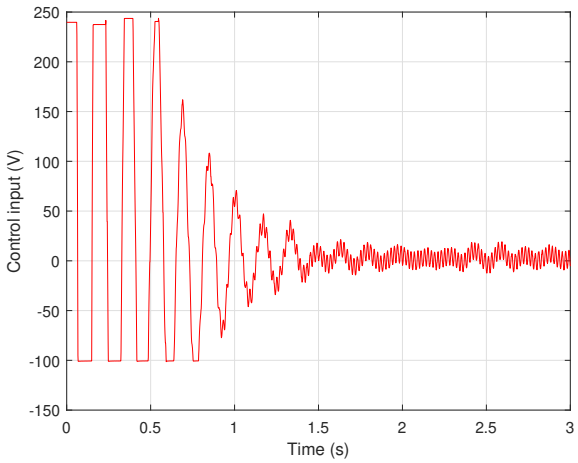

Figure 5.13: Control signal of the USDE-based control for the submerged beam (experiment results)

to unknown external disturbances. The stability and convergence properties of the proposed control is proved by using Lyapunov theory. In the simulation, the convergence performance of the proposed estimator and the vibration suppression performance are demonstrated. The proposed control method is further verified on a distributed model. The results show that the proposed control has a better performance compared to the PD control. At last, experiment results show the effectiveness of the proposed control method.

Chapter 6

Adaptive Vibration Control for the Beam System

6.1 Introduction

For the systems with uncertainties and parameter perturbations, adaptive control is one of the most effective control methods [140]. A salient feature in adaptive control is the unknown parameters can be online updated. This feature makes it possible to control systems under different conditions.

In the past several decades, adaptive control has been widely applied in many systems such as robots [141], aircrafts [142] and navigation systems [143]. The advantage of adaptive control lies in the self-adjusting parameters of the system with regard to various operating conditions. In [144], a robust adaptive control strategy is proposed for teleoperatioin systems. Time-varying delay and uncertainties are addressed with the help of adaptive control. For robot manipulators, [145] provides an adaptive motion control method, where the gravity can be online compensated. In [146], the adaptive control is extended to the unmanned vehicles. It is shown the adaptive control can address the motion control problem for the unmanned systems with hydrodynamical uncertainties.

For the beam system, adaptive control has been investigated in a few articles. In [147], an adaptive shape control is proposed for the flexible beam. The composite beam was modelled by using piezoelectric actuators and sensors. Dynamic response of the integrated laminated beam was studied. In [148], adaptive barrier control was introduced to suppress the vibration and cope with the system uncertainties. A new barrier Lyapunov function was proposed for the control design and stability analysis to prevent the constraint violation. In [149], a model reference adaptive control was investigated. The adaptive law was developed based on the Lyapunov redesign method on an infinite dimensional Hilbert space.

In this chapter, a new adaptive parameter estimation and control scheme will be introduced for the beam system. Different to the existing adaptive control methods, the proposed adaptive law will be driven by the parameter estimation error instead of the prediction error. In addition to online estimate the unknown parameters, the vibration of the beam can be suppressed by using the proposed adaptive controller.

6.2 Adaptive control for the beam system

In this section, we will propose a new adaptive control strategy for the flexible beam. The dynamics of the beam under different flow loads behaves like other beams with different parameters. Therefore, we can design adaptive control as long as the parameters can be online estimated. We recall the beam model as

$$\begin{cases} \dot{x}_1 = x_2 \\ \dot{x}_2 = -\Theta_1 x_1 - \Theta_2 x_2 + b_1 u \\ y = x_1 \end{cases} \tag{6.1}$$

where Θ_1 and Θ_2 are the unknown system parameters, b_1 is a known piezoelectric coefficient.

6.2.1 Adaptive parameter estimation

Before introducing the adaptive controller, an adaptive law should be designed to update the unknown parameters of the beam system. In stead of designing traditional adaptive laws using the prediction error, we will construct a new adaptive law driven by the parameter estimation error. For this purpose, we define a set of filtered variables as

$$\begin{cases} k_f \dot{x}_{1f} + x_{1f} = x_1, & x_{1f}(0) = 0 \\ k_f \dot{x}_{2f} + x_{2f} = x_2, & x_{2f}(0) = 0 \\ k_f \dot{u}_f + u_f = u, & u_f(0) = 0 \end{cases} \tag{6.2}$$

To facilitate the parameter estimation, we can reconstruct the second equation in (6.1) as the following compact form

$$\dot{x}_{2f} = \Phi_f^T \Theta \tag{6.3}$$

where

$$\Phi_f = [-x_{1f}, -x_{2f}]^T, \quad \Theta = [\Theta_1, \Theta_2]^T. \tag{6.4}$$

Moreover, we define the auxiliary variables P and Q as [87]

$$\begin{cases} \dot{P} = -lP + \Phi_f^T \Phi_f \\ \dot{Q} = -lQ + \Phi_f^T \left[(x_2 - x_{2f}) / k_f - b_1 u_f \right]^T \end{cases} \tag{6.5}$$

where $l > 0$ is a positive constant.

By integrating (6.5) we can obtain its solution as

$$\begin{cases} P = \int_0^t e^{-l(t-r)} \Phi_f^T(r) \Phi_f(r) dr \\ Q = \int_0^t e^{-l(t-r)} \Phi_f^T(r) \left[(x_2 - x_{2f}) / k_f - b_1 u_f \right]^T dr \end{cases} \tag{6.6}$$

Then a crucial variable can be derived as

$$M = P\hat{\Theta} - Q = -P\tilde{\Theta} \tag{6.7}$$

where $\hat{\Theta}$ is the estimated parameter and $\tilde{\Theta}$ is the estimation error fulfills $\tilde{\Theta} = \Theta - \hat{\Theta}$. From (6.5) we can find that the variable M contains the information of the estimation error $\tilde{\Theta}$. As a result, M can be used to drive the adaptive law. As shown in [150], the variable M can guarantee the convergence of the parameter error and enhance the control performance as well.

6.2.2 Adaptive controller design and stability analysis

In order to suppress the vibration of the beam system, we define a sliding surface variable z with the control error x_1 and its derivative x_2 as

$$z = \alpha_1 x_1 + x_2 \tag{6.8}$$

By differentiating (6.8), one can derive $\dot{z}$ along with (6.1) as

$$\dot{z} = \alpha_1 x_2 + \dot{x}_2 = \alpha_1 x_2 - \Theta_1 x_1 - \Theta_2 x_2 + b_1 u \tag{6.9}$$

The adaptive control law can be designed as

$$u = \frac{1}{b_1}(-\beta_1 z + \hat{\Theta}_1 x_1 + \hat{\Theta}_2 x_2 - \alpha_1 x_2) \tag{6.10}$$

where $\hat{\Theta}_1$ and $\hat{\Theta}_2$ are the unknown system parameters that can be online estimated with the lumped vector Θ.

Then, we can design the parameter updating law to online estimate the unknown parameters $\hat{\Theta}_1$ and $\hat{\Theta}_2$ with the help of (6.7) as

$$\dot{\hat{\Theta}} = \Gamma(\Phi^T z - M) \tag{6.11}$$

where $\Gamma > 0$ is a designed diagonal matrix. The overall structure of the proposed adaptive control scheme for the beam system is shown in Figure. 6.1.

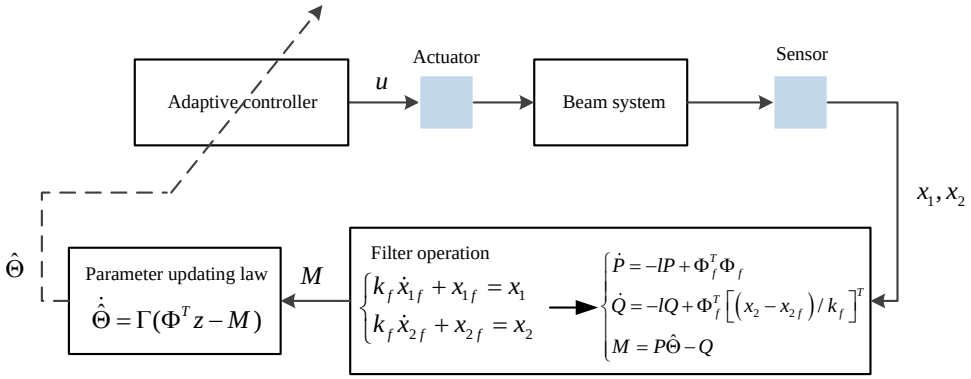

Figure 6.1: Structure of the proposed adaptive control scheme for the beam system

Remark 6.1. *Different to the existing adaptive control strategies, a new leakage term M is included in the parameter updating law (6.11). The new leakage term M contains the parameter estimation error, thus the parameter convergence can be guaranteed. Consequently, the convergence of the control error can be guaranteed by using the proposed adaptive control (6.10).*

The following Theorem summarizes the main results of this chapter:

Theorem 6.1. *Consider system (6.1) with the adaptive control (6.10) and the parameter updating law (6.11), if the regressor matrix Φ is persistently excited, the filtered regressor matrix P satisfies $\lambda_{min}(P) > \sigma > 0$ and both the control error x_1 and the parameter error $\tilde{\Theta}$ exponentially converge to zero.*

Proof. We select the Lyapunov function as

$$V_1 = \frac{1}{2} z^2 + \frac{1}{2} \tilde{\Theta}^T \Gamma^{-1} \tilde{\Theta} \tag{6.12}$$

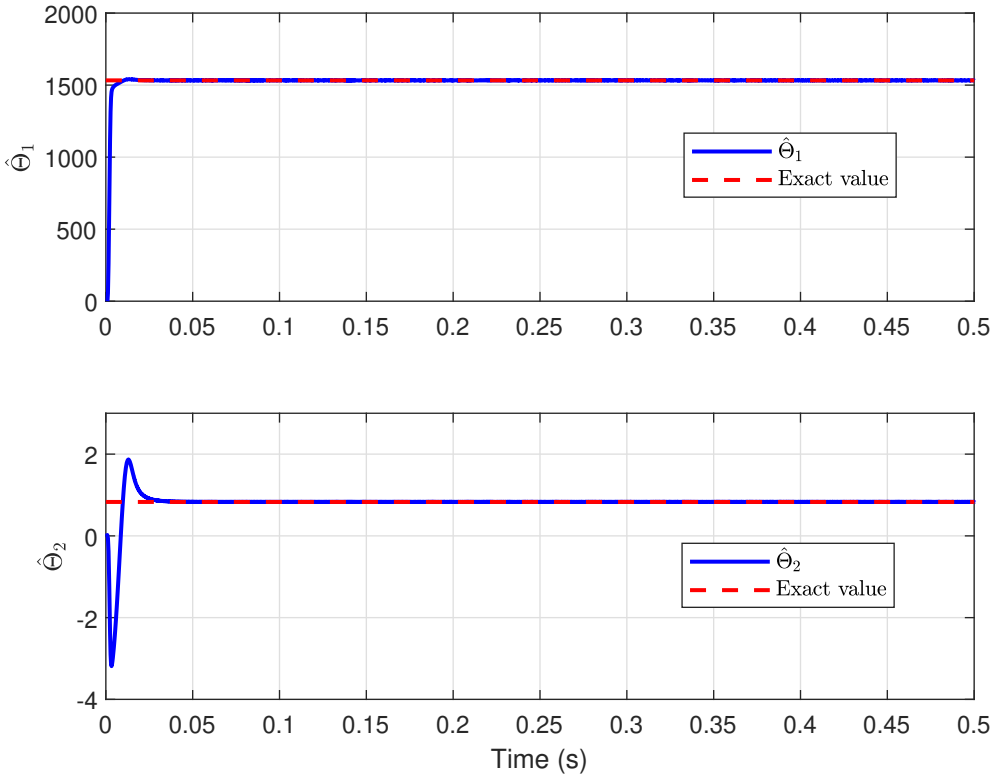

Figure 6.2: Estimated parameters of the beam system with the proposed adaptive control scheme

One can obtain the time derivative of V_1 from (6.12), (4.20) and (6.9) as

$$\begin{aligned}
\dot{V}_1 &= z\dot{z} + \tilde{\Theta}^T\Gamma^{-1}\dot{\tilde{\Theta}} \\
&= z(-\beta_1 z + \Phi\tilde{\Theta}) + \tilde{\Theta}^T\Gamma^{-1}(-\Gamma\Phi^T z - \Gamma P\tilde{\Theta}) \\
&= -\beta_1 z^2 - \tilde{\Theta}^T P\tilde{\Theta} \\
&\leq -\beta_1 z^2 - 2\sigma k_m/\lambda_{\max}\left(\Gamma^{-1}\right)\tilde{\Theta}^T\Gamma^{-1}\tilde{\Theta} \\
&\leq -\tau V_1
\end{aligned} \tag{6.13}$$

where $\tau = 2\min\{\beta_1, \sigma k_m/\lambda_{\max}\left(\Gamma^{-1}\right)\}$ is a positive constant for all $t > 0$. Based on Lyapunov's Theorem and Theorem 6.1, both z and the parameter error $\tilde{\Theta}$ exponentially converge to zero. This implies the control error x_1 converge to zero. □

6.3 Simulations

In order to verify the effectiveness of the proposed adaptive control. The parameters of the adaptive law (4.20) are set as $\Gamma = 1 \cdot \text{diag}(1 \cdot 10^{11}, 1 \cdot 10^8)$, $k_f = 0.001$, $l = 1 \cdot \text{diag}(0.1, 0.1)$. The parameters of the control law (6.10) are chosen as $\beta_1 = 20, \alpha_1 = 120$. For the tuning of these parameters, large learning gain Γ can increase the convergence rate while may cause parameter shifting at the transient response. Large β_1 and α_1 can improve the control performance while requiring a larger-range control signal depends on the actuator. The filter coefficient k_f and the forgetting factor l should be chosen by making a trade-off between the estimation performance and the robustness.

We release the tip of the beam at a distance of 0.01m to show the effectiveness of the proposed

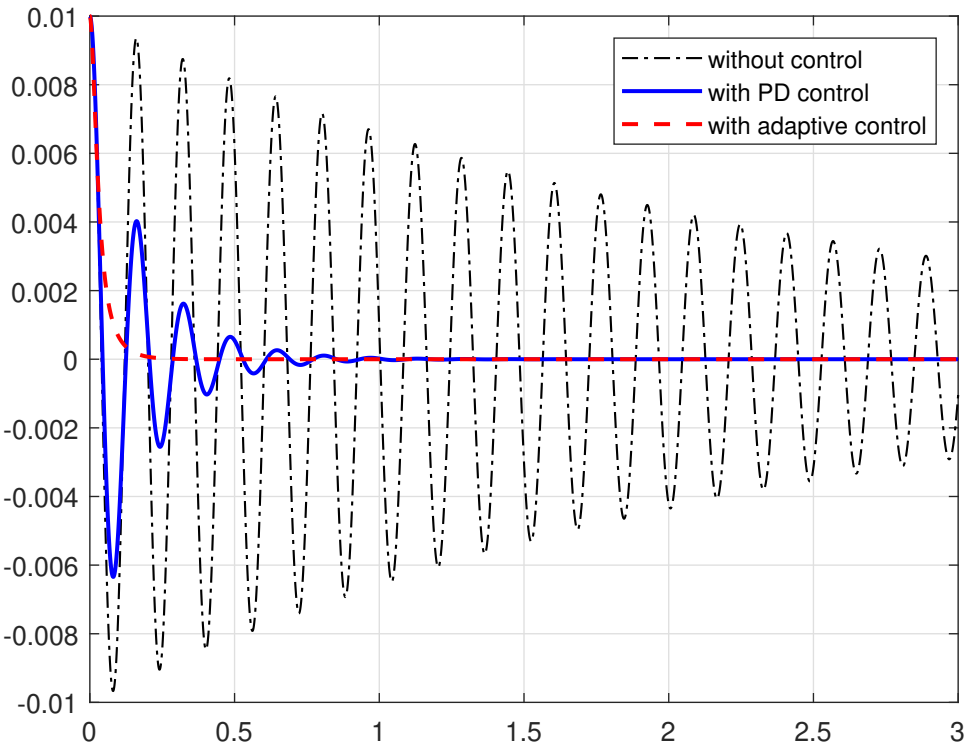

Figure 6.3: Vibration control performance with PD control and the proposed adaptive control scheme

adaptive control. This is a regular case in the turbine system encountering flows. The vibration of the beam makes the system fulfills the persistent excitation condition. Therefore, the unknown system parameters can be estimated as mentioned in Theorem 6.1.

The parameter estimation results and vibration control results are shown in Figure 6.2 and Figure 6.3. From Figure 6.2 we can see the parameters can be exactly estimated in a short time. Figure 6.3 shows both the PD control and the adaptive control can suppress the vibration of the beam. The adaptive control has a better control performance compared with the PD control.

To further illustrate the effectiveness of the proposed adaptive control, a higher order (20th-order) model will be used to simulate the system dynamics which is more close to the reality. We select the number of nodes in (2.85) as $K = 10$. Then a twentieth-order model is constructed to describe the system dynamics. In the controller design, the second order model (6.1) is retained. The comparative results are shown in Figure 6.4-Figure 6.6. From Figure 6.4 we can see the free vibration of the beam without control vibrates around 15 seconds after release. With the PD control, the beam can be stabilized at around 5 seconds as shown in Figure 6.5. With the proposed adaptive control, the vibration of the beam can be suppressed within a very short time around 2 seconds, which illustrate the effectiveness and the advantage of the proposed adaptive control method.

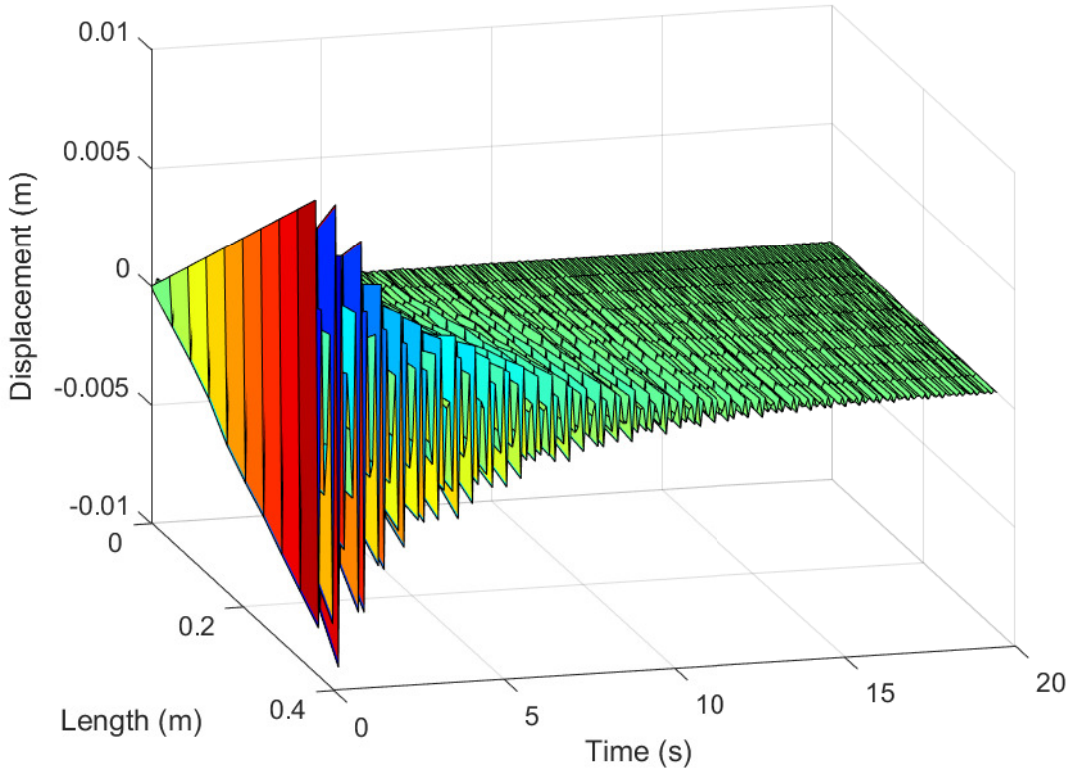

Figure 6.4: Vibration of the beam without control

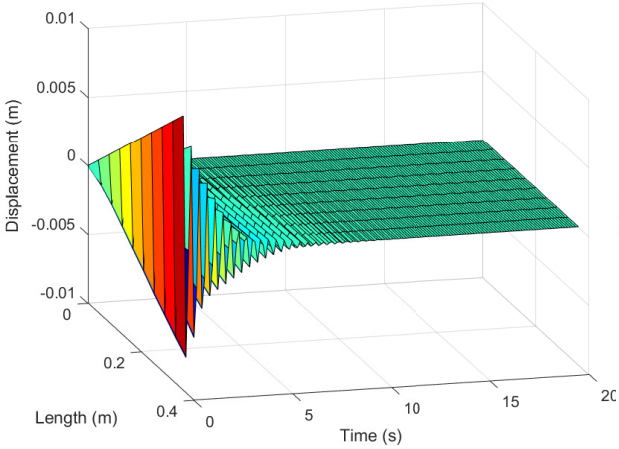

Figure 6.5: Vibration control of the beam with PD control

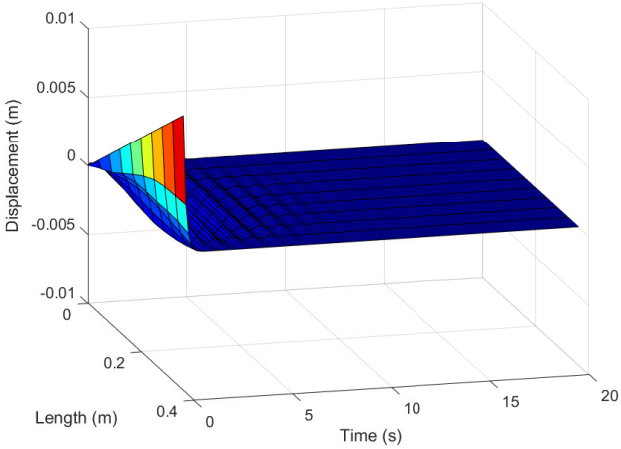

Figure 6.6: Vibration control of the beam with the proposed adaptive control

6.4 Conclusions

This chapter proposes an adaptive control for the beam with uncertainties. In the adaptive law design, a new parameter estimation error based algorithm is introduced which is different to the classical prediction error based methods (e.g. gradient method). By using the new adaptive law, the unknown system parameters can be online updated. To suppress the vibration of the beam, the adaptive controller is designed and the stability is proved by using Lyapunov theorems. Simulation results show the effectiveness of the proposed adaptive control scheme.

Part V

Concluding Remarks and Future Work

Chapter 7

Conclusions and Future Work

7.1 Conclusions and contributions

In this thesis, the dynamic model for the piezoelectric cantilever beam is build by using PDE. To facilitate the parameter estimation procedure and the controller design, a simplified control-oriented ODE-based model is constructed. Adaptive parameter estimation strategies are developed for the system with the first mode and the system with multi-modes respectively. In order to suppress the vibration of the beam, an USDE-based controller is introduced for the beam. To further take into account the unknown parameters, adaptive control is proposed which can online update the parameters. The main contributions of the thesis can be summarized as follows:

- **Development of the PDE-based model and the ODE-based model for the submerged piezoelectric cantilever beam**
  The system is described by both the PDE-based model and ODE-based model. The motion equation of the cantilever beam is build with the help of Hamilton's principle. The piezoelectric actuator model is included in the derived PDE and the deflection-strain relationship is presented for the purpose of experimental validation. To make it convenient for parameter estimation, Galerkin method is adopted to convert the PDE to ODE.

- **Adaptive parameter estimation strategy design for the beam system with one mode**
  A new adaptive parameter estimation framework is proposed to online estimate unknown system parameters considering the first vibration mode. To obtain the system states, the Levant exact differentiator via sliding mode technique is constructed. Instead of using the observer/predictor error as in the classical parameter estimation methods, a novel adaptive law which is driven by the parameter estimation error is proposed.

- **Adaptive parameter estimation for the beam system with multi-modes by using input and output**
  In order to cope with multiple vibration modes of the beam, a novel parameter estimation strategy is formulated to identify the beam system. A novel adaptive law is introduced to estimate the unknown system parameters in real time. Specifically, a time-varying gain is designed to handle the effects of regressor to enhance convergence performance and simplify the tuning of learning gains.

- **Development of the USDE-based vibration control for the beam system**
  An estimator based vibration control strategy is introduced to both suppress the vibration and estimate the unknown system dynamics. Different to the function approximation based methods, the proposed control has a simple structure which is more realistic to implement in practice. In the proposed estimator, only one parameter need to be tuned depends on the bandwidth of the filter. The estimated unknown dynamics is compensated into the controller and thus makes the system more robust to unknown external disturbances. The stability and convergence properties of the proposed control is proved by using Lyapunov theory.

- **Adaptive control design for the beam system**
  To suppress the vibration of the beam with unknown system parameters, an adaptive control is proposed. By using the parameter estimation error based adaptive law, the unknown system parameters can be online updated. To suppress the vibration of the beam, the adaptive controller is designed and the stability is proved.

7.2 Future work

In the future work, some issues not fully resolved would be investigated. Although we have developed a framework on modelling, identification and control on the beam system, there are still lots of interested points deserve to be studied. The major future work would be the investigation of the PDE systems. The learning-based controller and the strict persistent excitation condition would be two other important aspects. The specific discussion about the future work is given as follows:

- **Design parameter estimation algorithms and controllers directly on PDE systems**
  In the current work, an accurate PDE model and the reduced order model are constructed. For the control purpose, we designed the parameter estimation strategies and controllers based on the simplified ODE model. Although we have tested the estimation algorithms and the UDE-based control on the real plant by using the ODE model, it is always desired to operate with the accurate PDE model to describe the complete dynamics of the system. With the rapid growth of the hardware's processor, PDE-based algorithms would be realized on the applications. As a result, it is promising to investigate PDE systems.

- **Reduce the computation cost of learning-based controller**
  In Chapter 6, we have proposed adaptive control to suppress the vibration of the beam. Although we have good simulation results, there are still some problems on conducting the experiments. The major problem is the high computation cost, which led to a long delay for the real-time control. At the same time, a small sampling time is needed to correctly online estimate the parameters. These two reasons make it not able to be realized on the test bench. For the well-established systems with current processor, it is important to explore more efficient algorithms to reduce the computation cost of learning-based controller.

- **Relax persistent excitation condition in parameter estimation**
  For the adaptive parameter estimation in Chapter 3 and Chapter 4, there is a strong assumption named persistent excitation condition. In real applications, not all the systems can fulfill this condition. In such cases, the parameters will not converge to the true values. The adaptive estimation

and the adaptive control may not work at a feasible range at such cases thus my deteriorate the system. Consequently, investigation on relaxing persistent excitation condition is of great importance for real applications.

Part VI

Appendix

Appendix A

Computation of theoretical frequencies and mode shapes of the beam

In the absence of the damping term, piezoelectric effect and the external load, we have the free vibration equation

$$\rho A \frac{\partial^2 w}{\partial t^2} + EI \frac{\partial^4 w}{\partial x^4} = 0, \tag{A.1}$$

and the boundary conditions

$$w|_{x=0} = 0; \qquad \left.\frac{\partial w}{\partial x}\right|_{x=0} = 0 \tag{A.2}$$

$$\left.\frac{\partial^2 w}{\partial x^2}\right|_{x=L} = 0; \qquad \left.\frac{\partial^3 w}{\partial x^3}\right|_{x=L} = 0. \tag{A.3}$$

The free vibration solution can be obtained by using the method of separation of variables as [56]

$$w(x,t) = W(x)T(t). \tag{A.4}$$

Substituting (A.4) into (A.1), we have

$$\rho A W(x) \frac{d^2 T(t)}{dt^2} + EI \frac{d^4 W(x)}{dx^4} T(t) = 0. \tag{A.5}$$

Rearranging (A.5), one yields

$$\frac{c^2}{W(x)} \frac{d^4 W(x)}{dx^4} = -\frac{1}{T(t)} \frac{d^2 T(t)}{dt^2} = \beta^2 \tag{A.6}$$

where

$$c = \sqrt{\frac{EI}{\rho A}}. \tag{A.7}$$

Then, we have the following ordinary differential equations

$$\frac{d^4 W(x)}{dx^4} - \beta^4 W(x) = 0 \tag{A.8}$$

$$\frac{d^2 T(t)}{dt^2} + \omega^2 T(t) = 0 \tag{A.9}$$

where

$$\beta^4 = \frac{\omega^2}{c^2} = \frac{\rho A \omega^2}{EI}. \tag{A.10}$$

The solution of (A.8) can be given as

$$W(x) = C_1 \cos \beta x + C_2 \sin \beta x + C_3 \cosh \beta x + C_4 \sinh \beta x. \tag{A.11}$$

The solution of (A.9) can be expressed as

$$T(t) = A \cos \omega t + B \sin \omega t. \tag{A.12}$$

Substituting boundary condition (A.2) into (A.11), one have

$$C_1 + C_3 = 0, C_2 + C_4 = 0 \tag{A.13}$$

and then

$$W(x) = C_1(\cos \beta x - \cosh \beta x) + C_2(\sin \beta x - \sinh \beta x). \tag{A.14}$$

Substituting boundary condition (A.3) into (A.14) yields

$$-C_1(\cos \beta L + \cosh \beta L) - C_2(\sin \beta L + \sinh \beta L) = 0, -C_1(-\sin \beta L + \sinh \beta L) - C_2(\cos \beta L + \cosh \beta L) = 0. \tag{A.15}$$

Since C_1 and C_2 are nonzero, the determinant of the coefficients must be zero

$$\begin{vmatrix} -(\cos \beta L + \cosh \beta L) & -(\sin \beta L + \sinh \beta L) \\ -(-\sin \beta L + \sinh \beta L) & -(\cos \beta L + \cosh \beta L) \end{vmatrix} = 0 \tag{A.16}$$

or

$$(\cos \beta L + \cosh \beta L)^2 - \left(\sinh^2 \beta L - \sin^2 \beta L\right) = 0. \tag{A.17}$$

Equation (A.17) can be simplified to obtain the frequency equation as

$$\cos \beta L \cosh \beta L + 1 = 0. \tag{A.18}$$

In Table A.1, we list five solutions of (A.18) computed by using MAPLE.

$\beta_1 L$	1.875104069
$\beta_2 L$	4.694091133
$\beta_3 L$	7.854757438
$\beta_4 L$	10.99554073
$\beta_5 L$	14.13716839
$\beta_6 L$	17.27875953

Table A.1: Six solutions of (A.18)

The natural frequency can be obtained as

$$\omega_i = (\beta_i L)^2 \sqrt{\frac{EI}{\rho A L^4}}, i = 1, 2, \ldots \tag{A.19}$$

where $\beta_n L$ is the nth root of the frequency equation (A.18).

Equation (A.15) gives

$$C_2 = -\frac{\cos \beta L + \cosh \beta L}{\sin \beta L + \sinh \beta L} C_1. \tag{A.20}$$

Then the mode shape can be obtained as

$$W_i(x) = C_i \left[(\cos \beta_i x - \cosh \beta_i x) - \frac{\cos \beta_i L + \cosh \beta_i L}{\sin \beta_i L + \sinh \beta_i L} (\sin \beta_i x - \sinh \beta_i x) \right]. \tag{A.21}$$

$$w(x, t) = \sum_{i=1}^{n} W_i(x) \eta_i(t) \tag{A.22}$$

The unknown constant C_i is unique for each frequency and is determined by the information (the dis-

placement and velocity) of initial conditions at $t = 0$. The first to fifth mode shapes (a typical value $C_i = 1$ is used) are shown in Figure A.1.

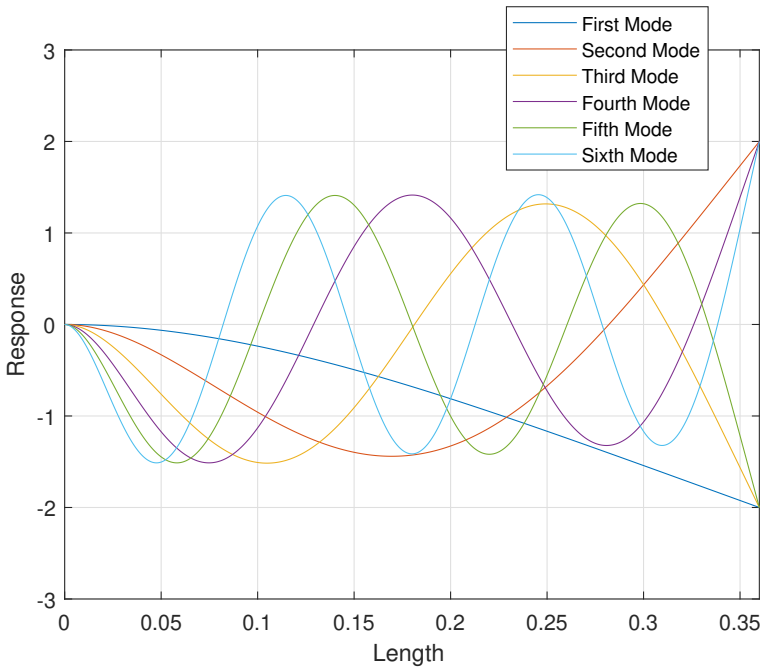

Figure A.1: First six mode shapes of the beam system

Bibliography

[1] Zhengwei Wang and Lingjiu Zhou. Simulations and measurements of pressure oscillations caused by vortex ropes. *Journal of Fluids Engineering*, 128(4):649–655, 2006.

[2] Steven L Garrett. *Understanding Acoustics: An Experimentalist's View of Acoustics and Vibration*. Springer, 2017.

[3] AG Olabi and Mohammad Ali Abdelkareem. Renewable energy and climate change. *Renewable and Sustainable Energy Reviews*, 158:112111, 2022.

[4] Enas Taha Sayed, Tabbi Wilberforce, Khaled Elsaid, Malek Kamal Hussien Rabaia, Mohammad Ali Abdelkareem, Kyu-Jung Chae, and AG Olabi. A critical review on environmental impacts of renewable energy systems and mitigation strategies: Wind, hydro, biomass and geothermal. *Science of the total environment*, 766:144505, 2021.

[5] Riman Sipahutar, Siti Masreah Bernas, Momon Sodik Imanuddin, et al. Renewable energy and hydropower utilization tendency worldwide. *Renewable and Sustainable Energy Reviews*, 17:213–215, 2013.

[6] Chirag Trivedi. A review on fluid structure interaction in hydraulic turbines: A focus on hydrodynamic damping. *Engineering Failure Analysis*, 77:1–22, 2017.

[7] Active flow control system for improving hydraulic turbine performances at off-design operation, available online: http: //www.afc4hydro.com.

[8] Abid Memon, M Asif Memon, Kaleemullah Bhatti, Kavikumar Jacob, Thanin Sitthiwirattham, Chanon Promsakon, et al. Modelling and simulation of fluid flow through a circular cylinder with high reynolds number: A comsol multiphysics study. *Journal of Mathematics*, 2022, 2022.

[9] Oscar de la Torre, Ignazio Floris, Salvador Sales, and Xavier Escaler. Fiber bragg grating sensors for underwater vibration measurement: Potential hydropower applications. *Sensors*, 21(13):4272, 2021.

[10] Eduard Egusquiza, Carme Valero, Xingxing Huang, Esteve Jou, Alfredo Guardo, and Cristian Rodriguez. Failure investigation of a large pump-turbine runner. *Engineering Failure Analysis*, 23:27–34, 2012.

[11] Mohd-Zulhilmi Paiz Ismadi, Patrice Meunier, Andreas Fouras, and Kerry Hourigan. Experimental control of vortex breakdown by density effects. *Physics of fluids*, 23(3):034104, 2011.

[12] Jean-Pierre Franc and Jean-Marie Michel. *Fundamentals of cavitation*, volume 76. Springer science & Business media, 2006.

[13] Xian-wu Luo, Bin Ji, and Yoshinobu Tsujimoto. A review of cavitation in hydraulic machinery. *Journal of Hydrodynamics*, 28(3):335–358, 2016.

[14] VL Okulov, VG Meledin, and IV Naumov. Experimental investigation of a swirling flow in a cubic container. *Technical Physics*, 48(10):1249–1254, 2003.

[15] JB Yang, LJ Jiang, and D CH Chen. Dynamic modelling and control of a rotating euler–bernoulli beam. *Journal of sound and vibration*, 274(3-5):863–875, 2004.

[16] MSM Fouzi, KM Jelani, NA Nazri, and Mohd Shahrir Mohd Sani. Finite element modelling and updating of welded thin-walled beam. *International Journal of Automotive and Mechanical Engineering*, 15(4):5874–5889, 2018.

[17] Vincenzo Gattulli, Marco Lepidi, Francesco Potenza, and Umberto Di Sabatino. Modal interactions in the nonlinear dynamics of a beam–cable–beam. *Nonlinear Dynamics*, 96(4):2547–2566, 2019.

[18] Alessandro Macchelli and Claudio Melchiorri. Modeling and control of the timoshenko beam. the distributed port hamiltonian approach. *SIAM Journal on Control and Optimization*, 43(2):743–767, 2004.

[19] BZ Guo. Basis property of a rayleigh beam with boundary stabilization. *Journal of optimization theory and applications*, 112(3):529–547, 2002.

[20] Davood Younesian and Ebrahim Esmailzadeh. Non-linear vibration of variable speed rotating viscoelastic beams. *Nonlinear Dynamics*, 60(1-2):193–205, 2010.

[21] Jer-Rong Chang, Wei-Jr Lin, Chun-Jung Huang, and Siu-Tong Choi. Vibration and stability of an axially moving rayleigh beam. *Applied Mathematical Modelling*, 34(6):1482–1497, 2010.

[22] Hemanshu R Pota and Thomas E Alberts. Multivariable transfer functions for a slewing piezoelectric laminate beam. *Journal of Dynamic Systems, Measurement, and Control*, 1995.

[23] OA Garcia-Perez, G Silva-Navarro, and JF Peza-Solis. Flexible-link robots with combined trajectory tracking and vibration control. *Applied Mathematical Modelling*, 70:285–298, 2019.

[24] SM Khot, Nitesh P Yelve, Rajat Tomar, Sameer Desai, and S Vittal. Active vibration control of cantilever beam by using pid based output feedback controller. *Journal of Vibration and Control*, 18(3):366–372, 2012.

[25] Wei He, Shuang Zhang, and Shuzhi Sam Ge. Boundary output-feedback stabilization of a timoshenko beam using disturbance observer. *IEEE Transactions on Industrial Electronics*, 60(11):5186–5194, 2012.

[26] Ian R Petersen and Himanshu R Pota. Minimax lqg optimal control of a flexible beam. *Control Engineering Practice*, 11(11):1273–1287, 2003.

[27] Bartłomiej Dyniewicz, Jacek M Bajkowski, and Czesław I Bajer. Semi-active control of a sandwich beam partially filled with magnetorheological elastomer. *Mechanical Systems and Signal Processing*, 60:695–705, 2015.

[28] Philip Beckley. *Electrical steels for rotating machines (Power and energy series no. 37)*. IET, 2002.

[29] R Zeng, Kin Wing Kwok, Helen LW Chan, and CL Choy. Longitudinal and transverse piezoelectric coefficients of lead zirconate titanate/vinylidene fluoride-trifluoroethylene composites with different polarization states. *Journal of applied physics*, 92(5):2674–2679, 2002.

[30] Seon M Han, Haym Benaroya, and Timothy Wei. Dynamics of transversely vibrating beams using four engineering theories. *Journal of Sound and vibration*, 225(5):935–988, 1999.

[31] J Chung and Hong Hee Yoo. Dynamic analysis of a rotating cantilever beam by using the finite element method. *Journal of Sound and vibration*, 249(1):147–164, 2002.

[32] Jintai Chung, Duhan Jung, and Hong Hee Yoo. Stability analysis for the flapwise motion of a cantilever beam with rotary oscillation. *Journal of sound and vibration*, 273(4-5):1047–1062, 2004.

[33] Hong Hee Yoo, Seung Hyun Lee, and Sang Ha Shin. Flapwise bending vibration analysis of rotating multi-layered composite beams. *Journal of sound and vibration*, 286(4-5):745–761, 2005.

[34] Jarosław Latalski and Jerzy Warminski. Nonlinear vibrations of a rotating thin-walled composite piezo-beam with circumferentially uniform stiffness (cus). *Nonlinear Dynamics*, 98(4):2509–2529, 2019.

[35] D Younesian and E Esmailzadeh. Vibration suppression of rotating beams using time-varying internal tensile force. *Journal of sound and vibration*, 330(2):308–320, 2011.

[36] Yii-Mei Huang and Cheun-Yuan Lee. Dynamics of a rotating rayleigh beam subject to a repetitively travelling force. *International journal of mechanical sciences*, 40(8):779–792, 1998.

[37] Mergen H Ghayesh and Sara Balar. Non-linear parametric vibration and stability of axially moving visco-elastic rayleigh beams. *International Journal of Solids and Structures*, 45(25-26):6451–6467, 2008.

[38] Peter Hagedorn and Anirvan DasGupta. *Vibrations and waves in continuous mechanical systems*. Wiley Online Library, 2007.

[39] David P Thambiratnam and H Max Irvine. Microcomputer analysis of torsionally coupled multistorey buildings—i. shear beam model. *Computers & structures*, 32(5):1175–1182, 1989.

[40] V Gičev and MD Trifunac. Rotations in a shear-beam model of a seven-story building caused by nonlinear waves during earthquake excitation. *Structural Control and Health Monitoring: The Official Journal of the International Association for Structural Control and Monitoring and of the European Association for the Control of Structures*, 16(4):460–482, 2009.

[41] Stephen P Timoshenko. Lxvi. on the correction for shear of the differential equation for transverse vibrations of prismatic bars. *The London, Edinburgh, and Dublin Philosophical Magazine and Journal of Science*, 41(245):744–746, 1921.

[42] NFJ Van Rensburg and AJ Van der Merwe. Natural frequencies and modes of a timoshenko beam. *Wave motion*, 44(1):58–69, 2006.

[43] CM Wang, VBC Tan, and YY Zhang. Timoshenko beam model for vibration analysis of multi-walled carbon nanotubes. *Journal of Sound and Vibration*, 294(4-5):1060–1072, 2006.

[44] Xin-She Yang. *Mathematical modelling for earth sciences*. Dunedin, 2008.

[45] Saeid Bashash, Amin Salehi-Khojin, and Nader Jalili. Forced vibration analysis of flexible euler-bernoulli beams with geometrical discontinuities. In *2008 American Control Conference*, pages 4029–4034. IEEE, 2008.

[46] Cassio T Faria and Daniel J Inman. Modeling energy transport in a cantilevered euler–bernoulli beam actively vibrating in newtonian fluid. *Mechanical Systems and Signal Processing*, 45(2):317–329, 2014.

[47] Wafik Abassi, Adil El Baroudi, and Fulgence Razafimahery. Vibration analysis of euler-bernoulli beams partially immersed in a viscous fluid. *Physics Research International*, 2016, 2016.

[48] Matteo Luca Facchinetti, Emmanuel De Langre, and Francis Biolley. Coupling of structure and wake oscillators in vortex-induced vibrations. *Journal of Fluids and structures*, 19(2):123–140, 2004.

[49] Wang Lin and Ni Qiao. Vibration and stability of an axially moving beam immersed in fluid. *International journal of solids and structures*, 45(5):1445–1457, 2008.

[50] F Gosselin, MP Paidoussis, and AK Misra. Stability of a deploying/extruding beam in dense fluid. *Journal of sound and vibration*, 299(1-2):123–142, 2007.

[51] SA Eftekhari and AA Jafari. A mixed modal-differential quadrature method for free and forced vibration of beams in contact with fluid. *Meccanica*, 49(3):535–564, 2014.

[52] SA Eftekhari. A differential quadrature procedure for linear and nonlinear steady state vibrations of infinite beams traversed by a moving point load. *Meccanica*, 51(10):2417–2434, 2016.

[53] Qiao Ni, Mingwu Li, Min Tang, and Lin Wang. Free vibration and stability of a cantilever beam attached to an axially moving base immersed in fluid. *Journal of Sound and Vibration*, 333(9):2543–2555, 2014.

[54] Mohaamad Rezaiee-Pajand, Mohammad Sadegh Kazemiyan, et al. Solving coupled beam-fluid interaction by dtm. *Ocean Engineering*, 167:380–396, 2018.

[55] Ali H Nayfeh and P Frank Pai. *Linear and nonlinear structural mechanics*. John Wiley & Sons, 2008.

[56] Singiresu S Rao. *Vibration of continuous systems*, volume 464. Wiley Online Library, 2007.

[57] SN Mahmoodi, SE Khadem, and M Kokabi. Non-linear free vibrations of kelvin–voigt viscoelastic beams. *International Journal of Mechanical Sciences*, 49(6):722–732, 2007.

[58] Hyungrae Kim and Jintai Chung. Nonlinear modeling for dynamic analysis of a rotating cantilever beam. *Nonlinear Dynamics*, 86(3):1981–2002, 2016.

[59] Hong Hee Yoo, RR Ryan, and Richard A Scott. Dynamics of flexible beams undergoing overall motions. *Journal of Sound and vibration*, 181(2):261–278, 1995.

[60] H Tzou. Piezoelectric shells: Distributed sensing and control of continua: vol. 19, 2012.

[61] Yaowen Yang, Zhanli Jin, and Chee Kiong Soh. Integrated optimal design of vibration control system for smart beams using genetic algorithms. *Journal of Sound and Vibration*, 282(3-5):1293–1307, 2005.

[62] William F Riley, Leroy D Sturges, and Don H Morris. *Mechanics of materials*. John Wiley & Sons Incorporated, 2007.

[63] GJ Wagner, Nicolas Moës, WK Liu, and Ted Belytschko. The extended finite element method for rigid particles in stokes flow. *International Journal for Numerical Methods in Engineering*, 51(3):293–313, 2001.

[64] Giovanni Di Ilio, Iskender Sahin, and Angelantonio Tafuni. Unsteady stokes flow for a vibrating cantilever under a free-surface. In *ASME International Mechanical Engineering Congress and Exposition*, volume 46583. American Society of Mechanical Engineers, 2014.

[65] R Byron Bird, Warren E Stewart, and Edwin N Lightfoot. *Transport phenomena*, volume 1. John Wiley & Sons, 2006.

[66] Stephen D Senturia. *Microsystem design*. Springer Science & Business Media, 2007.

[67] Mousa Rezaee and Naser Sharafkhani. Out-of-plane vibration of an electrostatically actuated microbeam immersed in flowing fluid. *Nonlinear Dynamics*, 102(1):1–17, 2020.

[68] Tomomichi Nakamura, Shigehiko Kaneko, Fumio Inada, Minoru Kato, Kunihiko Ishihara, Takashi Nishihara, Njuki W Mureithi, and Mikael A Langthjem. *Flow-induced vibrations: classifications and lessons from practical experiences*. Butterworth-Heinemann, 2013.

[69] E Harald van Brummelen. Added mass effects of compressible and incompressible flows in fluid-structure interaction. *Journal of Applied Mechanics*, 76, 2009.

[70] Cho-Chung Liang, Ching-Chao Liao, Yuh-Shiou Tai, and Wen-Hao Lai. The free vibration analysis of submerged cantilever plates. *Ocean Engineering*, 28(9):1225–1245, 2001.

[71] QW Liang, Cristian G Rodríguez, Eduard Egusquiza, Xavier Escaler, Mohamed Farhat, and François Avellan. Numerical simulation of fluid added mass effect on a francis turbine runner. *Computers & Fluids*, 36(6):1106–1118, 2007.

[72] Benoît Debbaut and Ken Thomas. Simulation and analysis of oscillatory squeeze flow. *Journal of non-newtonian fluid mechanics*, 124(1-3):77–91, 2004.

[73] Ünal Dikmen. Modeling of seismic wave attenuation in soil structures using fractional derivative scheme. *Journal of Balkan Geophysical Society*, 8(4):175–188, 2005.

[74] James William Thomas. *Numerical partial differential equations: finite difference methods*, volume 22. Springer Science & Business Media, 2013.

[75] John C Strikwerda. *Finite difference schemes and partial differential equations*, volume 88. Siam, 2004.

[76] Emmanuel Grenier, Violaine Louvet, and Paul Vigneaux. Parameter estimation in non-linear mixed effects models with saem algorithm: extension from ode to pde. *ESAIM: Mathematical Modelling and Numerical Analysis*, 48(5):1303–1329, 2014.

[77] Hu Ding, Li-Qun Chen, and Shao-Pu Yang. Convergence of galerkin truncation for dynamic response of finite beams on nonlinear foundations under a moving load. *Journal of Sound and Vibration*, 331(10):2426–2442, 2012.

[78] Murat Subaşı, Sıdıka Şule Şener, and Yeşim Saraç. A procedure for the galerkin method for a vibrating system. *Computers & Mathematics with Applications*, 61(9):2854–2862, 2011.

[79] Elena Blokhina, Joan Pons, Jordi Ricart, Orla Feely, and Manuel Dominguez Pumar. Control of mems vibration modes with pulsed digital oscillators: Part i—theory. *IEEE Transactions on Circuits and Systems I: Regular Papers*, 57(8):1865–1878, 2010.

[80] Tehuan Chen, Junqiang Lou, Yiling Yang, Jianqiang Ma, GuoPing Li, and Yanding Wei. Auto-regressive moving average with exogenous excitation model based experimental identification and optimal discrete multi-poles shifting control of a flexible piezoelectric manipulator. *Journal of Vibration and Control*, 24(24):5707–5725, 2018.

[81] Clarence W Rowley and Scott TM Dawson. Model reduction for flow analysis and control. *Annu. Rev. Fluid Mech*, 49(1):387–417, 2017.

[82] Myungsoo Jun, Kandler Smith, and Peter Graf. State-space representation of li-ion battery porous electrode impedance model with balanced model reduction. *Journal of Power Sources*, 273:1226–1236, 2015.

[83] Andreu Fargas-Marques and Ramon Costa-Castelló. Energy-efficient full-range oscillation analysis of parallel-plate electrostatically actuated mems resonators. *Nonlinear Dynamics*, 89(4):2889–2904, 2017.

[84] Petros A Ioannou and Jing Sun. *Robust adaptive control*. Courier Corporation, 2012.

[85] Adrian Wills and Brett Ninness. On gradient-based search for multivariable system estimates. *IEEE Transactions on Automatic Control*, 53(1):298–306, 2008.

[86] Constantin Paleologu, Jacob Benesty, and Silviu Ciochina. A robust variable forgetting factor recursive least-squares algorithm for system identification. *IEEE Signal Processing Letters*, 15:597–600, 2008.

[87] Jing Na, Muhammad Nasiruddin Mahyuddin, Guido Herrmann, Xuemei Ren, and Phil Barber. Robust adaptive finite-time parameter estimation and control for robotic systems. *International Journal of Robust and Nonlinear Control*, 25(16):3045–3071, 2015.

[88] K Kunisch and E Graif. Parameter estimation for the euler-bernoulli beam. *Matematica Aplicada e Computacional*, 4:95–124, 1985.

[89] Gergely Takács, Tomáš Polóni, and Boris Rohal'-Ilkiv. Adaptive model predictive vibration control of a cantilever beam with real-time parameter estimation. *Shock and Vibration*, 2014, 2014.

[90] ZS Ma, L Liu, SD Zhou, and W Yang. Modal parameter estimation of the coupled moving-mass and beam time-varying system. In *Proceedings of the International Conference on Noise and Vibration Engineering (ISMA'14)*, pages 587–596, 2014.

[91] Arie Levant. Higher-order sliding modes, differentiation and output-feedback control. *International journal of Control*, 76(9-10):924–941, 2003.

[92] Arie Levant and Xinghuo Yu. Sliding-mode-based differentiation and filtering. *IEEE Transactions on Automatic Control*, 63(9):3061–3067, 2018.

[93] Jean-Jacques E Slotine, Weiping Li, et al. *Applied nonlinear control*, volume 199. Prentice hall Englewood Cliffs, NJ, 1991.

[94] Jing Na, Xuemei Ren, and Yuanqing Xia. Adaptive parameter identification of linear siso systems with unknown time-delay. *Systems & Control Letters*, 66:43–50, 2014.

[95] Yonghun Kim, Seok-Kyoon Kim, and Choon Ki Ahn. Variable cut-off frequency observer-based positioning for ball-beam systems without velocity and current feedback considering actuator dynamics. *IEEE Transactions on Circuits and Systems I: Regular Papers*, 68(1):396–405, 2020.

[96] Huifang Min, Shengyuan Xu, Jason Gu, and Guozeng Cui. Adaptive finite-time control for high-order nonlinear systems with multiple uncertainties and its application. *IEEE Transactions on Circuits and Systems I: Regular Papers*, 67(5):1752–1761, 2019.

[97] C Atkinson and M Manrique de Lara. The frequency response of a rectangular cantilever plate vibrating in a viscous fluid. *Journal of Sound and Vibration*, 300(1-2):352–367, 2007.

[98] Bao-Zhu Guo and Wei Guo. Stabilization and parameter estimation for an Euler-Bernoulli beam equation with uncertain harmonic disturbance under boundary output feedback control. *Nonlinear Analysis: Theory, Methods & Applications*, 61(5):671–693, 2005.

[99] Andres San-Millan and Vicente Feliu. A fast online estimator of the two main vibration modes of flexible structures from biased and noisy measurements. *IEEE/ASME Transactions on Mechatronics*, 20(1):93–104, 2014.

[100] Gregor Gelbert, Jonas P Moeck, Christian O Paschereit, and Rudibert King. Advanced algorithms for gradient estimation in one-and two-parameter extremum seeking controllers. *Journal of Process Control*, 22(4):700–709, 2012.

[101] Md Zulfiquar Ali Bhotto and Andreas Antoniou. New improved recursive least-squares adaptive-filtering algorithms. *IEEE Transactions on Circuits and Systems I: Regular Papers*, 60(6):1548–1558, 2012.

[102] XM Ren, Ahmad B Rad, PT Chan, and Wai Lun Lo. Online identification of continuous-time systems with unknown time delay. *IEEE Transactions on Automatic Control*, 50(9):1418–1422, 2005.

[103] Jing Na, Anthony Siming Chen, Guido Herrmann, Richard Burke, and Chris Brace. Vehicle engine torque estimation via unknown input observer and adaptive parameter estimation. *IEEE Transactions on Vehicular Technology*, 67(1):409–422, 2017.

[104] Jingqing Han. From pid to active disturbance rejection control. *IEEE transactions on Industrial Electronics*, 56(3):900–906, 2009.

[105] Bao-Zhu Guo and Zhi-liang Zhao. On the convergence of an extended state observer for nonlinear systems with uncertainty. *Systems & Control Letters*, 60(6):420–430, 2011.

[106] Mehmet Avcar and Kemal Saplioglu. An artificial neural network application for estimation of natural frequencies of beams. *International Journal of Advanced Computer Science and Applications*, 6(6):94–102, 2015.

[107] Wei He and Jinkun Liu. *Active vibration control and stability analysis of flexible beam systems*. Springer, 2019.

[108] Goong Chen. Control and stabilization for the wave equation in a bounded domain. *SIAM Journal on Control and Optimization*, 17(1):66–81, 1979.

[109] Jong Uhn Kim and Yuriko Renardy. Boundary control of the timoshenko beam. *SIAM Journal on Control and Optimization*, 25(6):1417–1429, 1987.

[110] Omer Morgul. Dynamic boundary control of a euler-bernoulli beam. *IEEE Transactions on automatic control*, 37(5):639–642, 1992.

[111] Stephen W Taylor and Stephen CB Yau. Boundary control of a rotating timoshenko beam. *ANZIAM Journal*, 44:143–184, 2002.

[112] Mustafa Dogan and Ömer Morgül. Boundary control of a rotating shear beam with observer feedback. *Journal of Vibration and Control*, 18(14):2257–2265, 2012.

[113] Genqi Xu and Hongxia Wang. Stabilisation of timoshenko beam system with delay in the boundary control. *International Journal of Control*, 86(6):1165–1178, 2013.

[114] Bao-Zhu Guo and Kun-Yi Yang. Dynamic stabilization of an euler–bernoulli beam equation with time delay in boundary observation. *Automatica*, 45(6):1468–1475, 2009.

[115] Thomas Bailey and James E Hubbard Jr. Distributed piezoelectric-polymer active vibration control of a cantilever beam. *Journal of Guidance, Control, and Dynamics*, 8(5):605–611, 1985.

[116] IS Sadek, S Adali, JM Sloss, and JC Bruch Jr. Optimal distributed control of a continuous beam with damping. *Journal of sound and vibration*, 117(2):207–218, 1987.

[117] Wei He, Chuan Yang, Tingting Meng, and Changyin Sun. Distributed control of a class of flexible mechanical systems with global constraint. *International Journal of Control*, 89(1):128–139, 2016.

[118] Juntao Fei. Active vibration control of flexible steel cantilever beam using piezoelectric actuators. In *Proceedings of the Thirty-Seventh Southeastern Symposium on System Theory, 2005. SSST'05.*, pages 35–39. IEEE, 2005.

[119] M Naushad Alam et al. Active vibration control of a piezoelectric beam using pid controller: Experimental study. *Latin American Journal of Solids and Structures*, 9(6):657–673, 2012.

[120] Miroslav M Jovanović, Aleksandar M Simonović, Nemanja D Zorić, Nebojša S Lukić, Slobodan N Stupar, and Slobodan S Ilić. Experimental studies on active vibration control of a smart composite beam using a pid controller. *Smart materials and structures*, 22(11):115038, 2013.

[121] Gustavo LCM Abreu, José F Ribeiro, and Valder Steffen Jr. Experiments on optimal vibration control of a flexible beam containing piezoelectric sensors and actuators. *Shock and vibration*, 10(5-6):283–300, 2003.

[122] Guo-Ping Cai and Simon X Yang. A discrete optimal control method for a flexible cantilever beam with time delay. *Journal of Vibration and Control*, 12(5):509–526, 2006.

[123] Ismail Kucuk, Ibrahim Sadek, and Yalcin Yilmaz. Optimal control of a distributed parameter system with applications to beam vibrations using piezoelectric actuators. *Journal of the Franklin Institute*, 351(2):656–666, 2014.

[124] Kathryn Lenz, Hitay Özbay, Allen Tannenbaum, Janos Turi, and Blaise Morton. Frequency domain analysis and robust control design for an ideal flexible beam. *Automatica*, 27(6):947–961, 1991.

[125] Atta Oveisi and Tamara Nestorović. Robust mixed h2/h8 active vibration controller in attenuation of smart beam. *Facta Universitatis, Series: Mechanical Engineering*, 12(3):235–249, 2014.

[126] Bao-Zhu Guo and Feng-Fei Jin. The active disturbance rejection and sliding mode control approach to the stabilization of the euler–bernoulli beam equation with boundary input disturbance. *Automatica*, 49(9):2911–2918, 2013.

[127] Wei He, Tingting Meng, Deqing Huang, and Xuefang Li. Adaptive boundary iterative learning control for an euler–bernoulli beam system with input constraint. *IEEE transactions on neural networks and learning systems*, 29(5):1539–1549, 2017.

[128] Mohammad Fadaee and Mostafa Talebitooti. Active vibration control of carbon nanotube-reinforced composite beam submerged in fluid using magnetostrictive layers. *Mechanics Based Design of Structures and Machines*, pages 1–18, 2020.

[129] Claus Abicht, Jens Bormann, Peter C Müller, Dirk Söffker, and Heinz Ulbrich. Model-based estimation of impact forces affecting elastic structures: Simulation and experiment. In *International Design Engineering Technical Conferences and Computers and Information in Engineering Conference*, volume 80289, pages 1701–1706. American Society of Mechanical Engineers, 2001.

[130] Idriz Krajcin and Dirk So¨ ffker. Modified pio design for robust unknown input estimation. In *International Design Engineering Technical Conferences and Computers and Information in Engineering Conference*, volume 37033, pages 1459–1464, 2003.

[131] MK Choudhary and G Naresh Kumar. Eso based lqr controller for ball and beam system. *IFAC-PapersOnLine*, 49(1):607–610, 2016.

[132] Ali Tavasoli. Active disturbance rejection boundary control of timoshenko beam with tip mass. *ISA transactions*, 80:221–231, 2018.

[133] Hua-Cheng Zhou and Hongyinping Feng. Disturbance estimator based output feedback exponential stabilization for euler–bernoulli beam equation with boundary control. *Automatica*, 91:79–88, 2018.

[134] Hongyinping Feng and Bao-Zhu Guo. Distributed disturbance estimator and application to stabilization for multi-dimensional wave equation with corrupted boundary observation. *Automatica*, 66:25–33, 2016.

[135] Yu Liu, Xiongbin Chen, Yilin Wu, He Cai, and Hiroshi Yokoi. Adaptive neural network control of a flexible spacecraft subject to input nonlinearity and asymmetric output constraint. *IEEE Transactions on Neural Networks and Learning Systems*, 2021.

[136] Amir Sharifahmadian. *Numerical models for submerged breakwaters: coastal hydrodynamics and morphodynamics*. Butterworth-Heinemann, 2015.

[137] Shuzhi Sam Ge and Cong Wang. Direct adaptive nn control of a class of nonlinear systems. *IEEE Transactions on Neural Networks*, 13(1):214–221, 2002.

[138] Jooyoung Park and Irwin W Sandberg. Universal approximation using radial-basis-function networks. *Neural computation*, 3(2):246–257, 1991.

[139] Jean-Jacques E Slotine and Weiping Li. Composite adaptive control of robot manipulators. *Automatica*, 25(4):509–519, 1989.

[140] Alessandro Astolfi, Dimitrios Karagiannis, and Romeo Ortega. *Nonlinear and adaptive control with applications*, volume 187. Springer, 2008.

[141] M Reza J Harandi, SA Khalilpour, Hamid D Taghirad, and Jose Guadalupe Romero. Adaptive control of parallel robots with uncertain kinematics and dynamics. *Mechanical Systems and Signal Processing*, 157:107693, 2021.

[142] Alberto Cavallo, Giacomo Canciello, and Antonio Russo. Integrated supervised adaptive control for the more electric aircraft. *Automatica*, 117:108956, 2020.

[143] Spyros G Tzafestas. Mobile robot control and navigation: A global overview. *Journal of Intelligent & Robotic Systems*, 91(1):35–58, 2018.

[144] Parham M Kebria, Abbas Khosravi, Saeid Nahavandi, Peng Shi, and Roohallah Alizadehsani. Robust adaptive control scheme for teleoperation systems with delay and uncertainties. *IEEE transactions on cybernetics*, 50(7):3243–3253, 2019.

[145] Tong Yang, Ning Sun, Yongchun Fang, Xin Xin, and He Chen. New adaptive control methods for n-link robot manipulators with online gravity compensation: Design and experiments. *IEEE Transactions on Industrial Electronics*, 69(1):539–548, 2021.

[146] Ali Haseltalab and Rudy R Negenborn. Adaptive control for autonomous ships with uncertain model and unknown propeller dynamics. *Control Engineering Practice*, 91:104116, 2019.

[147] Jin-Chein Lin and MH Nien. Adaptive control of a composite cantilever beam with piezoelectric damping-modal actuators/sensors. *Composite structures*, 70(2):170–176, 2005.

[148] Wei He and Shuzhi Sam Ge. Vibration control of a flexible beam with output constraint. *IEEE Transactions on Industrial Electronics*, 62(8):5023–5030, 2015.

[149] Kyung-Jinn Yang, Keum-Shik Hong, Wan-Suk Yoo, and Fumitoshi Matsuno. Model reference adaptive control of a cantilevered flexible beam. *JSME International Journal Series C Mechanical Systems, Machine Elements and Manufacturing*, 46(2):640–651, 2003.

[150] Shubo Wang and Jing Na. Parameter estimation and adaptive control for servo mechanisms with friction compensation. *IEEE Transactions on Industrial Informatics*, 16(11):6816–6825, 2020.